THE MEASUREMENT OF STATIC ELECTRIC QUADRUPOLE MOMENTS OF EXCITED NUCLEAR STATES BY COULOMB EXCITATION

Thesis by
Robert Grandin Stokstad

In Partial Fulfillment of the Requirements

For the Degree of
Doctor of Philosophy

California Institute of Technology
Pasadena, California
1967
(Submitted December 6 , 1966)

ACKNOWLEDGMENTS

The experiments reported here were carried out with the collaboration at various times of Dr. Jorrit de Boer, Dr. Ian Hall, Dr. Geoffry Symons and Dr. Aage Winther. The author wishes to thank these people for the opportunity to work with them. Special thanks are due to Dr. de Boer, who suggested the experiment and whose constant interest and participation in these measurements are greatly appreciated.

Professor Charles Barnes has maintained an interest and concern in the author's progress as a student beginning with the author's first days at Caltech. The author wishes to especially thank him for his guidance and encouragement.

Financial assistance was provided by the California Institute of Technology, General Atomic Corporation and Rand Corporation and is gratefully acknowledged.

Finally, thanks are due to the entire staff and personnel of the Kellogg Radiation Laboratory for creating the stimulating and pleasant atmosphere which have made the author's stay at Cal Tech a memorable experience.

ABSTRACT

Measurements of the probabilities for Coulomb excitation of the first 2^+ excited states in $^{114}_{48}Cd$, $^{116}_{48}Cd$, $^{126}_{52}Te$ and $^{128}_{52}Te$ have been made with ^{4}He, ^{12}C and ^{16}O ions. The deviations observed in a comparison of the experimental data with the predictions of first order perturbation theory are interpreted in terms of the static electric quadrupole moments, Q_2, of the first 2^+ excited states of the nuclei. The deduced values of Q_2 are found to lie in the ranges $-0.44 \geq Q_2 \geq -0.97$, $-0.67 \geq Q_2 \geq -1.18$, $-0.16 \geq Q_2 \geq -0.50$ and $-0.01 \geq Q_2 \geq -0.40$ e $\cdot$ 10^{-24} cm^2 for $^{114}_{48}Cd$, $^{116}_{48}Cd$, $^{126}_{52}Te$ and $^{128}_{52}Te$, respectively. The deduced values of Q_2 for $^{114}_{48}Cd$ and $^{116}_{48}Cd$ are found to be surprisingly large when compared with the predictions of the vibrational model.

TABLE OF CONTENTS

I. INTRODUCTION

The Coulomb excitation process is a powerful technique for the investigation of the structural properties of the nucleus. Its particular advantages arise from the fact that the energy of the bombarding particle is held below the Coulomb barrier. The Coulomb repulsion prevents the surface of the projectile from penetrating that of the target nucleus, thus restricting the interaction between the two nuclei to the well-understood electrical force and enabling an unambiguous, model-independent measurement of certain nuclear parameters.

Coulomb excitation has been used extensively to measure the energies, spins, parities and E2 radiative transition matrix elements of low-lying nuclear states (Alder, et al., 1956). The ensuing wealth of systematic information made available has been a major contributor to the development of the collective model of the nucleus. As experimental equipment and techniques improve, Coulomb excitation continues to provide the nuclear theorist with the additional information he needs to test and improve his models.

This thesis describes a series of experiments in which Coulomb excitation has been employed to measure the static electric quadrupole moments of first-excited 2^+ states in the even-even nuclei ^{114}Cd, ^{116}Cd, ^{126}Te and ^{128}Te. In Section II the nature and theory of the Coulomb excitation process are reviewed with emphasis on those aspects relevant to the design of these experiments. The experimental apparatus and method, and the analysis and results are presented in Sections III and IV, respectively. A discussion of the assumptions and approximations

used in the analysis is given in Section V. In Section VI the results are discussed in the light of existing nuclear models and are shown to represent a challenging problem for the theorist.

II. THE THEORY OF COULOMB EXCITATION

A. Fundamental Assumptions

Coulomb excitation refers to the production of nuclear excitations by a long-range electric interaction with a bombarding particle. In particular, when the energy of the bombarding particle is well below the top of the Coulomb barrier[1], E_c, the interaction between the projectile and target nucleus will be free from interference by any nuclear forces. There are, however, two additional conditions which must be satisfied before one may proceed to the assumption of a classical orbit for the projectile (Alder, et al., 1956). These conditions are:

(i) The de Broglie wavelength, λ, of the projectile must be much less than the distance of closest approach, 2a, in a head-on collision. This requirement may be expressed as

$$\eta = \frac{a}{\lambda} = \frac{Z_1 Z_2 e^2}{\hbar v} >> 1$$

where Z_1 and Z_2 are the respective nuclear charge numbers of the projectile and target, and v is the initial relative velocity of the projectile. One half the distance of closest approach in a head-on

---

1) If one takes $r = 1.44\, A^{1/3} \cdot 10^{-13}$cm for the nuclear radius, the formula for the Coulomb barrier energy, E_c, has the simple numerical form, $E_c = \frac{Z_1 Z_2}{A_1^{1/3} + A_2^{1/3}}$ (MeV).

collision is given by

$$a = \frac{Z_1 Z_2 e^2}{m_o v^2}$$

where m_o is the reduced mass.

(ii) The energy lost by the projectile in producing a nuclear excitation may constitute only a small fraction of its initial energy.

Conditions (i) and (ii) are satisfied most easily by using heavy projectiles, e.g., ^{4}He, ^{12}C or ^{16}O ions to excite low-lying ($\lesssim$ 1 MeV) collective states. This is illustrated in the following table in which the values of E_c and η are given for various projectiles incident on $^{114}_{48}$Cd and with energy equal to E_c (in MeV).

projectile	E_c	η
e^+	9.9	0.35
p	8.2	2.6
^{4}He	14.9	7.8
^{16}O	52.1	34.0

The energy of the first excited state in ^{114}Cd is 0.56 MeV.

B. The Semiclassical Approximation

A classical treatment of the projectile orbit produces the Rutherford differential cross section

$$\frac{d\sigma_R}{d\Omega} = \frac{1}{4} a^2 \sin^{-4}\left(\frac{\theta}{2}\right) \tag{1}$$

which describes the angular distribution of the scattered projectiles. The differential cross section[2] for the Coulomb excitation of a state f from an initial state i may be written as

$$\frac{d\sigma}{d\Omega} = P_{i\to f} \frac{d\sigma_R}{d\Omega} \tag{2}$$

where $P_{i\to f}$ is called the probability for Coulomb excitation. $P_{i\to f}$ is given in terms of the transition amplitudes, b_{if}, by

$$P_{i\to f} = (2I_i + 1)^{-1} \sum_{M_i, M_f} |b_{if}|^2 \tag{3}$$

where I_i is the spin of the initial state of the target nucleus and M_i and M_f denote the respective magnetic substates of the initial and final states. The central problem of Coulomb excitation theory is thus the calculation of the transition probability amplitudes b_{if}.

---

2) Hereafter, "cross section" is understood to mean the differential cross section.

The amplitudes b_{if} are obtained from the solution of the time-dependent Schrodinger equation

$$H\psi = i\hbar \frac{\partial \psi}{\partial t} \quad . \tag{4}$$

Since the electric field of the projectile may be regarded as a perturbation localized in time and space, one may write

$$H = H_o + H_{int}(t) \tag{5}$$

and

$$\psi = \sum_n a_n(t) \, | \, n \rangle \, e^{\frac{-i}{\hbar} E_n t} \quad . \tag{6}$$

H_o is the Hamiltonian of the free nucleus with eigenfunctions

$$\psi_n = | \, n \rangle \, e^{\frac{-i}{\hbar} E_n t} \quad .$$

$H_{int}(t)$ is the energy of the charge distribution of the nucleus in the known, time-dependent electric field of the projectile. One thus obtains the set of coupled differential equations

$$i\hbar \, \dot{a}_n(t) = \sum_m \langle n | H_{int}(t) | m \rangle e^{\frac{i}{\hbar}(E_n - E_m)t} a_m(t) \tag{7}$$

for the amplitudes a_n of the free nucleus eigenfunctions ψ_n. It is noted that b_{if} is equal to $a_f(t \to \infty)$ for a nucleus initially in state i, i.e., with $a_i(t \to -\infty) = 1$.

The classical treatment of the projectile orbit resulting in (1), together with the quantum mechanical treatment, (4), (5) and (6), of the nucleus in the time-dependent electric field, produces (7) as the equation for the amplitudes of the free nucleus eigenfunctions. Equation (7) is therefore referred to as the "semiclassical approximation".

C. Multipole Interactions

The interaction Hamiltonian, $H_{int}(t)$, is separated into its multipole components, of which there are four types (Alder and Winther, 1966):

(i) the monopole - monopole interaction. This is simply the interaction which produces the Rutherford scattering and is subtracted out in subsequent calculation.

(ii) the monopole - multipole interaction. The multipole moment of the target nucleus interacts with the point charge field of the projectile to cause an excitation.

(iii) the multipole - monopole interaction. Excitation of the projectile proceeds through this mechanism. Since (ii) and (iii) are incoherent, the latter need not be of concern here.

(iv) the multipole - multipole interaction. This is generally negligible.

Of the various monopole - multipole interactions, denoted by $E\lambda$ and $M\lambda$, $\lambda = 1, 2, 3, \ldots$, the electric quadrupole interaction (E2) has been observed to occur most frequently in the Coulomb excitation process[3]. This is a consequence of the quadrupole character of the collective oscillations and deformations prevalent in nuclear matter, and also of the selection rules to which the Coulomb excitation process is subject. For the case of E2 multipole interaction only, $H_{int}(t)$ becomes

$$H_{int}(t) = \frac{4\pi}{5} Z_1 e \sum_{\mu=-2}^{2} r_p^{-3}(t)\, Y_{2,\mu}(\theta_p(t),\, \varphi_p(t))\, \mathcal{M}^*(E2,\mu) \qquad (8)$$

where

$$\mathcal{M}(E2,\mu) = \int r^2\, Y_{2,\mu}(\theta,\varphi)\rho_n(\vec{r})\, d^3r \qquad (9)$$

and r_p, θ_p and φ_p denote the coordinates of the projectile relative to the nuclear mass center. $\rho_n(\vec{r})$ is the nuclear charge density; $\mathcal{M}(E2,\mu)$ is referred to as the E2 multipole moment operator of the nucleus.

---

3) A few cases of E1 excitation are known, notably in ^{19}F, and E3 excitations have also been observed (Litherland, et al., 1963, and McGowan, et al., 1965). The relevance of a virtual E1 excitation to these experiments will be discussed in Section V. Magnetic multipole excitations are inhibited by a factor $(v/c)^2$ and are further reduced for large angle scattering.

D. Methods of Solution

There are several methods which may be employed to solve (7) and thereby obtain the excitation probability. The approximations used in these various methods will serve to classify the various types or modes of Coulomb excitation.

(1) First order perturbation theory

The excitation probability is assumed small such that the amplitude a_i of the ground state remains constant and equal to unity with all other $a_f << 1$. In this case,

$$b_{if}^{(1)} = a_f = \frac{1}{i\hbar} \int_{-\infty}^{\infty} \langle f | H_{int}(t) | i \rangle e^{\frac{i}{\hbar} E_f t} \, dt \ . \tag{10}$$

A change of variable in (10) followed by integration over the orbit of the projectile yields (Alder, et al., 1956)

$$P_{i \to f}^{(1,1)} = \chi_{i \to f}^2 \frac{df_{E2}(\theta, \xi_{fi})}{df_{E2}(\pi, 0)} \sin^4\left(\frac{\theta}{2}\right) \tag{11}$$

where

$$\chi_{i \to f} = \frac{-14.36 A_1^{1/2} M_{fi} E^{3/2}}{(1 + A_1/A_2)^2 Z_1 Z_2^2 (2I_i + 1)^{1/2}} \ , \tag{12}$$

$$\xi_{fi} = \frac{Z_1 Z_2 A_1^{1/2} \Delta E'_{fi}}{12.65 \ E^{3/2}} \ , \tag{13}$$

$$\Delta E'_{fi} = (E_f - E_i)(1 + A_1/A_2) \quad , \tag{14}$$

and

$$M_{fi} = \langle I_i \| i^{\lambda}\, \mathcal{M}(E\lambda) \| I_f \rangle \quad , \quad \lambda = 2 \quad . \tag{15}$$

E is the initial laboratory energy in MeV of the projectile with charge Z_1 and mass A_1 in a. m. u. θ is the center-of-mass angle through which the projectile is scattered by the target nucleus (Z_2, A_2) and E_f and E_i are the energies in MeV of the final and initial nuclear states, respectively. The orbital integrals $d\sigma_{E2}(\theta, \xi)$ have been tabulated by Alder, et al., (1956); the parameter ξ_{fi} is the ratio of the collision time (a/v) to the nuclear period ($\hbar/\Delta E$) and indicates the extent to which the excitation process proceeds adiabatically. The reduced matrix element M_{fi} connecting the initial and final states is in units of $e \cdot 10^{-24}$ cm^2.

$\chi_{i\to f}$ is a measure of the strength with which the final state is coupled to the initial state through the interaction of the E2 multipole transition moment of the nucleus with the monopole field of the bombarding particle[4]. $\chi^2_{i\to f}$ is the excitation probability in a sudden, i. e., $\xi_{fi} = 0$, head-on collision. The assumption of perturbation theory may therefore be stated as $\chi_{i\to f} \ll 1$.

It is noted that

$$M^2_{rs} = B(E2,\ s \to r)(2I_s + 1) \tag{16}$$

---

4) $\chi_{i\to f}$ is analogous to the parameter η, which measures the strength of the monopole - monopole interaction.

where B(E2) is the same nuclear matrix element appearing in the expression for the E2 radiative decay of the state s to the state r. As a consequence of this, the Coulomb excitation process is subject to the same selection rules which apply to the radiative decay of the nucleus.

(2) Second order perturbation theory

The amplitude a_z of an intermediate state z is included in (7) to produce two coupled differential equations. The transition amplitude b_{if} in second order perturbation theory (Alder, et al., 1956) then becomes

$$b_{if}^{(2)} = b_{if}^{(1)} + \sum_z b_{izf}^{(2)} \tag{17}$$

where

$$b_{izf}^{(2)} = \frac{1}{(i\hbar)^2} \int_{-\infty}^{\infty} dt \langle f | H_{int}(t) | z \rangle e^{\frac{i(E_f - E_z)}{\hbar} t}$$

$$\times \int_{\infty}^{t} dt' \langle z | H_{int}(t') | i \rangle e^{\frac{i(E_z - E_i)}{\hbar} t'} . \tag{18}$$

The summation in z is to be performed over all intermediate states, including the initial and final states. Insertion of (17) into (3) yields the perturbation expansion

$$P_{i \to f} = P_{i \to f}^{(11)} + \sum_z P_{i \to z \to f}^{(12)} + \sum_z P_{i \to z \to f}^{(22)} .$$

The terms $P^{(12)}$ and $P^{(22)}$ describe the phenomenon of multiple Coulomb excitation. For example, $P^{(22)}_{0^+\to 2^+\to 4^+}$ is the probability of the projectile exciting a state of spin and parity 4^+ from a 0^+ ground state by two successive E2 transitions.

To illustrate a situation which corresponds to the actual measurements, one considers the excitation of a nucleus with 0^+ ground state and two excited 2^+ states, which are labeled with the indices i, f, and z, respectively (see Figure 1). The Coulomb excitation of the first 2^+ state can then proceed by direct excitation from the ground state (first order, $i \to f$) or by double excitation with either of the 2^+ states as the intermediate state (second order, $i \to z \to f$ or $i \to f \to f$). Neglecting terms higher than third power in $\chi_{i\to f}$, the probability of excitation of the first 2^+ state is

$$P_{i\to f} = P^{(11)}_{i\to f} + P^{(12)}_{i\to z\to f} + P^{(12)}_{i\to f\to f} \quad . \tag{19}$$

The first term $P^{(11)}_{i\to f}$ (proportional to $\chi^2_{i\to f}$) is the first order excitation probability defined by (11). The other two terms (proportional to $\chi^3_{i\to f}$) arise from the interference between first and second order excitation of the state f where, in the second order excitation, the states z and f are the respective intermediate states. The term $P^{(12)}_{i\to f\to f}$ gives rise to a dependence of

the excitation probability on the static electric quadrupole moment of the 2^+ state (the so-called "reorientation effect" [5]).

The second order terms $P^{(22)}$ in Figure 2 are proportional to $\chi^4_{i\to f}$ and are of the same order as the terms arising from the interference between first and third order excitation. Calculations to this order have been made by Masso and Lin (1965).

The probability $P^{(12)}_{i\to z\to f}$ in (19) is given by

$$P^{(12)}_{i\to z\to f} = \frac{27\,\pi^{3/2}}{5}\,\chi^3_{i\to f}\,\frac{M_{zi}\,M_{fz}}{M^2_{fi}}\,J(\xi_{zi},\xi_{fz},\theta)\ . \qquad (20)$$

The quantity $J(\xi_{zi},\xi_{fz},\theta)$ is related to the orbital integrals $I_{\lambda\mu}(\theta,\xi)$ and $\beta_{k\kappa}(\lambda_1\lambda_2\xi_1\xi_2,\theta)$ defined by Alder, et al., (1956), by the relation

---

5) The term "reorientation effect" was introduced about ten years ago by Breit and Lazarus (1955) who were the first authors to suggest the possibility of measuring a static quadrupole moment by Coulomb excitation. Recently, "reorientation effect" has been used as a general expression to cover any effects of the static quadrupole moment in Coulomb excitation. Strictly speaking, however, it should be applied (Breit and Lazarus, 1955) only to virtual transitions among, and a redistribution of the final populations of the magnetic substates of the final state. This "reorientation" of the spin of the final state may be manifest, for example, in the angular distribution of de-excitation gamma rays. However, for 180 degree scattering such virtual transitions and redistributions are excluded and only the $m = 0$ substate is populated. On the other hand, the effect of the static quadrupole moment on the magnitude of the cross section is a maximum for 180^o scattering. In the experiments described here it is this latter property which has been exploited.

$$J(\xi_{zi}, \xi_{fz}, \theta) = \sum_{\mu} (-1)^{\mu} Y_{2\mu}\left(\frac{\pi}{2}, 0\right) I_{2\mu}(\theta, \xi_{zi}+\xi_{fz})\ \beta_{2-\mu}(22\xi_{zi}\xi_{fz}, \theta)\ . \tag{21}$$

Tables of the quantities $\beta_{k\kappa}$ have been computed for positive ξ-values by A. C. Douglas (1962). The term $P^{(12)}_{i\to f\to f}$ is obtained from (20) by setting z equal to f.

The largest contribution to $P_{i\to f}$ arises from $P^{(11)}_{i\to f}$, which is proportional to $B(E2, i\to f)$. The term $P^{(12)}_{i\to f\to f}$, which is of the order of magnitude of $\chi^3_{i\to f}$, is proportional to $B(E2, i\to f)$ and to the static quadrupole moment of the state f. In order to obtain an estimate of the size of this term relative to the excitation probability of the first 2^+ state it is convenient to consider the quantity

$$\rho = P^{(12)}_{i\to f\to f} / P^{(11)}_{i\to f}\ . \tag{22}$$

By substituting (11) and (20) into (22), one finds

$$\rho = 1.68\ \chi_{i\to f}\ \frac{M_{ff}}{M_{fi}}\ \frac{J(\xi_{fi}, 0, \theta)}{df_{E2}(\theta, \xi_{fi})/d\Omega}\ \sin^{-4}\left(\frac{\theta}{2}\right)\ . \tag{23}$$

Writing $\chi_{i\to f}$ in terms of ξ_{fi} using (12), (13) and (14), one may rewrite (23) in the form

$$\rho = -\frac{A_1}{Z_2}\ \frac{1}{(1 + A_1/A_2)^2}\ \Delta E'_{fi}\ M_{ff} \times K(\xi_{fi}, \theta) \tag{24}$$

where

$$K(\xi_{fi}, \theta) = 1.90 \frac{J(\xi_{fi}, 0, \theta)}{\xi_{fi}\, df_{E2}(\theta, \xi_{fi})/d\Omega} \sin^{-4}\left(\frac{\theta}{2}\right) . \qquad (25)$$

The dependence of $K(\xi_{fi}, \theta)$ on ξ_{fi} and θ is illustrated in Figure 2.

The static quadrupole moment Q_f of the state f is related to the reduced matrix element M_{ff} by

$$Q_f = -0.758\, M_{ff} = +0.758 \langle I_f \| \mathcal{M}(E2) \| I_f \rangle . \qquad (26)$$

From (24) and Figure 2, it can be seen that:

1) the ratio ρ is directly proportional to M_{ff}, and thus to the static quadrupole moment of the state f; a determination of the sign as well as the magnitude of Q_2 is therefore possible.

2) ρ is roughly independent of ξ_{fi}, and therefore of the energy of the projectile;

3) ρ is roughly proportional to A_1, the mass of the projectile;

4) ρ is largest at backward scattering angles.

In the present experiments, therefore, one compares the excitation probabilities for various projectiles scattered at angles close to 180^{o}.

Since $P^{(11)}_{i\to f}$ and $P^{(12)}_{i\to f\to f}$ are both proportional to $(M_{12})^2$, the ratio of the excitation probabilities for different projectiles is independent of $B(E2,\ 0^+ - 2^+)$, leaving M_{22} as the only nuclear parameter in the ratio. Similarly, if the data are obtained under the same experimental conditions, many factors important to the determination of the absolute excitation probability will tend to cancel in the ratio. Notably, this removes the uncertainty in the efficiency of the NaI detector ($\pm$ 8%) from the determination of the quadrupole moment.

By way of numerical illustration of the above procedure, the values of $P^{(11)}_{i\to f}$ and ρ are $0.175 \cdot (M_{12})^2$ and $-0.131 \cdot M_{22}$, respectively for 40 MeV ^{16}O ions scattered from ^{114}Cd at 165^o in the laboratory system. The corresponding values for 10 MeV ^4He bombardment are $0.0163 \cdot (M_{12})^2$ and $-0.036 \cdot M_{22}$. If the term $P^{(12)}_{i\to z\to f}$ in (19) is small relative to $P^{(12)}_{i\to f\to f}$, the excitation probability for the first 2^+ state may be written as

$$P_{i\to f} = P^{(11)}_{i\to f}\ (1 + \rho) \quad .$$

In this case, the ratio of the excitation probabilities obtained for bombardment by 40 MeV ^{16}O and 10 MeV ^4He ions is given by

$$\frac{P_{i\to f}\ (^{16}O)}{P_{i\to f}\ (^4He)} = 10.74\ \frac{1 - 0.131\ M_{22}}{1 - 0.036\ M_{22}} \quad .$$

Implicit in this treatment is the assumption that $P^{(12)}_{i\to f\to f}$ dominates $P^{(12)}_{i\to z\to f}$ and other higher order terms which are not included in the expansion (19). This condition is found to be satisfied in these experiments.

(3) Symmetrization of first order cross sections

It is shown by Alder, et al., (1956) that the use of symmetrized expressions for the adiabaticity parameter ξ_{fi} and the distance of closest approach 2a brings the classical first order cross sections into closer agreement with the more accurate quantum mechanical calculations. The symmetrized expressions for ξ_{fi} and $d\sigma/d\Omega$ are

$$\xi_{fi} = \frac{Z_1 Z_2 A_1}{6.325}^{1/2} \left[(E - \Delta E'_{fi})^{-1/2} - E^{-1/2} \right] \qquad (27)$$

and

$$\frac{d\sigma^{(11)}_{E2}}{d\Omega} = P^{(1,1)}_{i\to f}(\theta, \xi_{fi}) \left(1 - \frac{\Delta E'_{fi}}{E}\right) \frac{d\sigma_R}{d\Omega} \qquad (28)$$

where ξ_{fi} is given by (27), and $d\sigma_R/d\Omega$ is the (unsymmetrized) Rutherford cross section. These symmetrized expressions for ξ and for the first order cross section $d\sigma^{(11)}$ are used throughout the remainder of this thesis.

(4) Numerical integration of the coupled differential equations

A perturbation theory treatment of the excitation process loses validity rapidly as the size of $\chi_{i\to f}$ increases. Figure 3 shows for ^{114}Cd the range of values of $\chi_{i\to f}$ as a function of projectile and bombarding energy[6]. For large $\chi_{i\to f}$, either the slowly converging perturbation expansion must be extended to higher orders in $\chi_{i\to f}$ or a different method of calculation must be employed to account for the presence of non-negligible amplitudes a_z in (7).

The latter approach has been pursued by A. Winther and J. de Boer (1965). These authors have written a computer program which computes the cross sections for electric quadrupole excitation in the semiclassical approximation by numerically integrating the time-dependent Schrodinger equation (7) for a system consisting of a nucleus with a finite number of states and a projectile moving on a classical orbit. In addition to the bombarding conditions, spins and energies of the target nucleus levels, the program requires as input data the matrix M_{rs} between all nuclear states considered in the calculation. A brief description of this computer program is given in Appendix I.

By varying the values of the reduced E2 matrix elements M_{rs} in the input to the computer program, one can study the dependence of the excitation cross sections on the different nuclear

---

6) In the experiments $\chi_{i\to f}$ was typically 0.3 for ^{16}O bombardment of ^{114}Cd. One experimental datum was taken with 46 MeV ^{16}O ions; $\chi_{i\to f}$ in this case was about 0.5.

matrix elements for various bombarding conditions. Since, in the present experiments, it is found that this dependence is roughly approximated by a perturbation analysis, it will be convenient to retain the language of perturbation theory in discussing the results of the computer calculations. For example, in discussing the effects of a change in sign of any of the matrix elements in (20) one may speak of the sign of the interference term involving these matrix elements, indicating that these effects are in fact roughly proportional to the product $M_{fi}\, M_{zi}\, M_{fz}$.

In the analysis the computed cross sections have been fitted to the experimental data in order to obtain values for B(E2, $0^+ \rightarrow 2^+$) and for the static electric quadrupole moment, Q_2, of the first excited state.

E. Summary

It has been seen that the Coulomb excitation process provides a means of investigating certain features of nuclear structure, notably the nuclear transition matrix elements B(E2). It was further shown that an extension of Coulomb excitation theory beyond that of a first order approximation enables a determination of static quadrupole moments. It is interesting to note at this point two significant features of these measurements: (i) nowhere in the development of the theory has any reference been made to a nuclear model, and (ii) the deduction of Q_2 from the measured cross sections does not require a separate estimation of an electronic electric field gradient at the nuclear site, as would be the case in a measurement of hyperfine structure. The electric field gradient here is provided by the bombarding particle, whose orbit is assumed to be known.

III. EXPERIMENTAL APPARATUS AND METHOD

The experimental quantities to be measured were the probabilities for Coulomb excitation of the first 2^+ states of ^{114}Cd, ^{116}Cd, ^{126}Te and ^{128}Te when bombarded with various heavy ions, viz., ^{4}He, ^{12}C and ^{16}O. These probabilities were measured by counting the de-excitation gamma rays in coincidence with the scattered projectiles.

A. Heavy Ion Beam Production

The experiments described here were carried out with particle beams from the ONR-CIT tandem accelerator. The ^{4}He ion beam was produced by the injection into the tandem of a 700 keV neutral ^{4}He beam. Negative ion beams of ^{12}C or ^{16}O were obtained by charge exchange of positive ions from the duoplasmatron source, using as source gases methane and a mixture of 5 to 10% of oxygen in hydrogen, respectively.

B. Target Preparation

Separated isotopes in the form of CdO and Te were obtained from the Oak Ridge National Laboratory. The isotope enrichments varied upward from 97% with the remaining constitution of the sample known. The targets were prepared by the vacuum evaporation of the separated isotope onto thin carbon foils. A light-weight material such as carbon was used for the target backing in order to produce a wide separation in the energy of the ^{4}He ions scattered from the target material from those scattered from the backing.

The thicknesses of the targets were measured by recording the momentum profile of 1 MeV protons scattered at an angle of 140°. A second method also used was to compare the cross sections for elastic scattering of low energy (about 4 MeV) ^{4}He ions from the target and from a nickel foil of known thickness. Values which were estimated to be accurate to $\pm$ 20% were thus obtained for the energy loss of the projectile in the target.

Since the coincidence measurements do not require the resolution of the inelastically scattered ions from the elastically scattered ions, thicknesses corresponding to an energy loss of up to about 1.5 MeV for ^{16}O ions could be employed. The thicknesses of the various cadmium targets ranged from 250 to 450 $\mu gm/cm^2$. After the cadmium measurements were completed, it was realized that thinner targets were preferable because of a resulting lower random-coincidence count rate and count-rate loss. Furthermore, since the probability for Coulomb excitation is strongly energy dependent, thinner targets produced a smaller error in the correction applied for the energy loss of the bombarding particle in the target. For the tellurium measurements, therefore, targets of thickness about 80 $\mu gm/cm^2$ were prepared.

C. Detection System

The arrangement of the detectors is illustrated in Figure 4. The heavy ion beam was confined to an area of 1.5 mm diameter by a series of tantalum collimators before passing through the center-hole of an annular solid-state detector. The target was placed about one centimeter from the sensitive area of the counter which then accepted particles scattered between laboratory angles of 155° and

175^{o}. The depletion depth of the detector (about 300 μ) was more than sufficient to stop particles of all energies used in the experiments.

The gamma detector was a 7.62 - cm - long by 7.62 - cm - diameter NaI(Tl) crystal mounted at an angle of 58 degrees with respect to the incoming beam, with its face about 3 cm from the target center. This angle is near the zero of the Legendre polynomial P_2, which helps to minimize the effect of the anisotropic gamma-ray angular distribution. For this particular geometry the photopeak efficiency of the NaI detector is about 5% for gamma-ray energies near 500 keV.

The coincidence circuitry consisted of a conventional fast-slow coincidence system, with the fast coincidence unit modified to provide a time-to-pulse-height conversion. A block diagram of the electronic apparatus is given in Figure 5. A 400-channel analyzer was gated by the slow coincidence unit which could be arranged to require a time coincidence of some or all signal inputs from

(i) the fast coincidence unit;

(ii) a single-channel analyzer which selected pulses from the gamma-ray spectrum corresponding to the photopeak of the $2^{+} \rightarrow 0^{+}$ transition;

(iii) a single-channel analyzer which selected pulses from the particle spectrum corresponding to scattering from cadmium (or tellurium).

D. Procedure

Figures 6 and 7 show for ^{114}Cd and ^{128}Te respectively, singles gamma-ray spectra and spectra gated by the requirements (i) and (iii) above. Corresponding singles spectra of ^{16}O ions are shown in Figures 8 and 9. The relative thicknesses of the cadmium and tellurium targets are apparent from the widths of the peaks in these spectra. The single-channel analyzer level or "window" settings are also indicated in Figures 6 through 9.

The fast coincidence unit gave an output pulse proportional to the time overlap of 90-ns-long clipped pulses derived from the particle and gamma detectors. A time-to-pulse-height spectrum, gated by a coincidence of signals from (ii) and (iii) above, is shown in Figure 10. Delays were adjusted such that pulses in real coincidence had about half-maximum time overlap to facilitate the subtraction of the uniform random-coincidence background. This subtraction was typically about 2%, never more than 5%, and was known accurately enough so that negligible error was incurred. The shape of the time-to-pulse-height spectrum was independent of the bombarding particle.

After the subtraction of the random-coincidence background in the time-to-pulse-height spectrum, the experimental datum is the ratio, R, of the number of counts in the time-to-pulse-height peak to the number of particles (counted by a single-channel analyzer and scaler) scattered from cadmium or tellurium. Thus

$$R = \frac{\sum_{i=2}^{n} f_i \, d\sigma_i}{\sum_{i=1}^{n} d\sigma_i} \qquad (29)$$

where $d\sigma_i$ is the cross section for excitation of the i^{th} level and n is the number of levels significantly populated in the experiment. Figures 11 and 12 show the energies, spins and labelling indices, i , of the levels considered in the analysis. The quantity f_i is the probability that, after Coulomb excitation of the state i, the subsequent gamma decay produces a pulse in the window of the gamma-ray spectrum. For i = 2 this is just the photopeak efficiency of the gamma detector with a small correction for the anisotropy of the gamma-ray angular distribution.

E. Auxiliary Experiments

An alternative method of measuring the probability for Coulomb excitation is to detect the inelastically scattered particles by direct magnetic analysis of their energy. This method was employed in the case of ^{114}Cd to provide an independent check on the particle-gamma coincidence experiments. The results were found to corroborate those of the coincidence measurements. A description of the magnetic analysis experiment and its results is given in Appendix II. A.

For the purposes of analysis it was necessary to know some of the E2 matrix elements to the higher or "two phonon" states. In the cases of ^{114}Cd and ^{116}Cd this information was available from the work of McGowan, et al., (1965). Only some of the matrix elements required for the tellurium isotopes had been measured previously (Gangrskii and Lemberg, 1962); in particular, the value of B(E2, $4^+ \rightarrow 2^+$) was unavailable. A short experiment using the method of gamma-gamma coincidence was performed to obtain these values. This is described in Appendix II. B.

An attempt to extend the measurements to include bombardment by a ^{32}S ion beam was made. The difficulties encountered and results obtained are detailed in Appendix II. C.

The measurements and calculations performed with regard to the efficiency of the gamma-ray detector and the anisotropic angular distribution of the de-excitation gamma rays are presented in Appendix III.

IV. ANALYSIS AND RESULTS

A. Corrections Applied to the Raw Experimental Data

The experimental quantity obtained directly from the measurement is the ratio R, defined in (29). The quantity, P_{exp}, from which the quadrupole moment of the first 2^+ state, Q_2, is to be determined[7], is given by

$$P_{exp} = \frac{d\sigma_2}{\sum_{i=1}^{n} d\sigma_i} \qquad (30)$$

and is called the probability for Coulomb excitation of the first 2^+ state. A number of small corrections were made in order to extract P_{exp} from the raw experimental data.

1) Since the Coulomb excitation cross section is strongly energy dependent, the effective bombarding energy was taken to be the incident ion energy, E, minus half the target thickness, 1/2 ΔE; the cadmium targets were about 120, 800, and 1400 keV thick for ^4He, ^{12}C and ^{16}O ions, respectively and the tellurium targets were about 40 and 500 keV thick for ^4He and ^{16}O ions, respectively. A calculation of the effective bombarding energy correct to order $(\Delta E/E)^2$ proved the above method to be sufficiently accurate.

---

7) One could just as easily analyze the quantity R, but analysis of the quantity P has the advantage of exhibiting more clearly the effect of Q_2 on the cross section for the first excited state.

2) The anisotropy of the gamma-ray angular distribution necessitated a correction of about 9% to the absolute yield in normalizing the NaI crystal efficiency to 4π geometry. This correction, however, was essentially the same for all bombarding conditions used in the experiments. For large scattering angles the gamma-ray angular distribution depends only weakly on the type and energy of the particle which causes excitation of the state. Also, the effect of the quadrupole moment on the gamma-ray angular distribution is negligible for large scattering angles. The coefficients for calculating the gamma-ray angular distribution are obtained from the computer program mentioned in Section II.

3) The target nucleus possesses a recoil velocity after the collision with the projectile. This velocity, however, is reduced as the recoiling nucleus moves through, and loses energy in, the target. If the target nucleus decays while still in motion, the effective solid angle of the gamma detector will be altered slightly. The maximum possible change in this efficiency occurs for ^{16}O ion bombardment of a nucleus which then decays with its full recoil velocity, and this change amounts to only 0.3%. The application of this type of correction to the individual cases is discussed in Appendix III.

4) The contribution of cascade gamma rays to the coincidence yield R must be taken into account. This contribution can be calculated given the cross sections $d\sigma_i$ to the higher states and the cascade-to-crossover branching ratios. The finite width of the gamma-ray window may also permit acceptance of some or all of the gamma rays from the upper member of the cascade transition. The cross sections $d\sigma_i$ for the higher states were calculated with the computer program

using the E2 matrix elements M_{rs} given in Tables 1 and 2. These matrix elements were taken from the work of McGowan, et al., (1965), for the cadmium isotopes; the derivation of the matrix elements for the tellurium isotopes is given in Appendix II. B.

A correction of about 0.5% for ^{114}Cd was applied to the coincidence yield due to the de-excitation of the first excited state by the internal conversion process. This correction was, of course, the same for all bombarding particles.

5) The closer proximity to the single-channel-analyzer threshold of pulses from the inelastically scattered particles, and the pulse-height tail of the particle detector, resulted in slightly different efficiencies for detection of the elastically, and the inelastically, scattered particles. A correction for this was determined from the shape of the particle spectrum at each bombarding energy. This correction was made with great care since - at 4-5% for ^{4}He bombardment - its magnitude was comparable with the deviations being measured. A coincidence-gated particle spectrum (see Figure 13) showed the same peak-to-tail ratio as the singles spectra indicating that the counts in the pulse-height tail of the singles spectra above the single-channel-analyzer threshold were indeed substantially due to scattering from the relevant target isotope. An additional small correction was made to the particle count for particles scattered back into the annular counter from the tantalum beam stop, which was about two meters beyond the target.

6) The center-of-mass motion also introduces a small correction to the coincidence yield because of the difference in solid angle subtended by the particle detector for the elastically, and the inelastically, scattered projectiles. This correction amounted to

about 0.6% for ^{16}O ion bombardment of ^{114}Cd and was correspondingly smaller for the other ions used.

7) The ^{126}Te target contained a total of 3% of other Te isotopes. The known gamma-ray energies and values of $B(E2, 0^+ \rightarrow 2^+)$ of ^{124}Te, ^{128}Te, and ^{130}Te (Temmer and Heydenburg, 1956; Stelson and McGowan, 1958) enabled a correction (1.5%) to be made to the coincidence yield. This correction, however, was the same for ^{4}He and ^{16}O bombardment.

With the application of the above corrections to the measured ratios R, the experimental values, $P_{exp}(A_1, E)$, of the probability of excitation of the first 2^+ state were obtained as a function of bombarding particle and energy. These values are listed in Tables 3 and 4.

B. Presentation of the Data

A convenient way of presenting the experimental data to show the effect of Q_2 is to compare the measured values of P with those calculated from first order perturbation theory (28). This is done in Figures 14 through 17. The ratios $P_{exp}/P_{first\ order}$ for bombardment by the various heavy ions are plotted versus ξ. The values of $B(E2, 0^+ \rightarrow 2^+)$ used in calculating $P_{first\ order}$ were taken from an analysis to be described later.

C. Higher Order Effects

The large deviations from unity in Figures 14-17 indicate that matrix elements other than $\langle 0^+ \| \mathcal{M}(E2) \| 2^+ \rangle$ must also play a significant role in the

excitation process. These other matrix elements are those which, in the language of perturbation theory, lead to "higher order effects". It will be seen that the dominant higher order effect arises from the existence of an appreciable static quadrupole moment in the first excited state of the nuclei studied here.

The other higher order effects which can contribute to the excitation of the first 2^+ state are virtual transitions via the higher-lying 2^+ levels. These, however, may be accounted for by direct calculation provided the pertinent matrix elements M_{rs} are known. The magnitudes of these have either been measured or estimated and are given in Tables 1 and 2. The relative signs of these matrix elements are not known experimentally and this causes a considerable uncertainty in the deduction of Q_2.

In order to illustrate the above points and give a quantitative indication of the dependence of the cross sections on the projectile and its energy and on the magnitudes and signs of the matrix elements M_{rs}, the results of computer calculations of the cross sections, $d\sigma_i$, for various sets of inputs are given in Table 5[8]. The sign of M_{12} was taken to be negative in all cases. The last column of Table 5 shows in order the values of P derived from

(i) a computer evaluation including all the levels shown in Figure 11 for ^{114}Cd, (P_{comp});

(ii) a similar computation including only the ground and first excited states, ($P_{two\ level}$);

(iii) first order perturbation theory, (28).

---

8) The computer calculations for Table 5 were done at Rutgers by J. de Boer.

A study of Table 5 shows the following:

a) Apart from the matrix element M_{12} connecting the ground state to the first excited state, the largest contribution to the cross section for the excitation of the 2^+ state arises from M_{22}, which is proportional to the static electric quadrupole moment Q_2 of the first 2^+ state (26). Changing the value of M_{22} from 0 to +1.0 ($e \cdot 10^{-24}$ cm^2) decreases the cross section $d\sigma_2/d\Omega$ by about 13% for 40 MeV ^{16}O ions. The decrease is roughly proportional to M_{22}.

b) The change in the excitation cross section $d\sigma_2/d\Omega$ arising from a change in the signs of M_{14} and M_{17} amounts to 3.8% and 1.3%, respectively, for ^{16}O ions. The fact that the signs of M_{14} and M_{17} are unknown thus contributes a considerable uncertainty to the final analysis. The strong dependence of the cross section $d\sigma_2/d\Omega$ on the signs of these two matrix elements arises from the possibility of excitation of the first 2^+ state via virtual transitions through one of the higher 2^+ states. The interference of these virtual transitions with the direct transition from the ground state gives, in second order perturbation theory, contributions of the type $P^{(12)}_{0^+ \to 2'^+ \to 2^+}$ to the excitation of the first 2^+ state which are proportional to the third power of the interaction constant $\chi_{i \to f}$. These contributions have the same dependence on the projectile and its energy as the contribution $P^{(12)}_{0^+ \to 2^+ \to 2^+}$, which involves the static quadrupole moment. It is to be noted that changing the signs of both M_{14} and M_{24} produces only a very small effect on the cross sections; this is because the interference term $P^{(12)}_{0^+ \to 2'^+ \to 2^+}$ is proportional to the product $M_{12}\, M_{14}\, M_{24}$.

The excitation of the first 2^+ state by virtual transitions through higher states with spins different from two, i.e., zero or four, must also be considered. However, this process can only

produce interference effects involving terms of the order of χ^4, which are small and contain no ambiguity in sign.

c) Inclusion of the cascade-to-crossover branching ratio c_i (Stelson and McGowan, 1961) to calculate the cascade gamma-ray contribution,

$$\sum_{i=3}^{n} \frac{c_i}{1+c_i} d\sigma_i \tag{31}$$

to the population of the first 2^+ state yields values of about 4% for 40 MeV ^{16}O ions, 3% for 30 MeV ^{12}C ions and 1% for 10 MeV ^4He ions. This contribution is essentially independent of the signs of the matrix elements and absolute values of these are known to about ± 20%.

d) The E2 matrix elements between states in the two-phonon region have a negligible effect upon the excitation of the first 2^+ state. This has been illustrated in Table 5 by changing the value of M_{45} from 0 to 1.0. In the final analysis one is therefore justified in setting $M_{rs} = 0$ for $r, s > 2$.

e) The difference between P_{comp} and $P_{first\ order}$ arises only partly from the inclusion of the higher excited states in the calculation of P_{comp}. Computer calculations including only the ground and first excited states and with $M_{22} = 0$ yield values of $P_{two\ level}$ which differ from $P_{first\ order}$ by, for example, as much as 7% for 40 MeV ^{16}O bombardment. Deviations of this order of magnitude are, however, expected because of the decreasing accuracy of a first order perturbation treatment as $\chi_{1\to 2}$ becomes larger.

D. Least-Squares Fit to the Data

The experimental values for M_{12} and M_{22} were deduced by comparing the measured excitation probabilities with those calculated by the Winther-de Boer computer program. This comparison was done in the following manner.

a) Preliminary values of M_{12} and M_{22}, denoted by M'_{12} and M'_{22}, were obtained by using second order perturbation theory to analyze several of the data for ^{16}O ion and ^{4}He ion bombardment. This procedure is illustrated in Section II and Appendix II.C.

b) For a given projectile, A_1, and bombarding energy, E, the expression

$$P_{th}(A_1, E) = a_1(A_1, E)(M_{12})^2 + a_2(A_1, E)(M_{12})^2 M_{22} \qquad (32)$$

was taken to represent the dependence of the excitation probability on M_{12} and M_{22}. This is, of course, the prediction of second order perturbation theory. The coefficients a_1 and a_2, however, were not taken from second order perturbation theory, but were obtained from the computer program as follows.

c) Two values of $P_{th}(A_1, E)$ were calculated with the computer program, first using M'_{12}, M'_{22} and M_{rs} as input, and then using $M'_{12} + \Delta M'_{12}$, $M'_{22} + \Delta M'_{22}$ and M_{rs} as input, where $\Delta \ll 1$; the values of M_{rs}, the matrix elements to the levels above the first excited state, were taken from Tables 1 and 2. Equation (32) was used together with the above values of $P_{th}(A_1, E)$ to solve for a_1 and a_2.

The values obtained in this manner for a_1 and a_2 depend on the relative signs of the M_{rs}, and also depend (slightly) on the particular values of M'_{12} and M'_{22} (although this latter dependence vanishes in the limit of second order perturbation theory). However, for small changes in M_{12} and M_{22} about M'_{12} and M'_{22}, (32) reproduces to a high degree of accuracy the calculation of $P_{th}(A_1, E)$ by the computer program.

d) Steps b) and c) were repeated for all the bombarding particles and energies used in the experiments, thus obtaining a set of equations (32), each linear in $(M_{12})^2$ and $(M_{12})^2 M_{22}$. The method of least squares was then used to obtain the value of M_{12} and M_{22} which, when inserted in (32), best reproduced the set of experimental excitation probabilities, $P_{exp}(A_1, E)$.

Because of the dependence of a_1 and a_2 (and hence of the quadrupole moment) on the relative signs of the M_{rs}, a separate least-squares fit was performed for each possible sign combination. Thus, in the case of ^{114}Cd, four values of M_{12} and M_{22} have been deduced from the data.

The fitted values of M_{12} and M_{22} differed slightly from the values of M'_{12} and M'_{22} which were obtained from the preliminary analysis and used to calculate a_1 and a_2. The resultant error in the quadrupole moment has been carefully estimated and was found to be less than 5% in all cases. This error could be eliminated by an iteration of the fitting procedure or by using a more accurate expression for $P_{th}(A_1, E)$ than is given by (32). Such an expression is

$$P_{th} = a_0 + a_1(M_{12})^2 + a_2(M_{12})^2 M_{22} \,. \qquad (32a)$$

However, in view of the larger errors (± 30%) in Q_2 arising from other sources, it was felt that the small improvement in Q_2 afforded by an iteration of the analysis would not justify the cost of the necessary computing time.

It may be noted here that the value of M'_{12} used to calculate the a_1 and a_2 has itself a minimum uncertainty of ± 8% which arises from the uncertainty in the NaI crystal efficiency. This introduces an uncertainty of about 6% in the quadrupole moment.

E. Results

The solid curves shown in Figures 14 - 17 represent the least-squares fits to the experimental data obtained by using the values of M_{rs} given in Tables 1 and 2 and with all M_{rs} except M_{22} taken negative. Figures 15 and 16 for ^{114}Cd and ^{116}Cd both indicate a decline in the values of $P_{exp}/P_{first\ order}$ at the higher ^{4}He energies. A possible explanation of this is the onset of interference from nuclear reactions as the top of the Coulomb barrier (~ 15 MeV) is approached. These higher energy points (dotted) have accordingly excluded from the analysis. This has also been done for the ^{4}He data in the tellurium nuclei, although the departure of the yield from Coulomb excitation theory appears to be more gradual than in the cadmium isotopes.

The deduced values of M_{12} and M_{22} are given in Tables 6 and 7. Here and in Figures 14 - 17 the errors include only the counting statistics. The total errors for the various values of M_{12} and M_{22} deduced for each nucleus are given in parentheses in Tables 6 and 7. For M_{12} the predominant contribution to the total error arises from the uncertainty in the NaI crystal efficiency (± 8%),

while for M_{22} the uncertainties in target thickness, M_{12} and the higher matrix elements each contribute to the total error.

Tables 6 and 7 show that the value of M_{22} determined from the data may change by up to 30% depending upon the various choices of the signs of the M_{rs} while the quality of the fit, indicated by the value of chi-squared, is similar in all cases. It is therefore not possible on the basis of the present experiments to determine these signs. This is due to the fact that the interference term responsible for this sign dependence is similar in behavior to the interference term arising from a finite quadrupole moment.

It can be seen from Table 6 that, despite the fact that ρ depends only weakly on the bombarding energy (see (24) and Figure 2), an analysis using the oxygen data alone is capable of yielding a value of M_{22} which has the correct sign and order of magnitude. It should also be noted that the value of M_{12} derived from the analysis is rather insensitive to the signs of the M_{rs}.

In principle the B(E2) and quadrupole moment can be determined from any two experimental data, either of different energy or of a different bombarding particle, though the latter constitutes the more sensitive measurement. The fact that a good theoretical fit is obtained to the cadmium data points of three different bombarding particles, covering a wide range of energies, attests to the validity of the theory in describing the excitation process. Only two different ions were used in the measurements on the tellurium nuclei since the quadrupole effect itself was smaller and the validity of the method had already been established in the cadmium measurements.

To single out the effect of Q_2, the data and fits of Figures 14 - 17 are replotted in Figures 18 - 21, normalizing now to $P_{comp}(Q_2 = 0)$. $P_{comp}(Q_2 = 0)$ is a computer calculation of P using the fitted value of M_{12} and all the other matrix elements in Tables 1 and 2 but with $M_{22} = 0$. Thus, if the quadrupole moments had been zero, all the data points in these figures would be expected to yield, in the least-squares fit, a common line of ordinate unity. The slope of the ^{16}O curves in the figures in which P_{exp} is normalized to $P_{first\ order}$ is due partly to the decreasing accuracy of first order perturbation theory as the excitation probability increases.

From the above discussion and the similarities of Figures 14 - 17 and Figures 18 - 21, it is clear that the major part of the deviations from first order perturbation theory may be attributed to non-zero quadrupole moments of the first 2^+ states in these nuclei.

V. DISCUSSION OF THE ANALYSIS

The preceding analysis rests on certain assumptions concerning the excitation process; the validity of these will now be discussed.

1) The treatment of the Coulomb excitation process in the semiclassical approximation assumes that the projectile follows a classical hyperbolic orbit, an assumption which is valid for large values of η (see Section II). At the energies used in the present experiments the values of η for the bombardment of ^{114}Cd with ^{4}He, ^{12}C and ^{16}O ions are approximately 10, 30 and 40, respectively. The use of symmetrized expressions for the distance of closest approach and adiabaticity parameter further improves the accuracy of the semiclassical approximation such that, for the experiments reported here, the difference between a semiclassical and a quantum mechanical treatment is expected to be negligible (Alder, et al., 1956).

2) Only electric quadrupole interactions between projectile and target have been considered in the analysis.

Because of the selection rules applicable to the present case magnetic interactions can only contribute to higher order effects and not to the direct excitation of the 2^{+} state. Such contributions are, however, expected to be 100 to 1000 times smaller than the E2 effects since magnetic excitations are intrinsically much weaker for particles scattered at large angles (the cross section is zero for 180^{o} scattering) and for particles with non-relativistic velocities.

The effects of electric dipole interactions have been discussed by Eichler (1964). He considered the term in the perturbation expansion arising from the interference between virtual double E1 excitation via the giant dipole resonance and direct E2 excitation from the ground state. In the type of experiment reported here, the expected dependence of the double-E1 effect on the various bombarding conditions employed is sufficiently similar to that of the static-quadrupole-moment effect that an experimental distinction is impracticable. However, according to more recent calculations by MacDonald (1964), Douglas (1966), and Winther (1966) based on the collective model, the magnitude of the E1 effect is expected to be 5 - 10 times smaller than observed in these experiments. Accordingly, the effects of virtual double E1 excitation have been neglected in analysis and also in the estimation of the error in M_{22}.

The effects of E3 and higher multipoles have also been neglected. Although a weak E3 excitation of a 3^- state at about 2 MeV has been observed by McGowan, et al., (1965), the contribution of this process to the excitation of the 2^+ state is considerably smaller than the equivalent contribution from the second 2^+ state.

3) Only the lowest known excited states (6 for ^{114}Cd, 4 for ^{116}Cd, and 3 for ^{126}Te and ^{128}Te) have been included in the computer analysis although only about 10% of the energy weighted E2 sum-rule is accounted for by the transitions to these states. This limitation seems justified on the grounds that other low-lying states which could contribute significantly to the excitation of the first 2^+ state should also have been observed previously through their gamma decay. Furthermore, if the remaining 90% of the E2

strength is accounted for by a single "giant quadrupole" state at about 10 MeV, and if a matrix element of equal magnitude is assumed to connect this state with the first 2^+ state, then the resulting interference term in the probability of excitation of the first 2^+ state in ^{114}Cd is found to be negligible.

4) The possible effects of nuclear reactions have been ignored. While it is extremely unlikely that such effects are important for the ^{12}C and ^{16}O ion bombarding energies used here, it is known (Hansen and Nathan, 1963, and McGowan, et al., 1965) that nuclear reactions may become appreciable for ^4He bombardment as the energy approaches the top of the Coulomb barrier (about 15 MeV for ^4He on ^{114}Cd). It is therefore especially important in experiments of this type to establish the energy range within which one may have confidence in a purely electromagnetic description of the interaction. This is the reason why ^4He data were taken over a wider energy range than was ultimately analyzed in the present experiments.

An examination of the analyzed ^4He data points in Figures 18 - 21 suggests that a small but finite slope is present in the data for each nucleus. The significance of this slope, if real, is not understood. It has been assumed that the ^4He energies used in the experiments and included in the analysis are far enough below the top of the Coulomb barrier to make interference from nuclear reactions extremely unlikely. The validity of this assumption appears to be proven by the simultaneous fit to the data involving the three different bombarding ions. It is noted, however, that if a monotonic decrease in the ^4He yield with increasing energy due to nuclear reactions is actually present in the analyzed data, that

this would lead to an underestimation rather than an overestimation of the quadrupole moment. It would be interesting to extend the ^{4}He data to higher energies up to and beyond the top of the Coulomb barrier to examine this assumption further.

VI. DISCUSSION OF THE RESULTS

Before discussing the results of the experiment, a few comments on the collective model are necessary.

The collective model of the nucleus in its simplest form classifies the collective or correlated motion of the individual nucleons into two basic types - rotational and vibrational motion. Rotational motion is characterized by the existence of a permanent equilibrium deformation; the nucleus may rotate about an axis perpendicular to its (assumed) axis of symmetry. Vibrational motion corresponds to an oscillation of the nuclear surface much the same as can be experienced by a liquid drop. While it appears possible that a nucleus may vibrate about an equilibrium deformation, thus permitting a "mixing" of the characteristic features of rotational and vibrational motion, the energies associated with the two types of motion are usually sufficiently different that nuclei may be empirically classified as either rotational or vibrational according to the structure of their lowest-lying levels.

Rotational-type nuclei are found in the mass regions[9] A = 150 to 190 and above A = 220. The energy level structure of even-even nuclei[10] in these regions is characterized by a J(J + 1) energy spacing and a sequence of J-values 0^+, 2^+, 4^+, 6^+, etc.,

---

9) Examples of collective motion are also known in other regions of the periodic table, including probably the 1p-shell nuclei.

10) Only even-even nuclei will be considered in the discussion for reasons of simplicity and because the nuclei investigated in these experiments are all of the even-even type.

with the energy of the first excited state usually in the 100 to 300 keV range.

Vibrational nuclei, on the other hand, exhibit a quite different level sequence and spacing. A triad of excited states with $J^{\pi} = 0^+, 2^+, 4^+$ is usually found at about twice the excitation energy of the first excited state with $J^{\pi} = 2^+$. The excitation energy of the latter is typically 400 to 700 keV. Vibrational nuclei are found in the mass regions A = 60 to 150 and A = 190 to 220. It is apparent from an examination of their energy level spectra that the cadmium and tellurium isotopes investigated here are typical vibrational-type nuclei.

The simplest vibrational model considers pure harmonic quadrupole vibrations of the nuclear surface (Bohr and Mottelson, 1953). The equation of the surface may be expressed as

$$R(\theta, \varphi) = R_0 (1 + \sum_{\mu=-2}^{2} \alpha_{2,\mu} Y_{2,\mu}(\theta, \varphi))$$

where the $\alpha_{2,\mu}$ are functions of time and are assumed small. By expressing the Hamiltonian of the system in terms of the generalized coordinates, $\alpha_{2,\mu}$, and their associated generalized momenta, it may be seen that the surface oscillations are equivalent to a system of harmonic oscillators. The excitation quanta are Bose-Einstein particles or "phonons" of spin 2 and even parity. The first excited state is a one phonon state while the degenerate $(0^+, 2^+, 4^+)$ triad is obtained from the combination of two phonons. In the simple harmonic model (SHM) the matrix element of the E2 operator between states containing the same number of pure phonons vanishes identically. Thus, in this model, $Q_2 = 0$.

The fact that the experimental values of Q_2 determined in the present work, and also recently by others[11], are not zero is perhaps not too surprising, however, when one notices that the SHM provides only an approximate description of the actual nuclear motion. An examination of the known properties of most vibrational nuclei immediately reveals deviations from the SHM. (For the remainder of the discussion ^{114}Cd is taken as the case in point). The degeneracy of the two-phonon triad is removed and all of the levels are seen to lie at more than twice the energy of the one-phonon state. Furthermore, an examination of the matrix elements in Table 1 shows that the selection rule forbidding E2 transitions between states differing by other than one phonon is violated by the small but finite value of $B(E2, 2'^+ \rightarrow 0^+)$. There are also other similar examples of deviations from the pure-harmonic phonon model. It may be hoped that a more refined model which can account for some of these deviations will also predict the measured value of Q_2.

Within the framework of the SHM, deviations from harmonic structure are accompanied by the admixing of states of different numbers of phonons. In other words, the $2'^+ \rightarrow 0^+$ crossover

---

11) Measurements similar to those reported here have been done on ^{114}Cd also at Oak Ridge National Laboratory by Stelson, et al., (1965) and at A. W. R. E., Aldermaston by Simpson, et al., (to be published). Their values for Q_2, -0.6 ± 0.2 barn (Oak Ridge) and -0.49 ± 0.23 barn (Aldermaston), agree within the experimental errors with the value reported in this thesis, -0.7 ± 0.2 barn.

A part of the experiments described here has been reported in the literature (de Boer, Stokstad, Symons and Winther, 1964, and 1965).

transition is accounted for by the presence in the two-phonon state of a small admixture of the one-phonon state. Similarly the deviation of the transition moment ratio

$$R_1 \equiv \frac{B(E2,\ 2'^{+} \rightarrow 2^{+})}{B(E2,\ 2^{+} \rightarrow 0^{+})}$$

from the SHM prediction of 2 is an indication of phonon mixing. Tamura and Ugadawa (1965) have taken the experimental value $R_1 = 1.2 \pm 0.2$ (McGowan, et al., 1965) and used it to calculate the amount of two-phonon character present in the one-phonon state on the basis of a simple model. In their model the wave functions of the first and second excited 2^{+} states are written respectively as

$$\psi(2) = a_1|1\rangle + a_2|2\rangle$$

$$\psi(2') = -a_2|1\rangle + a_1|2\rangle$$

with

$$a_1^2 + a_2^2 = 1 .$$

The one-phonon amplitude a_1 and hence the admixture amplitude a_2 are fixed by the relation

$$R_1 = \frac{2(2a_1^2 - 1)^2}{a_1^2}$$

yielding $a_1^2 = 0.86$ and $a_2^2 = 0.14$. The magnitude of Q_2 is given by

$$Q_2 = \frac{12}{5} \frac{1}{(7\pi)^{1/2}} a_1 a_2 Z R_0^2 \beta$$

where β, a parameter related to the mean square amplitude of the surface vibration, is derived from the $B(E2, 0^+ \rightarrow 2^+)$ and is equal to 0.2. Evaluation of the above yields

$$|Q_2| = 0.58 \text{ barn.}$$

The sign of Q_2 is not predicted in this simple model but depends on the nature of the force producing the mixing. It would appear that the problem is solved by this simple model. This, however, is not the case. The quadrupole moment has been explained at the expense of the forbidden crossover transition. The model predicts

$$R_2 \equiv \frac{B(E2, 2'^+ \rightarrow 0^+)}{B(E2, 2^+ \rightarrow 0^+)} = 0.14$$

whereas the experimental value is $R_2^{(exp)} = 0.015 \pm 0.005$. The phonon admixture of 14% which explains R_1 and Q_2 produces in this model a crossover transition rate almost an order of magnitude too large. It is also possible that such a large phonon admixture violates the original assumptions on which the model is

based. One cannot therefore regard this model as satisfactory[12].

Rather than considering at this point the other vibrational model calculations, all of which incorporate individual particle structure to some extent, it is advantageous to look to another collective model, the rotational model, as it is known to predict large quadrupole moments. In the simple rotational model, all transition and static E2 moments are related by Clebsch-Gordan coefficients. In particular,

$$|Q_2| = 0.91 \, |\langle 0 \| \mathcal{M}(E2) \| 2 \rangle| \ .$$

The value of B(E2, $0^+ \rightarrow 2^+$) is known and the above relation gives

$$|Q_2| = 0.7 \text{ barn}$$

which agrees with the experimental value of -0.7 ± 0.2. The rotational model predicts Q_2 negative if the intrinsic deformation is prolate. Here one can see the fundamental theoretical difficulty posed by the measured value of Q_2; ^{114}Cd is a nucleus displaying what appears to be a vibrational character in all respects except one, the value of Q_2, which is rotational in character.

A rotational model capable of accounting for some apparently vibrational characteristics is the asymmetric rotator model of Davydov and Fillipov (1958). They consider the rotations of a permanently deformed, ellipsoidal nucleus with three unequal principal axes. The deviation from axial symmetry is expressed in terms of the parameter γ which is empirically fixed by the

---

12) Neither do Tamura and Ugadawa. They wish only to show by means of this model that a vibrational description can be found which accounts for Q_2. Whether this model actually accomplishes this is open to question.

ratio of the energies of the first and second 2^+ states. For ^{114}Cd, $\gamma = 26.8$ degrees. One other parameter is needed to determine Q_2; this is Q_0, the so-called "intrinsic" quadrupole moment, which is related to the $B(E2, 0^+ \rightarrow 2^+)$. The Davydov-Fillipov model predicts

$$|Q_2| = 0.3 \text{ barn} .$$

Q_2 is negative if one assumes a prolate equilibrium deformation, i.e., assumes Q_0 positive. Although this value of Q_2 is still too small, the asymmetric rotator model gives a more reasonable description of ^{114}Cd than the simple rotational model which has no second-excited 2^+ state. A difficulty with the Davydov-Fillipov model, however, is the lack of a 0^+ state to complete the two-phonon triad, which is frequently seen experimentally.

To summarize the above discussion, one may note that none of the phenomonological collective models considered thus far - the pure harmonic vibrator, phonon-mixing, simple rotational model and the asymmetric rotator models - has been able to explain all of the major characteristics of ^{114}Cd.

A suggestion of the next direction which one might take in searching for an explanation of this dilemma is provided by the presence of the additional 0^+ and 2^+ states in the two-phonon region of ^{114}Cd (see Figure 11). These are presumably intrinsic states arising from the excitation of individual nucleons and should serve as a reminder that individual particle aspects can influence the collective properties of the nucleus.

The simplest model based on individual particle motion is the ordinary shell model (Mayer and Jensen, 1955). For the cadmium nuclei (Z = 48) one may take as the relevant shell model

configuration for the first excited state two proton holes in a $(g_{9/2})^{-2}$ configuration coupled to angular momentum 2. Evaluation of Q_2 (Tamura and Ugadawa, 1965) gives

$$Q_2 = -0.10 \text{ barn} .$$

The sign is predicted correctly[13] but the magnitude is too small. This disagreement should not be taken too seriously, however, since one should not expect such a simple shell model description to work where collective motion is so clearly important.

A more realistic approach can be taken by coupling individual particle motion with collective surface oscillations (Bohr, 1953). In such a model two nucleons in the shell model configuration $(n\ell J)^2$ with principal, orbital and total angular quantum numbers n, ℓ and J are coupled to a phonon of spin R. The phonon and the shell model configuration states are then coupled to total angular momentum $\vec{I} = \vec{J} + \vec{R}$ for the nucleus. Detailed calculations by Macdonald (1963) yield

$$Q_2 = -0.30 \text{ barn} .$$

However, in this model the 4^+ state occurs below the second 2^+ state and the 0^+ state lies too high.

It is also possible to treat the collective motion on a microscopic scale. The nucleons outside the last closed shell are

---

13) This model, however, would predict the wrong sign for the tellurium isotopes.

coupled by a pairing force, and the coordinates of the paired particles are suitably transformed to those of quasi-particles in a manner directly analogous to that used in the theory of superconductors. A long-range quadrupole-type force is then used to couple the quasi-particles and produce a collective motion. The resulting equations are then "linearized" i. e., treated in various degrees of the random phase approximation (RPA). RPA calculations by Tamura and Ugadawa (1965) yield quadrupole moments on the order of

$$Q_2 = -0.08 \text{ barn} .$$

The reason for this small value of Q_2 is that the ordinary RPA treatment neglects precisely those diagonal terms which are responsible for producing a quadrupole moment. Noting this, Tamura and Ugadawa (1966) have made RPA calculations in which the otherwise neglected terms are treated as a perturbation. Their results show a more reasonable value of

$$Q_2 = -0.44 \text{ barn} .$$

This model, as have all others, experiences certain difficulties. It predicts

$$|Q_2, {}^{114}\text{Cd}| > |Q_2 {}^{116}\text{Cd}|$$

the opposite of which is observed experimentally. Also, it predicts a positive value of Q_2 for the tellurium isotopes, contradicting the experimental values.

Other authors (Dang, et al., 1966) have also made attempts to calculate the large quadrupole moments observed in ^{114}Cd. These calculations differ in some respects from those proposed by Tamura and Ugadawa but have in common the facts that i) they are only simplified, exploratory calculations and are not to be taken as final theories and ii) they both indicate that phonon mixing and particle mixing may provide the mechanism for producing a large quadrupole moment.

The present state of theoretical interpretation of the large quadrupole moments observed in ^{114}Cd and ^{116}Cd is thus seen to be far from satisfactory. Whether the final solution will be found in terms of a vibrational model description or within the context of some different, as yet unproposed, type of model must remain for the moment a matter of conjecture.

A summary of the present experimental results, together with some of the other known properties of the cadmium and tellurium isotopes is presented in Figure 22. This figure shows the ratios

$$\frac{B(E2,\ 2'^{+} \rightarrow 2^{+})}{B(E2,\ 2^{+} \rightarrow 0^{+})}\ ,$$

$$\frac{B(E2,\ 4^{+} \rightarrow 2^{+})}{B(E2,\ 2^{+} \rightarrow 0^{+})}\ ,$$

$$\frac{E_{2'^{+}}}{E_{2^{+}}}\ ,$$

$$\frac{E_{4^+}}{E_{2^+}} ,$$

and

$$\frac{M_{22}}{|M_{12}|} = - \frac{\langle 2^+ \| \mathcal{M}(E2) \| 2^+ \rangle}{|\langle 2^+ \| \mathcal{M}(E2) \| 0^+ \rangle|} .$$

It is apparent from Figure 22 that the variation in magnitude of the ratio $M_{22}/|M_{12}|$ for the four nuclei studied here follows a pattern suggested by the other properties of the cadmium and tellurium isotopes. In particular, as the transition moment ratios and energy level ratios approach the value 2 predicted by the SHM or "phonon" model, the magnitude of $M_{22}/|M_{12}|$ decreases toward the SHM prediction of zero. Tables 3 and 4 show also that the magnitudes of Q_2 for the tellurium isotopes are smaller than those of the cadmium isotopes; the neutron numbers of the latter are midway between the major closed shells at N = 50 and N = 82. Finally, it is noted that the sign of Q_2 does not change in crossing the closed proton shell at Z = 50.

In summary, the quadrupole moments of the first excited states of ^{114}Cd and ^{116}Cd, measured in these experiments, are surprisingly large. How large they are is emphasized by the fact that ^{114}Cd, a nucleus which otherwise shows characteristics of a vibrational nature, possesses a static electric quadrupole moment in its first excited state which is as large as would be obtained with a rotational model description. Theoretical models, introduced prior to the measurement of Q_2 to account for the other deviations

from vibrational-type structure, predicted a value of Q_2 which is too small. Models introduced subsequently, and designed to predict a large Q_2, experience difficulty in reproducing the other known properties of ^{114}Cd. The systematic variation of Q_2 for the four nuclei studied follows a pattern which appears to be consistent with the trend of the other observed deviations from pure harmonic structure. No satisfactory theory exists to describe all these deviations from pure harmonic behavior; the failure of the existing theories to explain the large values of Q_2 is especially striking.

APPENDIX I. SYNOPSIS OF THE MULTIPLE COULOMB EXCITATION COMPUTER PROGRAM

The computer program for multiple Coulomb excitation written by Winther and de Boer (1965) provides the experimentalist with an essential and convenient tool for the analysis of data obtained from this type of measurement. Although the input requirements and use of the program in the analysis for this particular experiment have already been mentioned in Section II, it is worthwhile to examine in brief some of the internal aspects of the program.

The program uses the semiclassical approximation (7) together with the E2 multipole interaction Hamiltonian (8) to solve for the amplitudes, $a_n(t)$, of the free nucleus eigenfunctions. The solution is obtained by direct numerical integration of the coupled differential equations (7). The variables t and $r_p(t)$ in (8) are replaced by

$$t = \frac{a}{v} (\epsilon \sinh w + w)$$

$$r_p(t) = a(\epsilon \cosh w + 1)$$

where

$$\epsilon = (\sin \frac{\theta}{2})^{-1}$$

such that (7) becomes

$$\frac{da_r(w)}{dw} = i \sum_{\mu, s} Q_{2,\mu}(\epsilon, \xi_{rs}, w) \times \zeta_{rs}^2 \times a_s(w) \qquad (33)$$

where

$$\zeta_{rs} \sim \frac{Z_1 e M_{rs}}{\hbar v a^2} \quad .$$

It is noted that ζ_{rs} is proportional to the interaction constant $\chi_{i \to f}$ defined in (12).

The probability for the Coulomb excitation of a state N from an unpolarized ground state (I_1) is given by

$$P(N) = \frac{1}{2I_1 + 1} \sum_{M_1, M_N} | a_{I_N M_N}(M_1) |^2 \qquad (34)$$

and the Coulomb excitation cross section for an unsymmetrized calculation would then be obtained from (2).

In determining a symmetrization procedure for a multiple excitation calculation, the conditions of time reversal invariance and unitarity were satisfied in addition to the requirement that the symmetrization reproduce the limit of a quantum mechanical calculation. A symmetrized form of ξ_{rs}, ξ_{rs}^{symm}, analogous to (27) was used in the factor $Q_{2,\mu}(\epsilon, \xi_{rs}, w)$ in (33).

$$\xi_{rs}^{symm} = \frac{Z_1 Z_2 A_1^{1/2}}{6.235} \left\{ [E - E_r']^{-1/2} - [E - E_s']^{-1/2} \right\} \qquad (35)$$

where

$$E_r' = (1 + A_1/A_2)(E_r - E_i) \qquad (36)$$

and E, E_r and E_i are the energies in MeV of the projectile, state r and the initial state, respectively. The procedure for symmetrizing ζ_{rs} was to replace v everywhere with $\sqrt{v_r v_s}$ where

$$v_r = \sqrt{\frac{2(E - E_r')}{M}} \qquad (37)$$

with M the mass of the projectile. Half the distance of closest approach, a, is replaced by a_{rs} where

$$a_{rs} = \frac{Z_1 Z_2 e^2}{m_o v_r v_s} \quad . \qquad (38)$$

This symmetrization procedure is exactly equivalent to an internally consistent shift of the energy of each level and a renormalization of the E2 matrix elements M_{rs}. The symmetrized calculation is thus equivalent to an unsymmetrized calculation performed for a slightly different nucleus. Unitarity is therefore not violated by the introduction of symmetrized parameters and $\sum_N P(N) = 1$.

The requirement of time reversal invariance is given by the relation

$$(2I_N + 1)v_N^2 \, d\sigma(N \to M) = (2I_M + 1)v_M^2 \, d\sigma(M \to N) \tag{39}$$

for the cross sections for the excitation processes $N \to M$ and $M \to N$. An examination of the differential equations (33), in which the symmetrized parameters ξ_{rs}^{symm} and ζ_{rs}^{symm} are employed, shows that the equations are invariant under the conditions of reversed motion; reversed motion is the situation in which the nucleus in state f is bombarded by a projectile of energy $E - E_f'$. This invariance results in the relation

$$a_{I_f M_f}(M_i) = a_{I_i M_i}(M_f) \tag{40}$$

from which follows

$$(2I_N + 1)P(N \to M) = (2I_M + 1)P(M \to N) \, . \tag{41}$$

Using (41), it is easily shown that

$$d\sigma(N \to M) = \frac{v_M}{v_N} P(N \to M, \zeta_{rs}^{symm}, \xi_{rs}^{symm}) \frac{a_{NM}^2}{4} \sin^{-4}\left(\frac{\theta}{2}\right) \tag{42}$$

satisfies (39).

P(2) as defined in (42) is seen to be slightly different from $P_{exp} = d\sigma_2/\sum_i d\sigma_i$ as defined in (30). The analysis has been performed in terms of the quantities actually measured, namely the ratios of cross sections as given by P_{exp}, rather than in terms of the excitation probabilities defined by (42).

It is noted that the symmetrized expressions II C. 15 in Alder, et al., (1956), (28), and (42) are all equivalent in the limit of first order perturbation theory.

The integration of (33) starts from the initial condition that all $a_r(w = -U_p) = 0$ except for the ground state amplitude. The range, U_p, and initial step width of the integration, $2\Delta w$, are determined by the required absolute accuracy which is stated in the input. A Runge-Kutta-Gill procedure is first used to generate the amplitudes and their derivatives for four consecutive steps. With these values as starting points, the faster Adams-Moulton predictor-corrector integration routine is then used to complete the calculation. A constant check on the accuracy of the integration is maintained and an adjustment in step width executed whenever necessary.

The differential cross sections for each level may be obtained either in the laboratory or center-of-mass systems. The program also calculates the coefficients for the gamma-ray angular distribution in various coordinate systems. The formulae given are sufficiently general to include the fact that, in multiple Coulomb excitation, the various levels may be populated not only by direct excitation from the ground state, but also by electron conversion and gamma-ray transitions from higher levels.

APPENDIX II. AUXILIARY MEASUREMENTS

A. Magnetic Analysis Measurement

It is also possible to detect Coulomb excitation by direct magnetic analysis of the energy of the scattered projectile. This method is particularly suitable when protons or alpha particles are employed as projectiles, since the energy losses in the target remain small. This type of measurement becomes more difficult when heavier ions are used; large dE/dx energy losses for heavy ions require an extremely thin target in order to be able to resolve the elastically and inelastically scattered particles. A measurement by magnetic analysis was made, nevertheless, in order to have an independent check on the particle-gamma coincidence method.

The magnetic analysis method offers several advantages over the particle-gamma coincidence method.

(i) It is not necessary to determine the efficiency of a NaI crystal to extract the excitation probability.

(ii) The population of the first 2^+ state by cascade gamma rays is no longer a factor to be considered in the analysis.

(iii) The measurement does not require electronic coincidence circuitry with its accompanying dead-time losses and random-coincidences. The principle difficulty encountered with this technique is the low counting rate.

Data were obtained by this method for the scattering of ^{4}He and ^{16}O ions from ^{114}Cd at a laboratory angle of 150 degrees. The ^{4}He and ^{16}O energies used were 9.76 and 40.7 MeV respectively, both corresponding to $\xi = 0.30$. Adequate resolution of the inelastic and elastic particle groups was obtained by using thin targets (200 $\mu gm/cm^2$ for ^{4}He and 20 $\mu gm/cm^2$ for ^{16}O bombardment) and a small spectrometer acceptance angle (about 2^{o} total) to minimize the kinematical variation of particle energy with angle (about 60 keV per degree for ^{16}O on ^{114}Cd at 150^{o}). The scattered particles were detected initially by a linear array of sixteen solid-state detectors placed in the focal plane of a 61-cm double-focusing magnetic spectrometer. The total energy region spanned by this detector array was quite adequate to cover the region of interest but, because of the wide gaps between the detectors, it was still necessary to scan across the spectrum in several overlapping steps. A typical momentum spectrum obtained with ^{4}He projectiles is shown in Figure 23. For ^{16}O bombardment, however, the counting rates were so low that it turned out to be impossible to obtain adequate statistical precision with the counter array. After taking an exploratory spectrum with poor statistics (see Figure 24), the sixteen counter array was replaced by a single large detector, collimated by a 1.27 cm slit. This detector spanned an energy region of approximately 200 keV, sufficient to cover either the complete inelastic peak or the complete elastic peak for one choice of the spectrometer magnetic field. By varying the magnetic field of the spectrometer, the detector was set on each peak separately; the number of particles scattered by the target was monitored by a solid state detector placed in the scattering chamber at an angle of 150^{o} on the opposite side of the beam axis. The back-

ground under the inelastic peak was estimated by counting on either side of this peak. This subtraction was about 2% of the inelastic yield.

In calculating the ratio of the cross sections for the ^{16}O case, it was necessary to allow for the small difference in the charge state populations for the elastically and inelastically scattered particles. This difference was measured by determining the yield of elastically scattered ^{16}O ions in the selected 6^+ charge state as a function of the energy of the incoming beam. The difference between the 6^+ charge state populations at the energies of the elastic and inelastic groups was measured to be 1.5%.

The results of the spectrometer measurements are given in the following table. The errors are almost entirely due to the limited statistical precision of the number of counts in the inelastic peak.

Projectile	E_{MeV}	ξ	$P_{exp} \times 1000$
^{16}O	40.70	0.301	75 ± 4
^{4}He	9.76	0.301	6.7 ± 0.2

The analysis of the above experimental quantities was done in a manner similar to that described in Section IV and yielded the values

$$M_{12} = -0.709 \pm 0.012 \quad e \cdot 10^{-24} cm^2$$
$$M_{22} = +1.0 \pm 0.3 \quad e \cdot 10^{-24} cm^2$$

These values compare favorably with those given in Table 6 for the particle-gamma coincidence method.

B. Gamma-gamma Coincidence Measurement

The analysis of the data required a knowledge of the matrix elements M_{rs} connecting the levels populated in the experiment. Gamma-gamma coincidence measurements performed by Stelson (1961) and McGowan et al., (1965) provided this information for the cadmium nuclei. Only part of the required information was available for ^{126}Te and ^{128}Te.

The values of B(E2, $0^+ \rightarrow 2^+$) and B(E2, $0^+ \rightarrow 2'^+$) for ^{126}Te had been measured by Stelson (1958) and Gangrskii, et al., (1962), respectively. These values together with the known cascade-to-crossover branching ratio (Perlman and Welker, 1954) determine the B(E2, $2'^+ \rightarrow 2^+$) since the $2'^+ \rightarrow 2^+$ transition is known to be 98% E2 (Wiedling, et al., 1960)[14].

In order to obtain a value for B(E2, $4^+ \rightarrow 2^+$), the following experiment was performed. A ^{126}Te target prepared on a clean gold backing was bombarded with 42 MeV oxygen ions. Two gamma-ray detectors - one, a 10.2-cm-long by 12.7-cm-diameter Na(Tl) crystal and the other, a 20-cc lithium-drifted germanium detector - were mounted on either side of, and close to, the target. The germanium detector spectrum was gated by gamma-gamma coincidences and the pulses from the NaI detector were required to fall within a window set around the 667 keV ($2^+ \rightarrow 0^+$) photopeak. The Li-Ge detector spectrum is shown in Figure 25; it consists

---

14) The SHM predicts the $2'^+ \rightarrow 2^+$ transition to be pure E2. Gamma-gamma angular correlation measurements by Lindquist and Marklund (1957) on a variety of nuclei show that the $2'^+ \rightarrow 2^+$ transition is generally greater than 90% E2. However, one of the exceptions was ^{124}Te with a 50 ± 10% M1 multipolarity. The decay of ^{122}Te was measured to be 92% E2.

almost entirely of a background of real coincidences whose source was most likely the $^{12}C(^{16}O, p\,\alpha)^{23}Na$ reaction from the carbon accumulated on the target during bombardment. The peak at 667 keV indicated by the arrow in Figure 25 is due to the $2^+ \rightarrow 0^+$ gamma rays from the $4^+ \rightarrow 2^+ \rightarrow 0^+$ and the $2'^+ \rightarrow 2^+ \rightarrow 0^+$ cascade transitions. Their presence in the spectrum arises from the fact that the window in the NaI detector spectrum also accepted the upper member of the $4^+ \rightarrow 2^+ \rightarrow 0^+$ cascade and a fraction of the upper member of the $2'^+ \rightarrow 2^+ \rightarrow 0^+$ cascade. The estimated random coincidence contribution to this peak was negligible.

The horizontal bar indicates the expected position of the $4^+ \rightarrow 2^+$ gamma ray. If the peak which appears under this bar is assumed to be due to the $4^+ \rightarrow 2^+$ transition, and if the 1.360 MeV state in ^{126}Te is indeed 4^+, one obtains[15] a value of $B(E2,\ 2^+ \rightarrow 4^+) = 0.23 \pm 0.10\ e^2 \cdot 10^{-48}\ cm^4$. This means a value of $B(E2,\ 4^+ \rightarrow 2^+)/B(E2,\ 2^+ \rightarrow 0^+)$ of 1.2 which is reasonable for these vibrational-type nuclei (see Figure 22). This value has been used in the analysis.

A similar experiment was not attempted for ^{128}Te since the energies of the upper and lower members of the cascade are so close as to make their resolution difficult even with a Li-Ge detector. To estimate the higher matrix elements for ^{128}Te, the values of the ratios $B(E2,\ 4^+ \rightarrow 2^+)/B(E2,\ 2^+ \rightarrow 0^+)$ and $B(E2,\ 2'^+ \rightarrow 2^+)/B(E2,\ 2^+ \rightarrow 0^+)$ were taken to be the same in ^{128}Te as in ^{126}Te. The $B(E2,\ 0^+ \rightarrow 2^+)$ used in these ratios was taken from the work of Stelson (1958) and the value for $B(E,\ 2'^+ \rightarrow 0^+)$ was assumed to be the same as in ^{126}Te. The resultant values of the M_{rs} for ^{126}Te and ^{128}Te are given in

---

15) Since the face of the NaI crystal was only 1.2 cm from the target, it was assumed that the effect of the angular correlation between the $4^+ \rightarrow 2^+$ and $2^+ \rightarrow 0^+$ gamma rays could be neglected.

Table 2. It should be mentioned that these values are not overly critical for the analysis, especially since their relative signs are unknown. This latter uncertainty effectively puts an error of $\pm$ 100% on these matrix elements. The error in Q_2 from this source is much larger than the corresponding error introduced by the cascade gamma-ray correction due to the uncertainty in the magnitude of M_{rs}.

C. Sulphur Beam Measurement

In Section II D. 2 it was shown that the magnitude of the effect of Q_2 on the excitation probability is roughly proportional to the mass of the bombarding particle. It was decided therefore to attempt an extension of the measurements to include a still heavier bombarding ion, ^{32}S. Sulphur was a natural choice because it had previously been accelerated with the tandem and because it is significantly heavier than oxygen.

Several difficulties were encountered in the production of the sulphur beam which seriously limited the utility of this method for measuring Q_2. Some of these difficulties, particularly those connected with the production of a negative ion beam, have already been described in detail by Miller (1966). Briefly, they were:

(i) the introduction of H_2S into the negative ion source had a detrimental effect on the ceramic insulators separating the various acceleration electrodes in the ion source. After typically twenty-four to thirty-six hours of operating time, conductive tracks developed across the surfaces of the insulators;

(ii) although no oxygen was deliberately introduced into the duoplasmatron source a negative oxygen beam of 80 keV energy was present with the same magnetic rigidity as the 40 keV S^- beam. This had the effects of loading the tandem with an unwanted beam and making the selection of, and regulation on, the desired sulphur beam more difficult. Post-terminal stripping produced a number of beams of intensity comparable to the desired beam at about the same terminal voltage;

(iii) the low net intensity of the S^- beam from the negative ion source effectively prohibited the use of the 8^+ sulphur charge state, limiting the maximum energy to about 45 MeV. As this is less than one half of the Coulomb barrier energy, the excitation probability was rather low. This together with a low beam intensity ($\sim$ 5 nanoampere) produced a very low counting rate.

It was nevertheless possible to obtain a measurement of the excitation probability of the first excited state in ^{116}Cd under bombardment by ^{32}S ions. The negative beam was produced by insertion of argon into the duoplasmatron source and H_2S into the exchange canal. Positive identification of the high-energy analyzed ^{32}S beam was obtained by scattering the beam from thin gold and nickel foils and observing the ratio of the scattered particle energies. With the tandem regulating on the 7^+ charge state, a beam of four nanoamperes at 44 MeV was available at the target. In a net beam time of about five hours, 1280 coincidences were obtained.

The methods described in Section II D. 2 suffice for an analysis of this datum. The experimental excitation probability

obtained was $0.38 \pm 0.04\%$. The $B(E2, 0^+ \rightarrow 2^+)$ obtained from a comparison of this value with first order perturbation theory was $0.55 \pm 0.05\ e^2 \cdot 10^{-48}\ cm^4$. To obtain a value for Q_2 one compares the ratios of the experimental excitation probabilities of, for example, ^4He ions and ^{32}S ions with the theoretical ratios by means of the following equation

$$\frac{P_{exp}(^{32}S)}{P_{exp}(^4He)} = \frac{P^{(1,1)}(^{32}S)(1 + \rho(^{32}S))}{P^{(1,1)}(^4He)(1 + \rho(^4He))}$$

(see (19), (22) and (24)). Using the ^4He datum taken at a bombarding energy of 9.02 MeV, one obtains

$$0.572 \pm 0.044 = 0.616\ (1 - 0.123\ M_{22})$$

$$M_{22} = +0.59 \pm 0.59$$

and

$$Q_2 = -0.45 \pm 0.45 \quad \text{barn} .$$

The principle uncertainty in the value of Q_2 thus derived is due to the uncertainty in the measured target thickness. The ^{32}S ions lost 4.1 MeV in passing through the particular target used. Clearly, thinner targets would be required for measurements using ^{32}S ions, with even lower counting rates being the result.

APPENDIX III

GAMMA-RAY SPECTROMETRY

It was necessary to know the efficiency of the NaI gamma detector in order to deduce the probability for Coulomb excitation. This efficiency was determined in the following way. Point sources of gamma rays of various energies were prepared and placed at a distance of 10 cm from the face of the 7.62-cm-long by 7.62-cm-diameter NaI crystal. The total efficiency and peak-to-total ratios for the detector and source in this geometry were taken from the Nuclear Data Tables compiled by Marion (1960) and were used to determine the strength of the point sources. The calibrated sources were then placed at the intersection of the beam and target and used to measure the efficiency of the gamma-ray detector in the actual experimental configuration. The major uncertainty in the resultant efficiency is contained in the values of the total efficiency and peak-to-total ratios initially used to calibrate the sources. The uncertainty in the experimental efficiency was estimated to be $\pm$ 8%.

The anisotropic angular distribution of the $2^+ \rightarrow 0^+$ de-excitation gamma rays requires a correction to the isotropic-source efficiency measured above. The gamma-ray angular distribution is a function of θ only, where θ is the angle between the gamma-ray direction and the beam axis, because the particle detector has azimuthal symmetry. The probability, dW, that the nucleus in its first excited state will emit a gamma ray into a solid angle $d\Omega$ at an angle θ is given by

$$dW = 1 + a_2 P_2(\cos\theta) + a_4 P_4(\cos\theta) \quad . \qquad (43)$$

P_2 and P_4 are the Legendre polynomials. Typical values of a_2 and a_4 obtained from the computer program were 0.7 and -1.6, respectively.

The finite size of the NaI crystal tends to attenuate the effects of the anisotropic distribution. The above expression for dW must be folded with the efficiency of the NaI crystal (as a function of θ) and integrated over the volume of the crystal. This procedure has been described by Pearson (1963). The value of the correction factor K which multiplies the isotropic efficiency is then given by

$$K = 1 + a_2 \frac{J_2}{J_0} P_2(\cos\theta_1) + a_4 \frac{J_4}{J_0} P_4(\cos\theta_1) \qquad (44)$$

where θ_1 is the angle of the axis of symmetry of the NaI crystal with respect to the beam axis. The factors J_2/J_0 and J_4/J_0 are referred to as Rose's smoothing factors (Rose, 1953). Since they are dependent upon the source - detector geometry, they were measured experimentally using a narrowly collimated source of gamma rays. The results agreed with those obtained by interpolation of results found in the literature (Herskind and Yoshizawa, 1964). The correction to the isotropic efficiency due to the anisotropic angular distribution amounted to about 9% but was essentially the same for all bombarding particles and energies.

The de-excitation gamma ray is emitted from the recoiling nucleus after a time $\sim 10^{-11}$ sec. which is long compared to the collision time ($a/v \sim 10^{-21}$ sec.). The gamma ray will be emitted at angle θ in a coordinate system moving with velocity $v = \beta c$ relative to the laboratory system, provided the velocity of the

recoiling nucleus is not appreciably attenuated by the target thickness. The gamma ray will appear to have an angle $\bar{\theta}$ in the laboratory system. For projectiles scattered at large angles, the component of the recoil velocity perpendicular to the beam axis may be neglected. A relativistic transformation of velocities then yields

$$\theta = \tan^{-1}\left(\frac{\sin\bar{\theta}}{\cos\bar{\theta} - \beta} \cdot \sqrt{1 - \beta^2}\right) . \qquad (45)$$

The net result of the change in angle is to introduce small P_1, P_3, and P_5 terms into the laboratory angular distribution. To first order in β, (44) becomes

$$K = 1 + a_2 \frac{J_2}{J_0} P_2 + a_4 \frac{J_4}{J_0} P_4 + 2\beta \left\{(1 - \frac{a_2}{5})\frac{J_1}{J_0} P_1 + (\frac{6}{5} a_2 - \frac{2}{2} a_4)\frac{J_3}{J_0} P_3 \right.$$

$$\left. + \frac{5}{3} a_4 \frac{J_5}{J_0} P_5 \right\} .$$

The maximum value of the term in β proved small (< 0.003) for 40 MeV ^{16}O bombardment of ^{114}Cd ($\beta = 0.018$), and was correspondingly smaller for bombardment by lighter ions.

The energy loss of the recoiling nucleus in the target effectively reduces the value of β to below that calculated for a freely recoiling nucleus. A calculation of the range of 17 MeV ^{114}Cd ions ($\beta = 0.018$) in ^{114}Cd using the formulae of Lindhard,

et al., (1963) yielded a value of 200 μgm/cm^2. This range, probably accurate to $\pm$ 50%, is less than the thickness of any of the ^{114}Cd or ^{116}Cd targets used in the experiments. If an average energy of 8 MeV is assumed over the range of the recoiling nucleus, the time in which the nucleus comes to rest is of the order of 10^{-13} second, which is much shorter than the lifetime of the excited nucleus. Therefore, no correction for nuclear recoil was applied to the gamma-ray angular distributions for the cadmium nuclei.

In the tellurium measurements however, in which the targets were only 80 μgm/cm^2 thick, a correction to the gamma-ray angular distribution for nuclear recoil was applied. Since, in this case, most of the gamma-ray de-excitations for ^{16}O ion bombardment took place in a region just behind the target, a slight difference in relative efficiency for ^{4}He ion and ^{16}O ion bombardment resulted. The corrections to the yield for this were less than 0.2%.

REFERENCES

1. Alder, K., Bohr, A., Huus, T. Mottelson, B. and Winther, A., Rev. Mod. Phys. 28, 432 (1956).

2. Alder, K. and Winther, W., Proceedings of the Symposium on "Recent Progress in Nuclear Physics with Tandems", Heidelberg (1966).

3. Bohr, A. and Mottelson, B., Kgl. Danske Videnskab. Selskab Mat. fys. Medd. 27 (1953).

4. Breit, G. and Lazarus, J. P., Phys. Rev. 100, 942 (1955).

5. Cookson, J. A. and Darcey, W., Nuclear Physics 62, 326 (1965).

6. Dang, G. D., Dreizler, R., Klein, A. and Wu, C. S., Phys. Rev. Letters 17, 709 (1966).

7. Davydov, A. S. and Fillipov, G. T., Nuclear Physics 8, 237 (1958).

8. de Boer, J., Stokstad, R. G., Symons, G. D. and Winther, A., Bull. Am. Phys. Soc. 9, 718 (1964).

9. de Boer, J., Stokstad, R. G., Symons, G. D. and Winther, A., Phys. Rev. Letters 14, 564 (1965).

10. Douglas, A. C., Atomic Weapons Research Establishment Report NR/P-2/62, Aldermaston, England (1962).

11. Douglas, A. C., private communication (1966).

12. Eichler, J., Phys. Rev. 133, B 1162 (1964).

13. Gangrskii, Yu. P. and Lemberg, I. Kh., JETP 15, 711 (1962).

14. Hansen, O. and Nathan, O., Nuclear Physics 42, 197 (1963).

15. Herskind, B. and Yoshizawa, Y., Nuclear Inst. and Methods 27, 104 (1964).

16. Lindhard, J., Scharff, M., Schott, H. E., Kgl. Danske Videnskab. Selskab Mat. fys. Medd. 33 (1963).

17. Lindquist, T. and Marklund, I., Nuclear Physics 4, 189 (1957).

18. Litherland, A. E., Clark, M. A. and Broude, C., Phys. Letters 3, 204 (1963).

19. MacDonald, N., Nuclear Physics 48, 500 (1963).

20. MacDonald, N., Phys. Letters 10, 334 (1964).

21. Marion, J. B., Nuclear Data Tables, Part 3, Nuclear Reaction Graphs, National Academy of Sciences, Washington, D. C., (1960).

22. Masso, J. F. and Lin, D. L., Phys. Rev. 140, B 1182 (1965).

23. Mayer, M. G. and Jensen, J. H. D., Elementary Theory of Nuclear Shell Structure (John Wiley and Sons, Inc., New York), (1955).

24. McGowan, F. K., Robinson, R. L., Stelson, P. H. and Ford, Jr., J. L. C., Nuclear Physics 66, 97 (1965).

25. Miller, R. G., Ph. D. Thesis, California Institute of Technology (1966).

26. Pearson, J. D., Ph.D. Thesis, California Institute of Technology (1963).

27. Perlman, M. L. and Welker, J. P., Phys. Rev. 95, 133 (1954).

28. Rose, M. E., Phys. Rev. 91, 610 (1953).

29. Simpson, J. J., Eccleshall, D., Yates, M. J. L. and Freeman, N. J., to be published.

30. Stelson, P. H. and McGowan, F. K., Phys. Rev. 110, 489 (1958).

31. Stelson, P. H. and McGowan, F. K., Phys. Rev. 121, 209 (1961).

32. Stelson, P. H., Milner, T. W., Ford, Jr., J. L. C., McGowan, F. K., and Robinson, R. L., Bull. Am. Phys. Soc. 10, 427 (1965).

33. Tamura, T. and Ugadawa, T., Phys. Rev. Letters 15, 765 (1965).

34. Tamura, T. and Ugadawa, T., Phys. Rev. 150, 783 (1966).

35. Temmer, G. M. and Heydenburg, N. P., Phys. Rev. 104, 967 (1956).

36. Wiedling, T. and Asplund, I., Arkiv Fysik 18, 65 (1960).

37. Winther, A. and de Boer, J., 1965, A Computer Program for Multiple Coulomb Excitation, Technical Report, November 18, 1965, California Institute of Technology.

38. Winther, A., private communication (1966).

TABLE 1

The matrix M_{rs} (*in units of* $e \cdot 10^{-24}$ cm^2) used in the computer calculations. $(M_{rs})^2 = B(E2, s \rightarrow r) \times (2I_s + 1)$. M_{12} and M_{22} were fitted to the experimental data, and the M_{rs} values for the higher transitions were taken from McGowan, et al., (1965). The assignments of the indices r and s are indicated in Fig. 11. Since no measured value for M_{26} was available for ^{114}Cd, this matrix element was taken to have the single particle value.

r \ s	1	2	3	4	5	6	7
			^{114}Cd				
1	0	M_{12}	0	±0.09	0	0	±0.09
2	M_{21}	M_{22}	-0.31	-0.83	-1.35	-0.13	-0.31
3	0	-0.31	0	0	0	0	0
4	±0.09	-0.83	0	0	0	0	0
5	0	-1.35	0	0	0	0	0
6	0	-0.13	0	0	0	0	0
7	±0.09	-0.31	0	0	0	0	0
			^{116}Cd				
1	0	M_{12}	±0.147	0	0		
2	M_{12}	M_{22}	-0.66	-1.32	-0.31		
3	±0.147	-0.66	0	0	0		
4	0	-1.32	0	0	0		
5	0	-0.31	0	0	0		

TABLE 2

The matrix M_{rs} (in units of $e \cdot 10^{-24}$ cm^2) used in the computer calculations. $(M_{rs})^2 = B(E2, s \rightarrow r) \times (2I_s + 1)$. M_{12} and M_{22} were fitted to the experimental data. The assignments of the indices r and s are indicated in Fig. 12. The derivation of the values of M_{14}, M_{23} and M_{24} is detailed in Appendix II. B.

r \ s	1	2	3	4
		^{126}Te		
1	0	M_{12}	0	±0.07
2	M_{21}	M_{22}	-1.10	-1.00
3	0	-1.10	0	0
4	±0.07	-1.00	0	0
		^{128}Te		
1	0	M_{12}	0	±0.07
2	M_{21}	M_{22}	-0.94	-0.90
3	0	-0.94	0	0
4	±0.07	-0.90	0	0

TABLE 3

Experimental values of $P = d\sigma_2 / \sum_{i=1}^{n} d\sigma_i$ measured at a mean laboratory angle of 165^{o}. E is the effective bombarding energy. The number in parentheses is the power of 10 by which the value of P_{exp} and its assigned error should be multiplied. Errors are random only. The data obtained at ^{4}He energies greater than 10 MeV have not been incorporated in the analysis.

^{114}Cd

Projectile	E_{MeV}	ξ	P_{exp}
^{16}O	46.03	0.250	0.134 ± 0.002 (0)
	40.80	0.300	0.868 ± 0.009 (-1)
	40.45	0.304	0.828 ± 0.010 (-1)
	40.05	0.308	0.802 ± 0.007 (-1)
	36.85	0.350	0.552 ± 0.007 (-1)
	36.10	0.361	0.505 ± 0.006 (-1)
	34.85	0.381	0.413 ± 0.007 (-1)
	33.73	0.400	0.362 ± 0.005 (-1)
	33.00	0.414	0.331 ± 0.004 (-1)
^{12}C	30.04	0.300	0.561 ± 0.006 (-1)
	27.14	0.350	0.356 ± 0.004 (-1)
	24.86	0.400	0.226 ± 0.003 (-1)
^{4}He	9.78	0.300	0.775 ± 0.012 (-2)
	9.74	0.302	0.781 ± 0.013 (-2)
	9.71	0.304	0.757 ± 0.008 (-2)
	8.78	0.354	0.472 ± 0.006 (-2)
	8.05	0.406	0.307 ± 0.005 (-2)

continued

TABLE 3 (continued)

Projectile	E_{MeV}	ξ	P_{exp}
	11.30	0.240	0.138 ± 0.002 (-1)
	10.73	0.260	0.120 ± 0.002 (-1)
		^{116}Cd	
^{16}O	41.63	0.269	0.110 ± 0.002 (0)
	37.65	0.313	0.709 ± 0.012 (-1)
	34.55	0.356	0.491 ± 0.007 (-1)
^{12}C	30.66	0.269	0.705 ± 0.009 (-1)
	27.73	0.313	0.457 ± 0.006 (-1)
	25.46	0.356	0.310 ± 0.005 (-1)
^{4}He	9.966	0.269	0.102 ± 0.001 (-1)
	9.019	0.314	0.659 ± 0.014 (-2)
	8.304	0.356	0.445 ± 0.009 (-2)
	12.08	0.200	0.211 ± 0.004 (-1)
	11.35	0.220	0.172 ± 0.003 (-1)
	10.73	0.240	0.131 ± 0.002 (-1)

TABLE 4

Experimental values of $P = d\sigma_2 / \sum_{i=1}^{4} d\sigma_i$ for ^{126}Te and ^{128}Te measured at a mean laboratory angle of 165°. E is the effective bombarding energy. The number in parentheses is the power of 10 by which the value of P_{exp} and its assigned error should be multiplied. Errors are random only. The data obtained at ^{4}He energies greater than 10.5 MeV have not been incorporated in the analysis.

Projectile	E_{MeV}	ξ	P_{exp}
		^{126}Te	
^{16}O	43.21	0.352	0.608 ± 0.006 (-1)
	39.56	0.403	0.395 ± 0.007 (-1)
	36.61	0.453	0.268 ± 0.003 (-1)
^{4}He	10.44	0.352	0.512 ± 0.006 (-2)
	9.58	0.403	0.328 ± 0.005 (-2)
	9.15	0.433	0.261 ± 0.005 (-2)
	8.89	0.453	0.219 ± 0.004 (-2)
	11.54	0.302	0.804 ± 0.008 (-2)
	11.06	0.322	0.662 ± 0.013 (-2)

continued

TABLE 4 (cont.)

Projectile	E_{MeV}	ξ	P_{exp}	
		^{128}Te		
^{16}O	42.96	0.396	0.437 ± 0.006	(-1)
	41.60	0.416	0.357 ± 0.004	(-1)
	39.75	0.446	0.289 ± 0.003	(-1)
	37.08	0.495	0.193 ± 0.002	(-1)
^{4}He	10.11	0.416	0.296 ± 0.004	(-2)
	9.67	0.446	0.229 ± 0.004	(-2)
	9.042	0.495	0.156 ± 0.002	(-2)
	11.58	0.337	0.576 ± 0.013	(-2)
	10.60	0.386	0.377 ± 0.004	(-2)

TABLE 5

Calculated cross sections and de-excitation probabilities P for ^{114}Cd at a laboratory angle of 165° obtained using the computer program described in Appendix I. The indices 1 to 7 refer to levels in ^{114}Cd as shown in Fig. 11. The first four lines show the energy dependence of the cross sections and de-excitation probabilities for ^{16}O bombardment. The next seven lines illustrate the dependence on M_{45} and on the relative signs of those matrix elements which, in perturbation theory, contribute to the

Projectile	Energy MeV	ξ	Signs or values of matrix elements ($e \cdot 10^{-24}$ cm^2)					Laboratory cross sections (barns/steradian, numbers in brackets denote powers of ten)							De-excitation probabilities		
			M_{22}	M_{14}	M_{17}	M_{24}	M_{45}	$d\sigma_1$	$d\sigma_2$	$d\sigma_3$	$d\sigma_4$	$d\sigma_5$	$d\sigma_6$	$d\sigma_7$	P_{comp}	$P_{two\ level}$	$P_{first\ order}$
^{16}O	46.0	0.250	+1.0	-	-	-	0.0	7.636(-2)	1.273(-2)	1.048(-4)	2.710(-4)	4.616(-4)	1.413(-5)	6.890(-5)	0.1414	0.1439	0.1840
	40.0	0.309	+1.0	-	-	-	0.0	1.088(-1)	9.757(-3)	4.090(-5)	1.091(-4)	1.673(-4)	5.012(-6)	2.859(-5)	0.0820	0.0813	0.0995
	36.0	0.362	+1.0	-	-	-	0.0	1.392(-1)	7.485(-3)	1.812(-5)	4.953(-5)	6.900(-5)	2.027(-6)	1.300(-5)	0.0510	0.0501	0.0599
	33.0	0.413	+1.0	-	-	-	0.0	1.689(-1)	5.735(-3)	8.531(-6)	2.381(-5)	3.027(-5)	8.714(-7)	1.188(-5)	0.0328	0.0323	0.0378
	40.0	0.309	-1.0	-	-	-	0.0	1.060(-1)	1.265(-2)	4.076(-5)	8.652(-5)	1.638(-4)	4.877(-6)	2.295(-5)	0.1066	0.1057	0.0995
	40.0	0.309	0.0	-	-	-	0.0	1.074(-1)	1.121(-2)	4.104(-5)	9.807(-5)	1.663(-4)	4.969(-6)	2.574(-5)	0.0942	0.0935	0.0995
	40.0	0.309	+1.0	-	-	-	+1.0	1.089(-1)	9.781(-3)	4.101(-5)	1.085(-4)	1.319(-4)	5.026(-6)	2.860(-5)	0.0823	0.0813	0.0995
	40.0	0.309	+1.0	-	+	-	0.0	1.090(-1)	9.633(-3)	4.066(-5)	1.092(-4)	1.664(-4)	4.985(-6)	3.080(-5)	0.0810	0.0813	0.0995
	40.0	0.309	+1.0	+	-	-	0.0	1.093(-1)	9.395(-3)	4.031(-5)	1.014(-4)	1.651(-4)	4.949(-6)	2.893(-5)	0.0789	0.0813	0.0995
	40.0	0.309	+1.0	+	+	-	0.0	1.093(-1)	9.275(-3)	4.008(-5)	1.005(-4)	1.642(-4)	4.922(-6)	3.027(-5)	0.0780	0.0813	0.0995
	40.0	0.309	+1.0	+	-	+	0.0	1.089(-1)	9.757(-3)	4.090(-5)	1.091(-4)	1.673(-4)	5.012(-6)	2.860(-5)	0.0820	0.0813	0.0995
^{12}C	30.0	0.301	0.0	-	-	-	0.0	1.133(-1)	7.607(-3)	1.783(-5)	5.148(-5)	7.286(-5)	2.177(-6)	1.710(-5)	0.0628	0.0624	0.0649
	30.0	0.301	+1.0	-	-	-	0.0	1.140(-1)	6.840(-3)	1.780(-5)	5.633(-5)	7.326(-5)	2.194(-6)	1.834(-5)	0.0565	0.0561	0.0649
^{4}He	10.0	0.290	0.0	-	-	-	0.0	1.222(-1)	1.150(-3)	3.222(-7)	3.724(-6)	1.282(-6)	3.788(-8)	2.090(-6)	0.00932	0.00928	0.00933
	10.0	0.290	+1.0	-	-	-	0.0	1.222(-1)	1.110(-3)	3.225(-7)	3.810(-6)	1.287(-6)	3.805(-8)	2.111(-6)	0.00900	0.00896	0.00933

lowest order interference term. The last four lines demonstrate how the effects of the static quadrupole moment depend on the projectile mass. The values of $P_{two\ level}$ were computed neglecting all levels with index $i > 2$. The values of $P_{first\ order}$ were calculated using first order perturbation theory according to Eq. (28): The magnitudes of the matrix elements were taken from Table 1 except where explicitly noted and M_{12} was taken to be -0.756 in all cases.

TABLE 6

Least-squares fit of the matrix elements M_{12} and M_{22} to the measured quantities P_{exp} given in Table 3. The values of the other E2 matrix elements are taken from Table 1. The sign of M_{12} is arbitrarily chosen negative. The number of experimental points used for a fit is denoted by N_{exp}. Only random errors were included in fitting the data. In parentheses are the total errors.

Projectiles	N_{exp}	Signs of M_{14}	Signs of M_{17}	M_{12} $e \cdot 10^{-24}$ cm^2	M_{22} $e \cdot 10^{-24}$ cm^2	Chi-squared
				^{114}Cd		
^{16}O, ^{12}C, ^{4}He	17	-	-	$-0.749 \pm 0.003 (0.03)$	$+1.10 \pm 0.07 (0.19)$	24
		-	+	$-0.748 \pm 0.003 (0.03)$	$+1.00 \pm 0.07 (0.19)$	22
		+	-	$-0.748 \pm 0.003 (0.03)$	$+0.86 \pm 0.07 (0.19)$	21
		+	+	$-0.748 \pm 0.003 (0.03)$	$+0.77 \pm 0.07 (0.19)$	20
^{16}O	9	-	-	$-0.787 \pm 0.019 (0.03)$	$+1.7 \pm 0.4 (0.6)$	7.4
				^{116}Cd		
		M_{13}				
^{16}O, ^{12}C, ^{4}He	9	-		$-0.788 \pm 0.005 (0.03)$	$+1.39 \pm 0.14 (0.17)$	2.7
		+		$-0.788 \pm 0.005 (0.03)$	$+1.07 \pm 0.15 (0.18)$	2.9

$$B(E2, 0^+ \rightarrow 2^+) = (M_{12})^2 \, e^2 \cdot 10^{-48} \text{ cm}^4$$

$$Q_2 = -0.758 \, M_{22} \, e \cdot 10^{-24} \text{ cm}^2$$

TABLE 7

Results of a least-squares fit of the matrix elements M_{12} and M_{22} to the measured quantities P_{exp} given in Table 4. The values of the other matrix elements are taken from Table 2. The sign of M_{12} is arbitrarily chosen negative. Only random errors were used in the least-squares fit to the data. In parentheses are the total errors. In all cases the number of experimental points used in the least-squares fit was 7.

Sign of M_{14}	M_{12} ($e \cdot 10^{-24}$ cm^2)	M_{22} ($e \cdot 10^{-24}$ cm^2)	Chi-squared
		^{126}Te	
-	$-0.698 \pm 0.004(0.025)$	$+0.53 \pm 0.10(0.13)$	8.7
+	$-0.697 \pm 0.004(0.025)$	$+0.32 \pm 0.10(0.11)$	6.5
		^{128}Te	
-	$-0.625 \pm 0.004(0.023)$	$+0.35 \pm 0.09(0.17)$	9.2
+	$-0.624 \pm 0.004(0.023)$	$+0.14 \pm 0.09(0.13)$	8.3

$$B(E2, 0^+ \rightarrow 2^+) = (M_{12})^2 \, e^2 \cdot 10^{-48} \text{ cm}^4$$

$$Q_2 = -0.758 \, M_{22} \, e \cdot 10^{-24} \text{ cm}^2$$

FIGURE 1

Illustration of the terms which contribute to the excitation of state f from state i. The first and second order excitations are denoted by double arrows and the interference terms by single arrows. (Page 12)

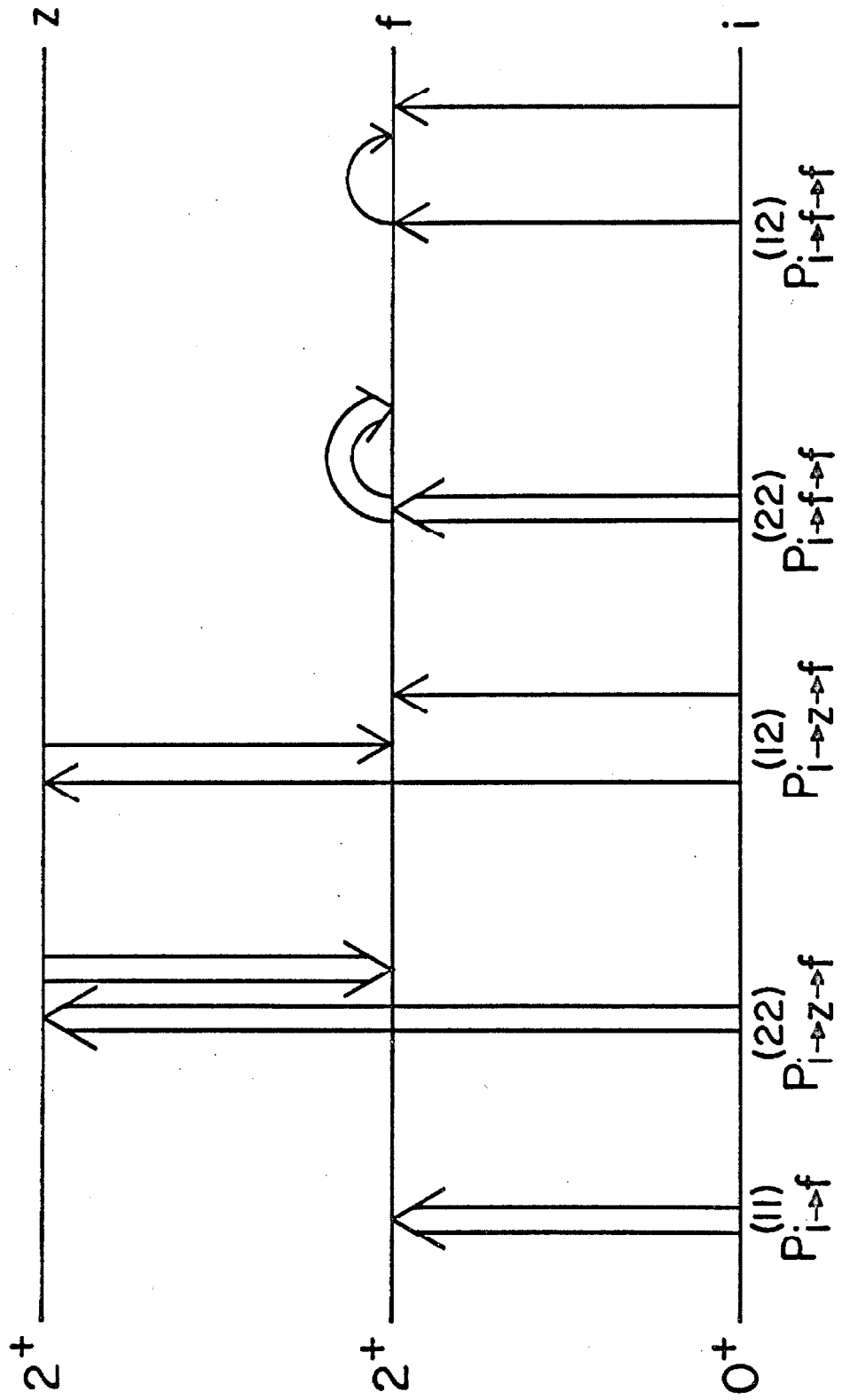
z
f
i
$P^{(12)}_{i\to f\to f}$
$P^{(22)}_{i\to f\to f}$
$P^{(12)}_{i\to z\to f}$
$P^{(22)}_{i\to z\to f}$
$P^{(11)}_{i\to f}$
2^+
2^+
0^+

FIGURE 1

FIGURE 2

The quantity $K(\xi_{fi}, \theta)$ defined in (25) plotted as a function of ξ_{fi}. The small slope of the curves indicates the weak dependence of the function ρ on the bombarding energy. (Page 15)

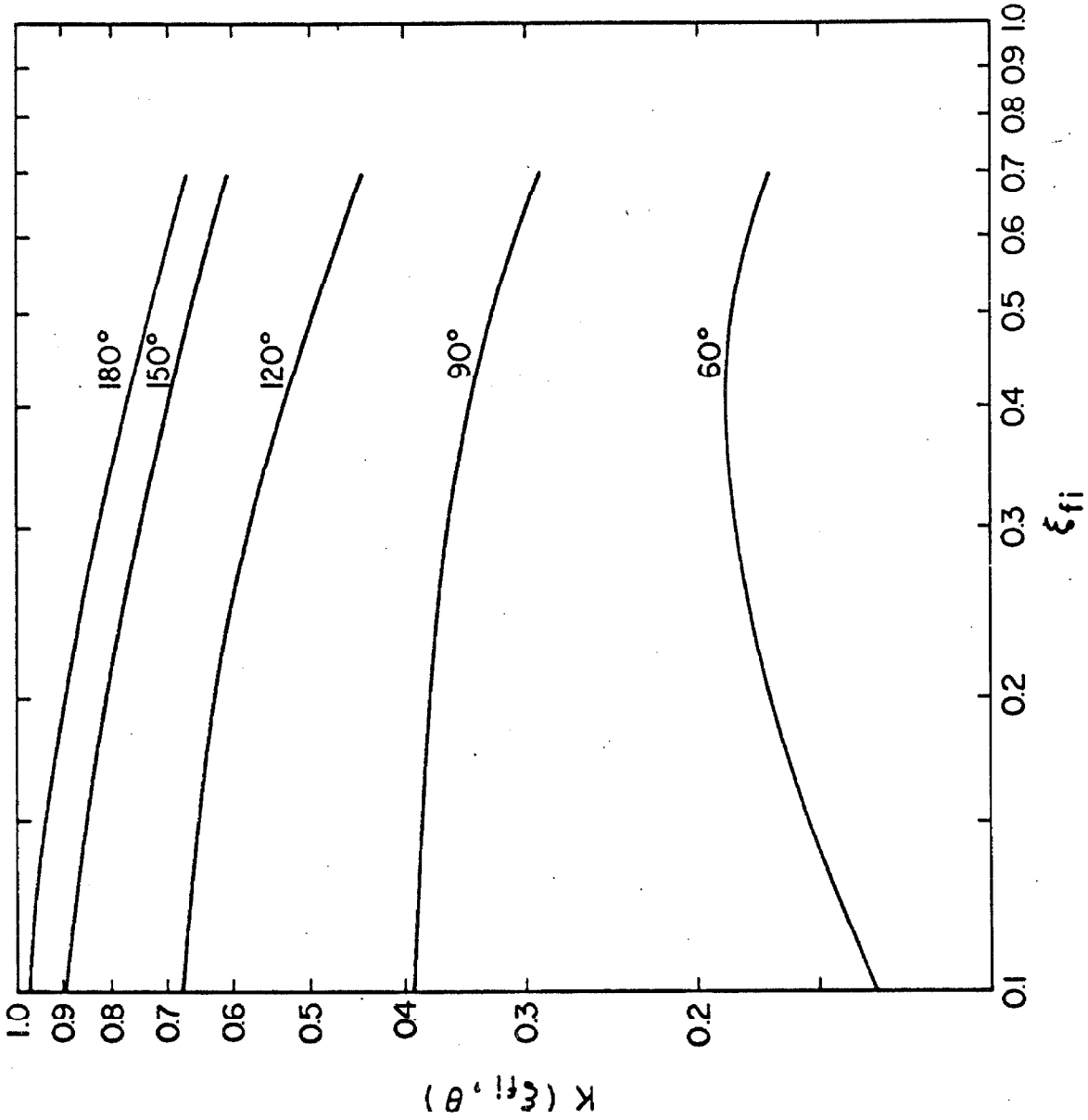

FIGURE 2

FIGURE 3

The interaction constant $\chi_{i \to f}$ defined in (12) calculated for the excitation of the first 2^+ state in ^{114}Cd. The curves span an energy range from 0.1 to 1.0 times the Coulomb barrier and were calculated using a value of B(E2, $0^+ \to 2^+$) = 0.50 $e^2 \cdot 10^{-48}$ cm^4. (Page 18)

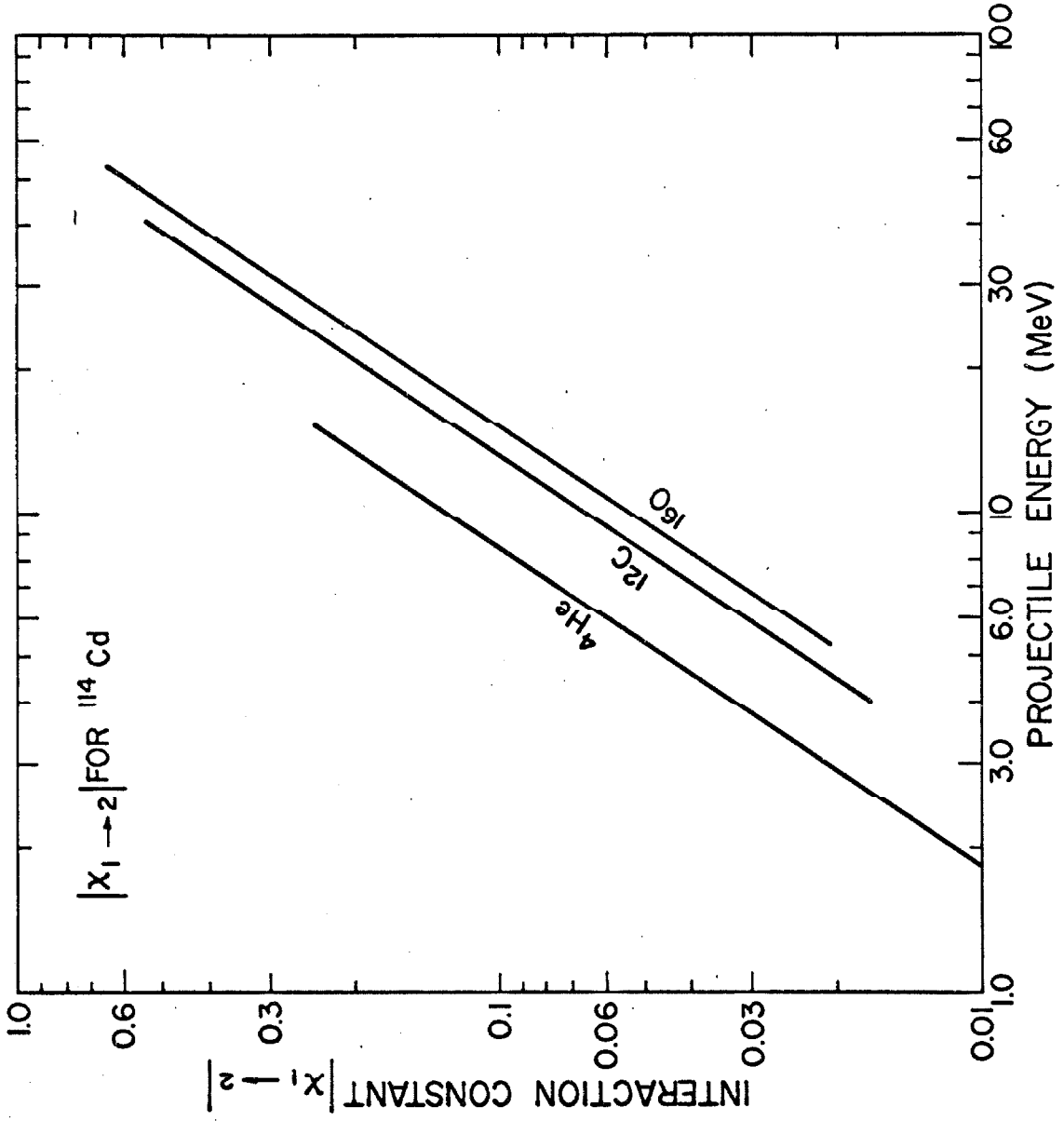
INTERACTION CONSTANT $|\chi_{1-2}|$
1.0
0.6
0.3
0.1
0.06
0.03
0.01
$|\chi_{1-2}|$ FOR ^{114}Cd
^{4}He
^{12}C
^{16}O
1.0
3.0
6.0
10
30
60
100
PROJECTILE ENERGY (MeV)

FIGURE 3

FIGURE 4

The arrangement of the detectors and beam collimation system within the target chamber (side view). The arrow indicates the direction of the beam. The items numbered (1) through (5) comprise the beam collimation system. (1), (3) and (5) denote tantalum collimators with inside diameters of 1.5, 1.8 and 2.0 mm, respectively. A lead spacer (2) minimized background gamma radiation from the first tantalum collimator (1). Collimators (3) and (5), separated by an aluminum spacer (4) prevented the beam scattered from (1) from striking the back-side of the solid state detector (6). The sensitive surface of the solid state detector had outside and inside diameters of 10 and 4 mm, respectively. The target (7) was placed about one centimeter from the sensitive area of the solid state detector. The face of the NaI detector (8) was 3.3 cm from the target and the beam stop (not shown) was about two meters from the target. (Page 21)

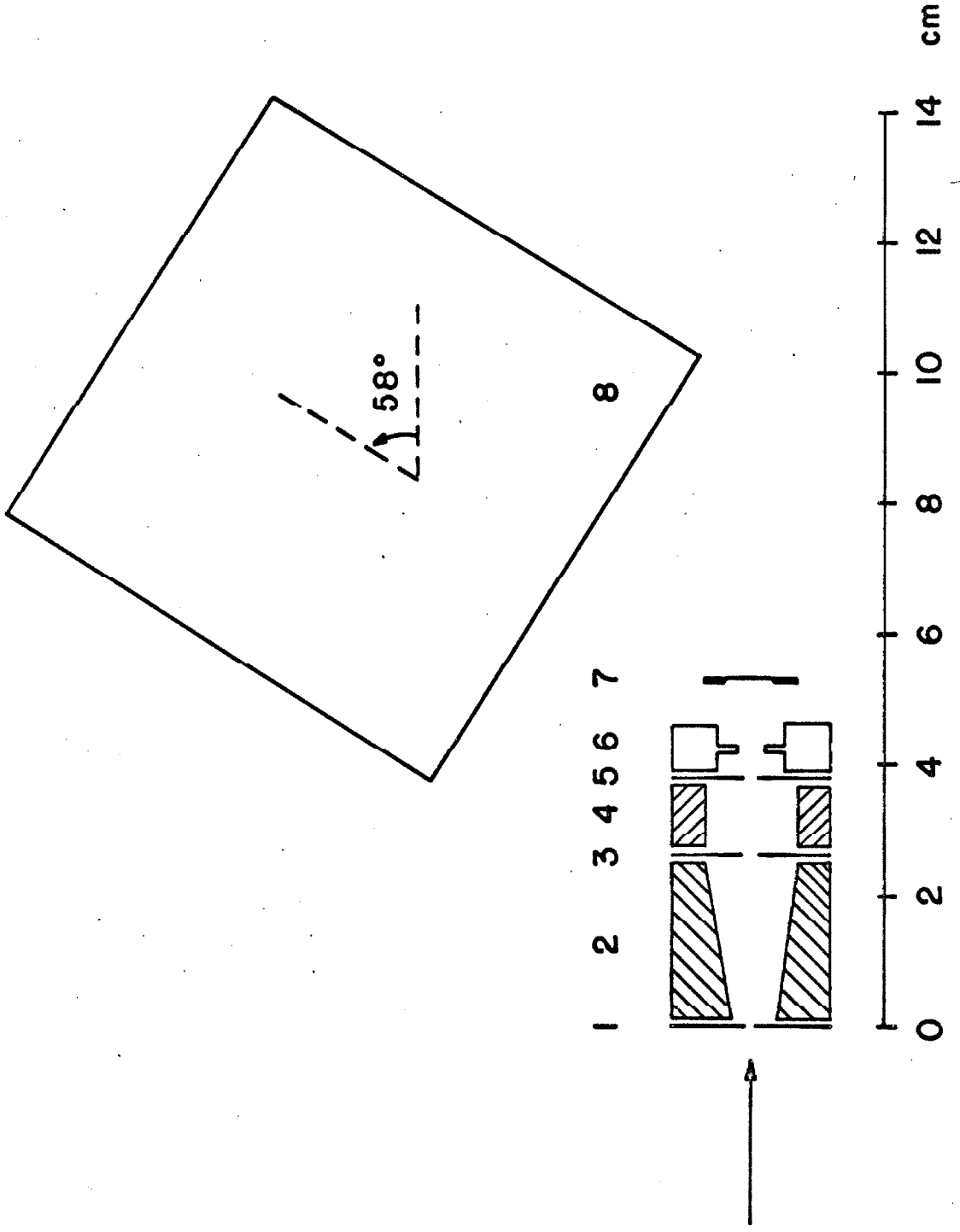

FIGURE 4

FIGURE 5

Block diagram of the electronic apparatus. (Page 22)

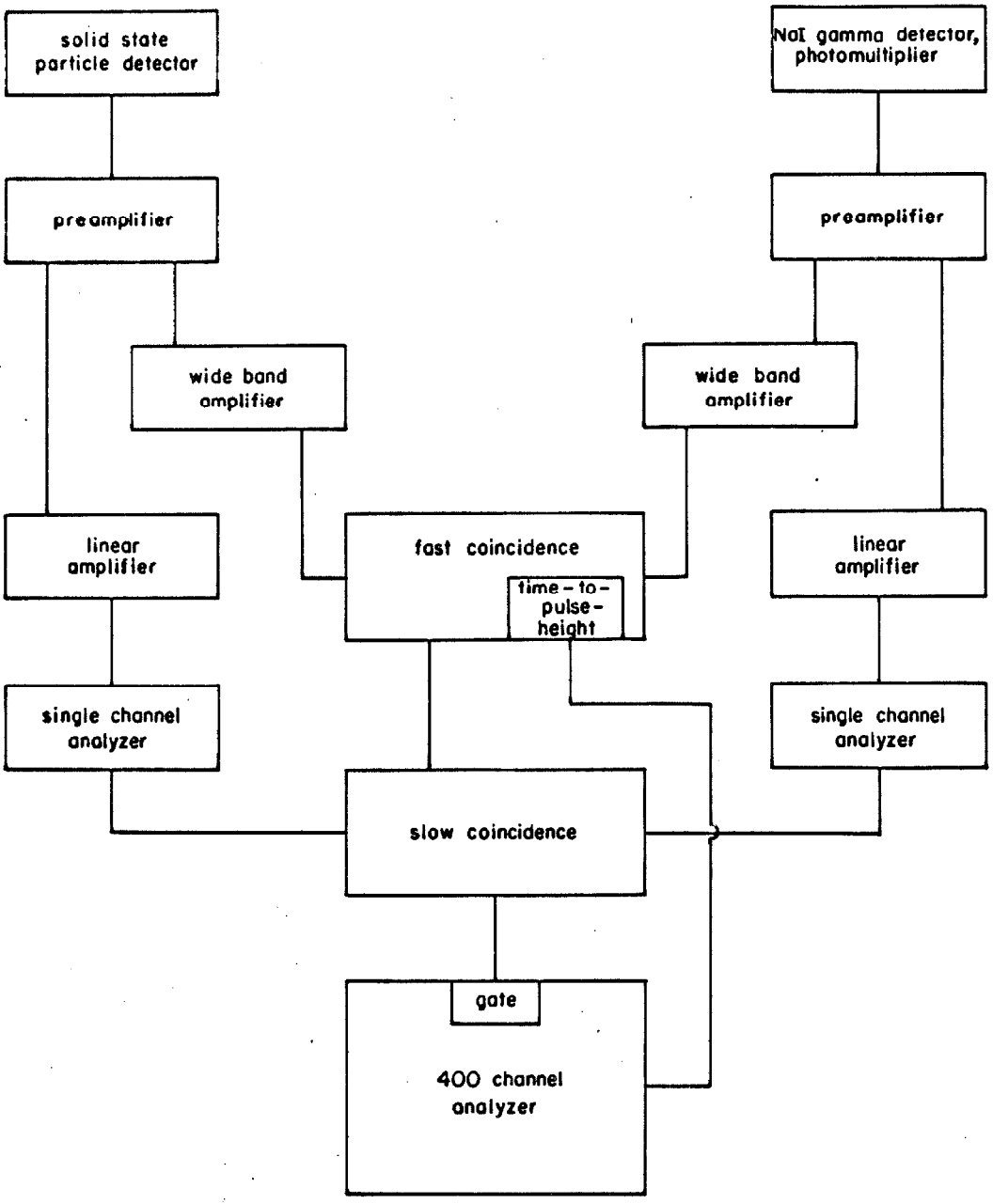
solid state particle detector
NaI gamma detector, photomultiplier
preamplifier
preamplifier
wide band amplifier
wide band amplifier
linear amplifier
fast coincidence
time-to-pulse-height
linear amplifier
single channel analyzer
single channel analyzer
slow coincidence
gate
400 channel analyzer

FIGURE 5

FIGURE 6

Gamma-ray spectra from the bombardment of ^{114}Cd by ^{16}O ions. The window used to gate the time-to-pulse-height spectrum is indicated. (Page 23)

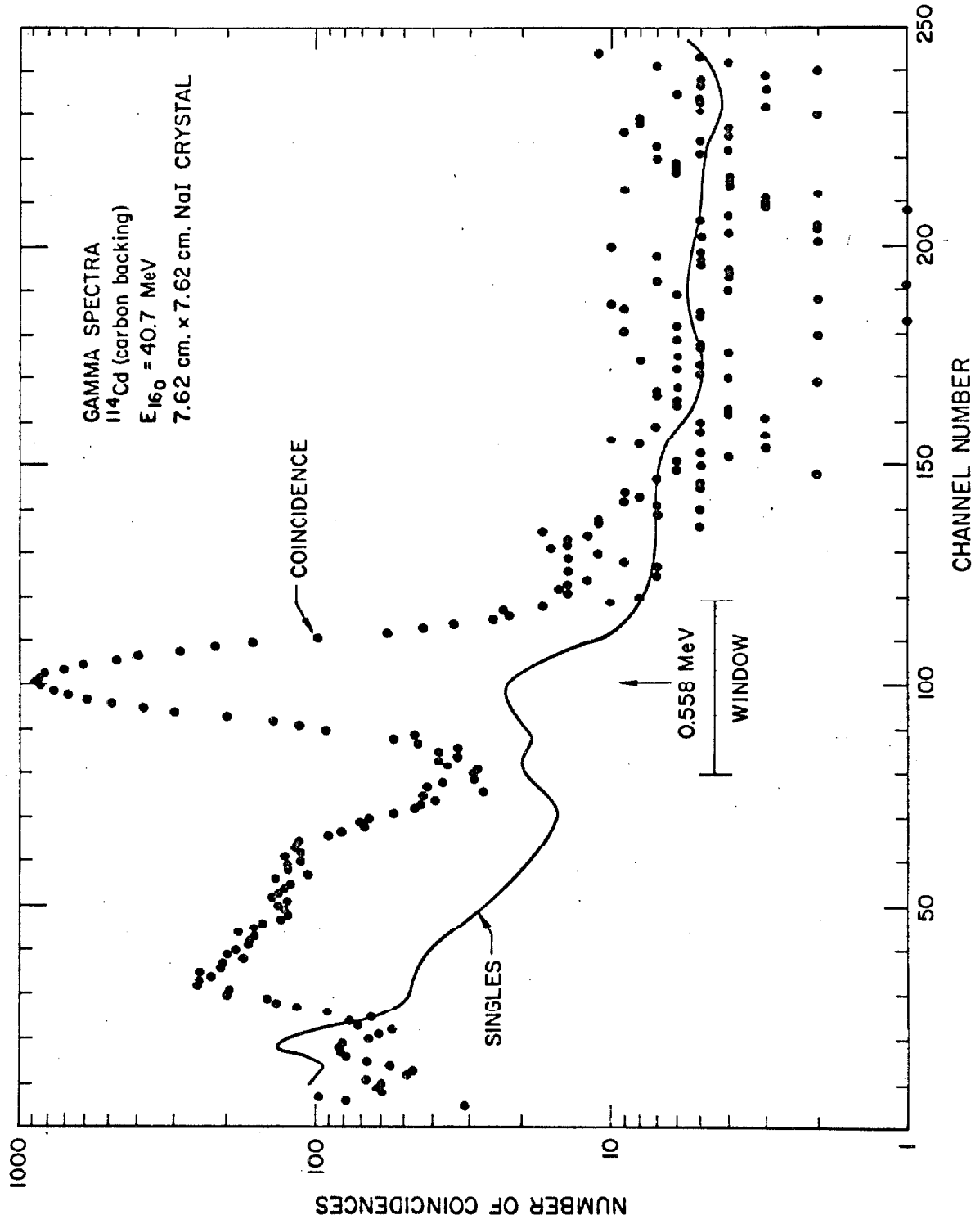
GAMMA SPECTRA
^{114}Cd (carbon backing)
E_{16_O} = 40.7 MeV
7.62 cm. x 7.62 cm. NaI CRYSTAL
COINCIDENCE
SINGLES
0.558 MeV
WINDOW
NUMBER OF COINCIDENCES
CHANNEL NUMBER
1000
100
10
1
50
100
150
200
250

FIGURE 6

FIGURE 7

Gamma-ray spectra from the bombardment of ^{128}Te by ^{16}O ions. The window used to gate the time-to-pulse-height spectrum is indicated. (Page 23)

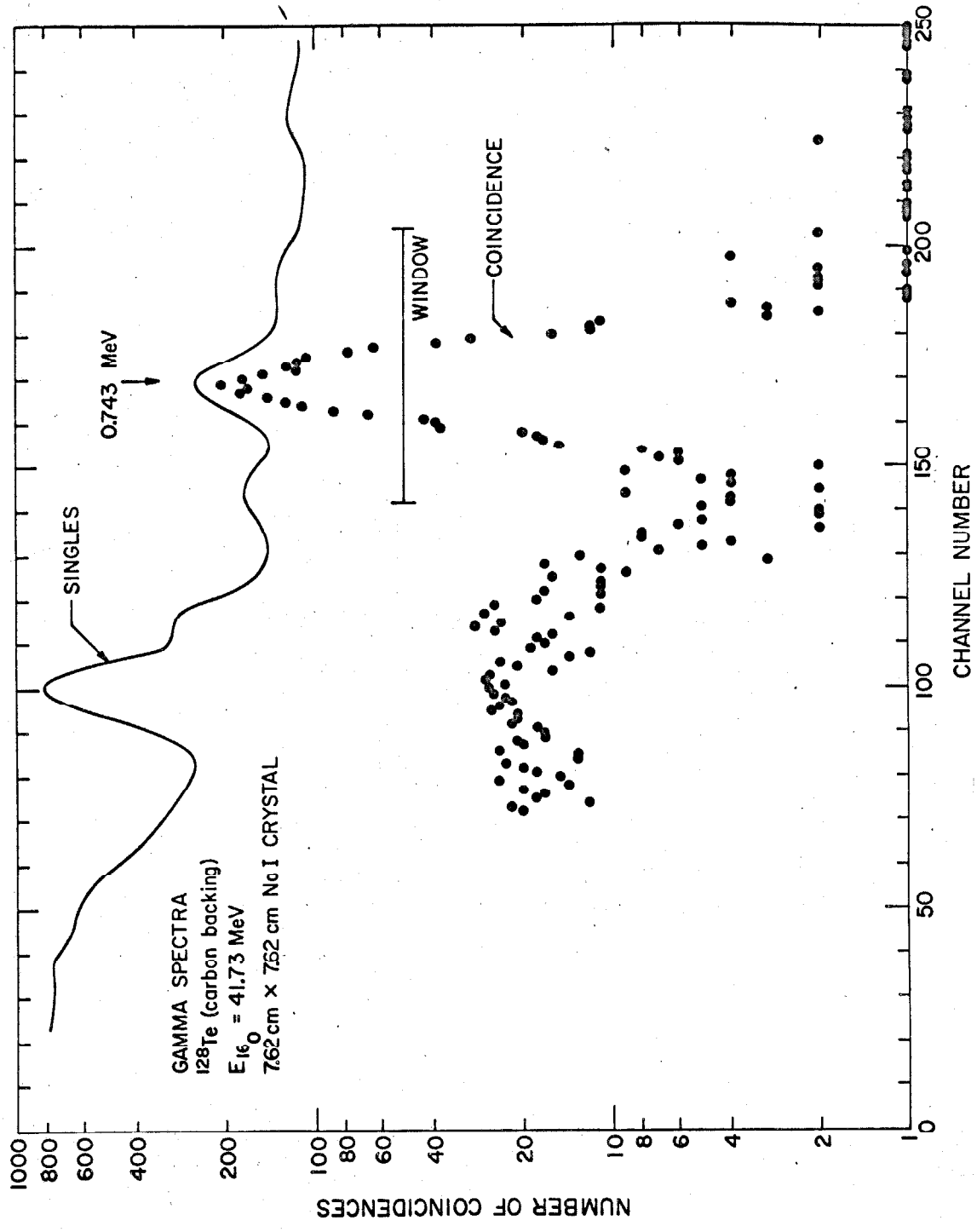
GAMMA SPECTRA
128Te (carbon backing)
E16O = 41.73 MeV
7.62 cm × 7.62 cm NaI CRYSTAL
SINGLES
0.743 MeV
WINDOW
COINCIDENCE
NUMBER OF COINCIDENCES
CHANNEL NUMBER
1000
800
600
400
200
100
80
60
40
20
10
8
6
4
2
1
0
50
100
150
200
250

FIGURE 7

FIGURE 8

Spectrum of ^{16}O ions scattered from ^{114}Cd in the angular range $155^{o} < \theta < 175^{o}$. The elastic and inelastic groups are not resolved. The window used to gate the time-to-pulse-height spectrum is indicated. (Page 23)

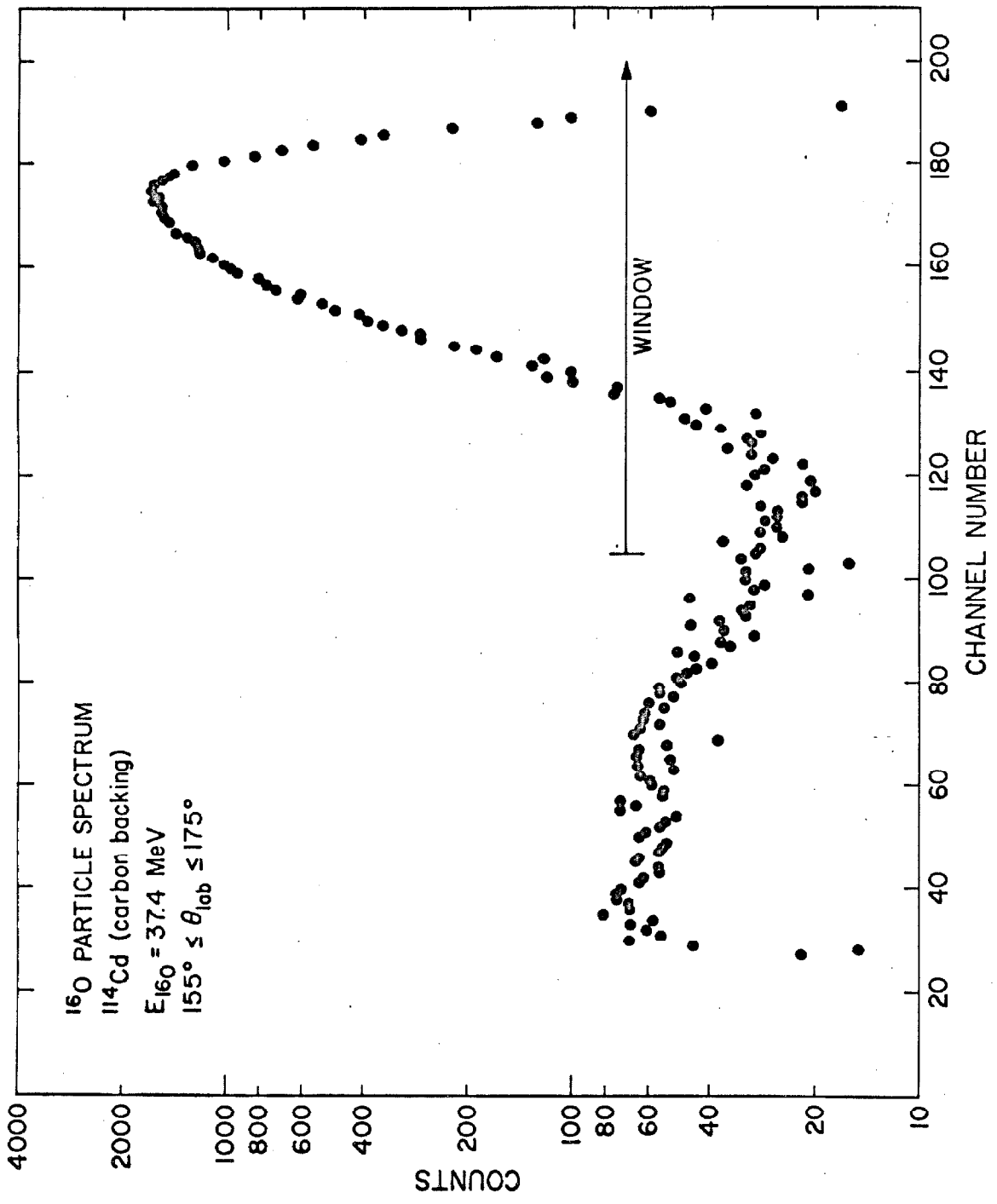
^{16}O PARTICLE SPECTRUM
^{114}Cd (carbon backing)
$E_{16O} = 37.4$ MeV
$155° \leq \theta_{lab} \leq 175°$
WINDOW
COUNTS
CHANNEL NUMBER
4000
2000
1000
800
600
400
200
100
80
60
40
20
10
20
40
60
80
100
120
140
160
180
200

FIGURE 8

FIGURE 9

Spectrum of ^{16}O ions scattered from ^{128}Te in the angular range $155^{o} < \theta < 175^{o}$. The elastic and inelastic groups are not resolved. The window used to gate the time-to-pulse-height spectrum is indicated. (Page 23)

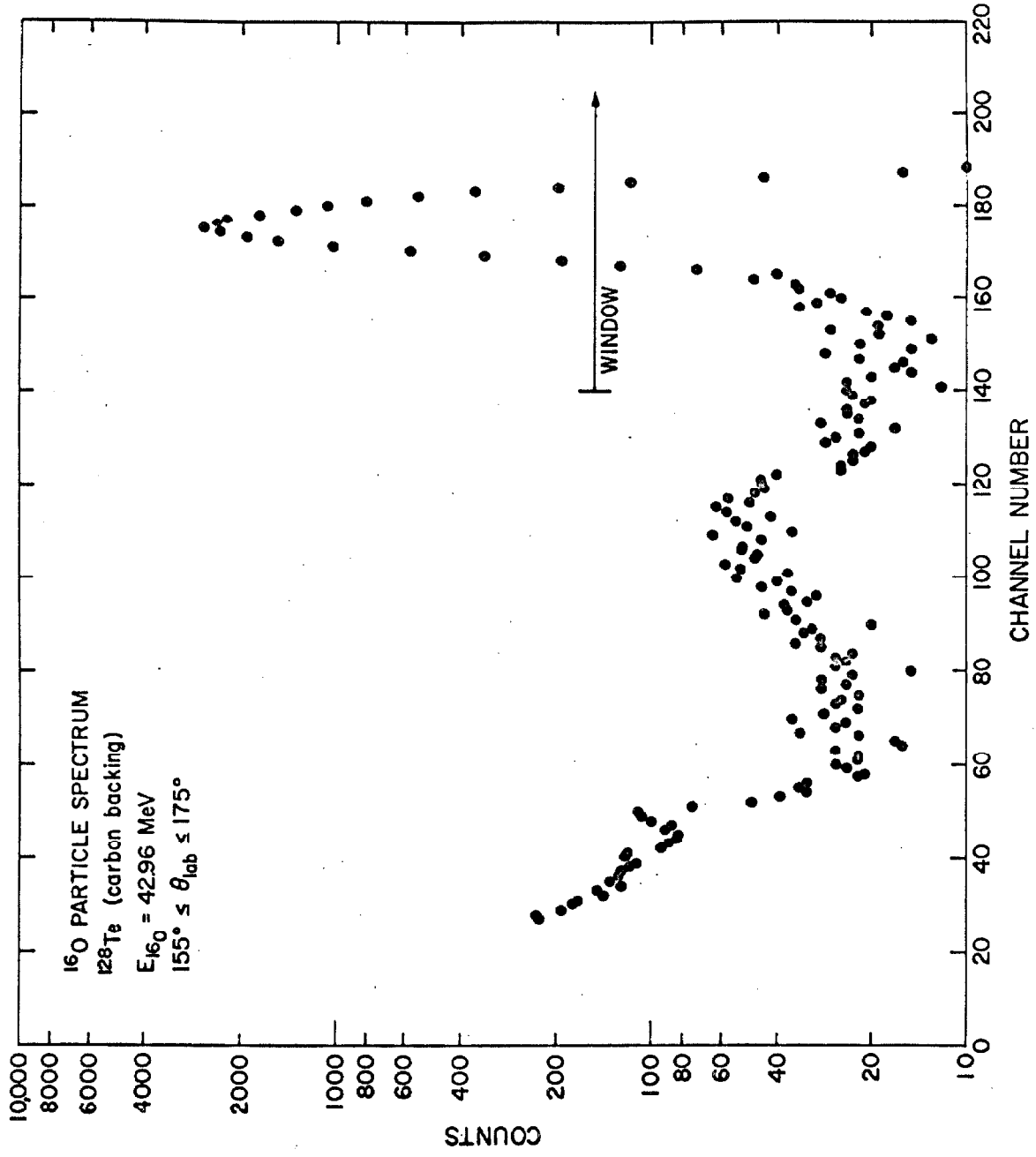
^{16}O PARTICLE SPECTRUM
^{128}Te (carbon backing)
$E_{^{16}O}$ = 42.96 MeV
155° ≤ θ_{lab} ≤ 175°
WINDOW
COUNTS
CHANNEL NUMBER
10,000
8000
6000
4000
2000
1000
800
600
400
200
100
80
60
40
20
10
0
20
40
60
80
100
120
140
160
180
200
220

FIGURE 9

FIGURE 10

Typical time-to-pulse-height spectrum; the spectra obtained in the bombardment of ^{114}Cd, ^{116}Cd, ^{126}Te and ^{128}Te were all similar. The small slope in the randoms background is due to a slight asymmetry in the timing pulses. The FWHM corresponds to a time resolution of 4.7 nanoseconds; the yield was counted over the base-width of about 22 nanoseconds. The subtraction of randoms background amounted typically to about 2% of the peak. (Page 23)

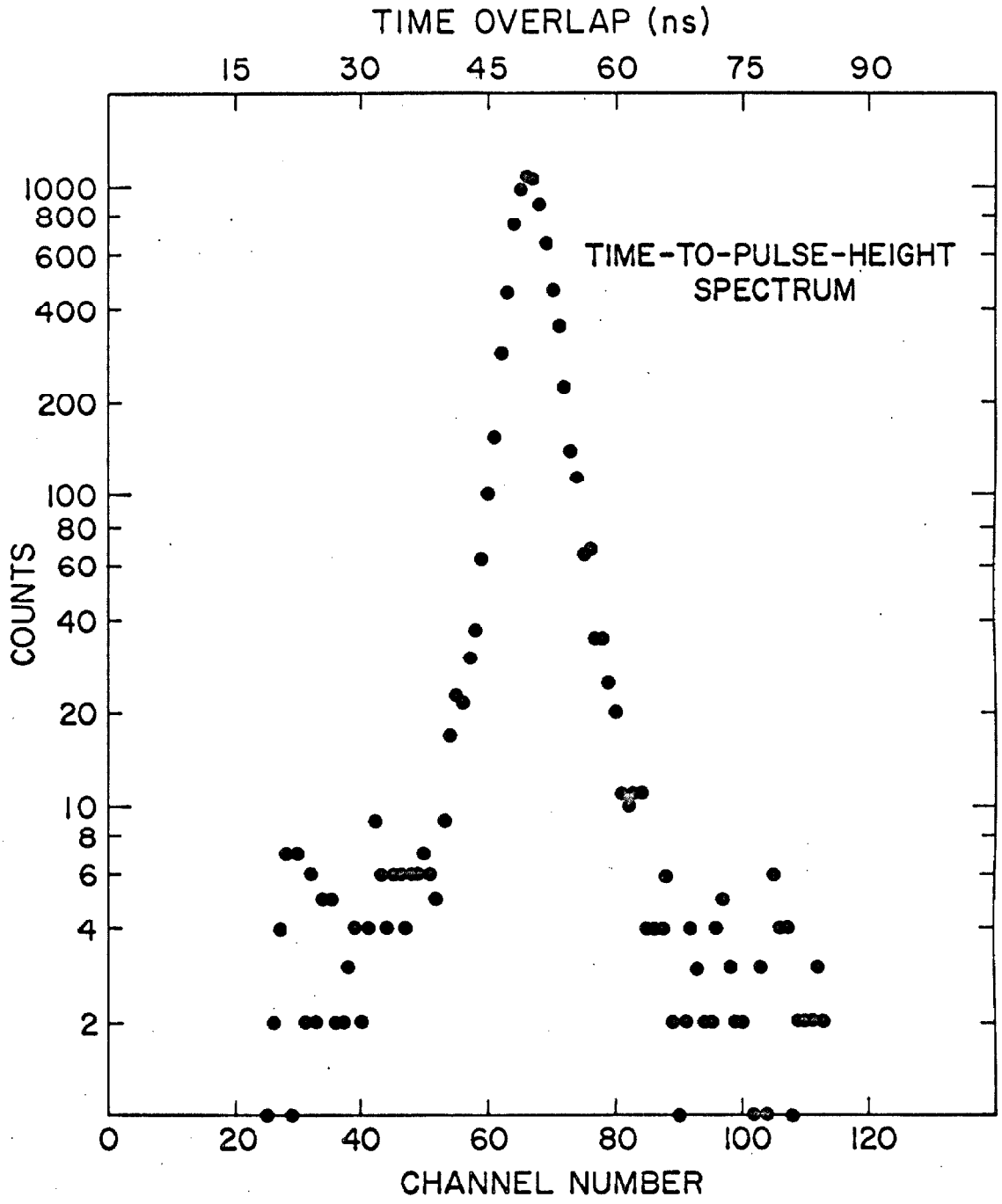
TIME OVERLAP (ns)
15
30
45
60
75
90
TIME-TO-PULSE-HEIGHT
SPECTRUM
COUNTS
1000
800
600
400
200
100
80
60
40
20
10
8
6
4
2
0
20
40
60
80
100
120
CHANNEL NUMBER

FIGURE 10

FIGURE 11

Level schemes of ^{114}Cd and ^{116}Cd. The matrix elements M_{rs} included in the analysis are indicated by arrows. The values of M_{rs} are given in Table 1. (Page 24)

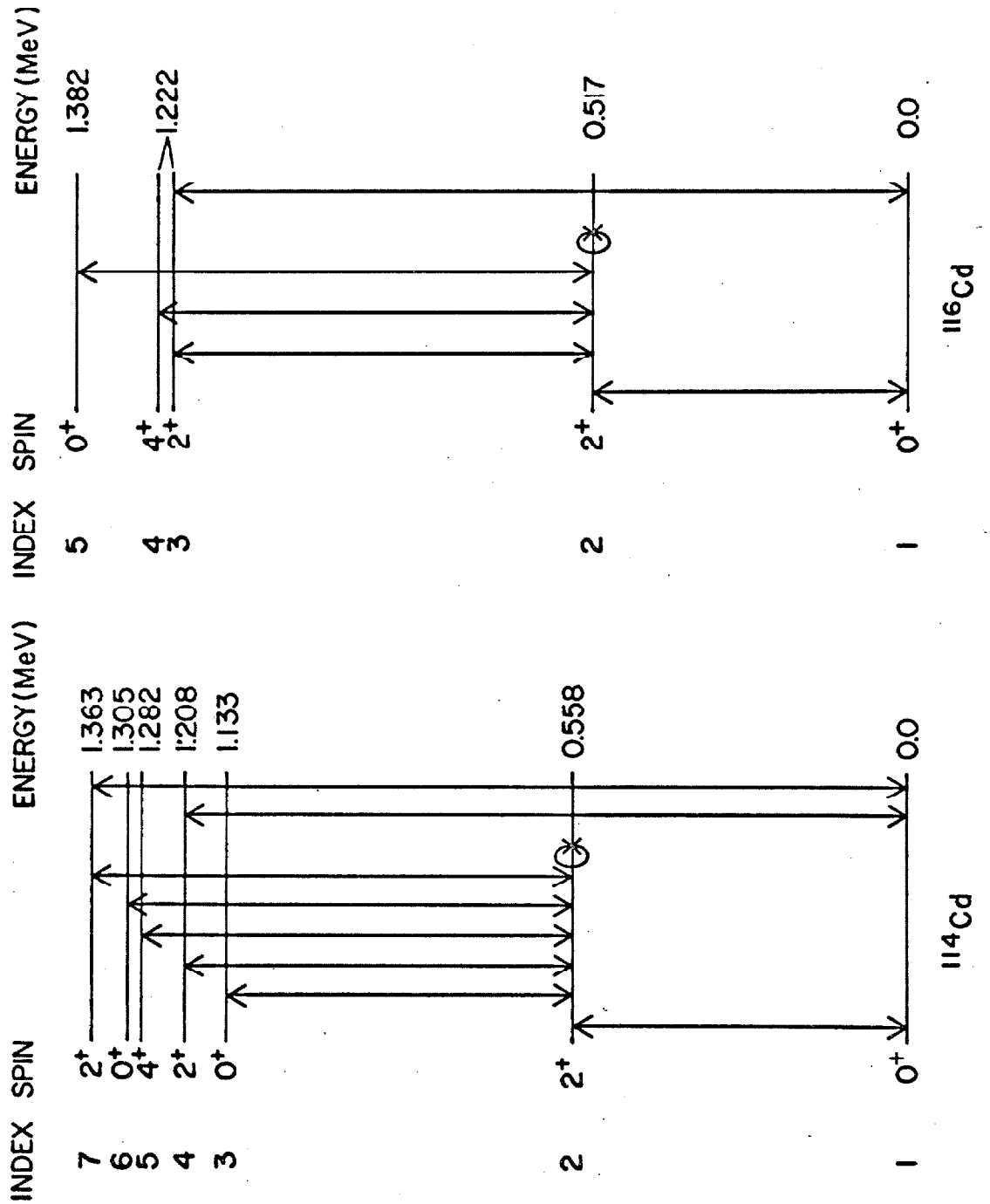
ENERGY (MeV)
INDEX
SPIN
1.382
1.222
0.517
0.0
5
4
3
2
1
0+
4+
2+
2+
0+
116Cd
ENERGY (MeV)
INDEX
SPIN
1.363
1.305
1.282
1.208
1.133
0.558
0.0
7
6
5
4
3
2
1
2+
0+
4+
2+
0+
2+
0+
114Cd

FIGURE 11

FIGURE 12

Level schemes of ^{126}Te and ^{128}Te. The energies and spins are taken from Cookson and Darcey, (1965). The matrix elements M_{rs} included in the analysis are indicated by arrows and are given in Table 2. (Page 24)

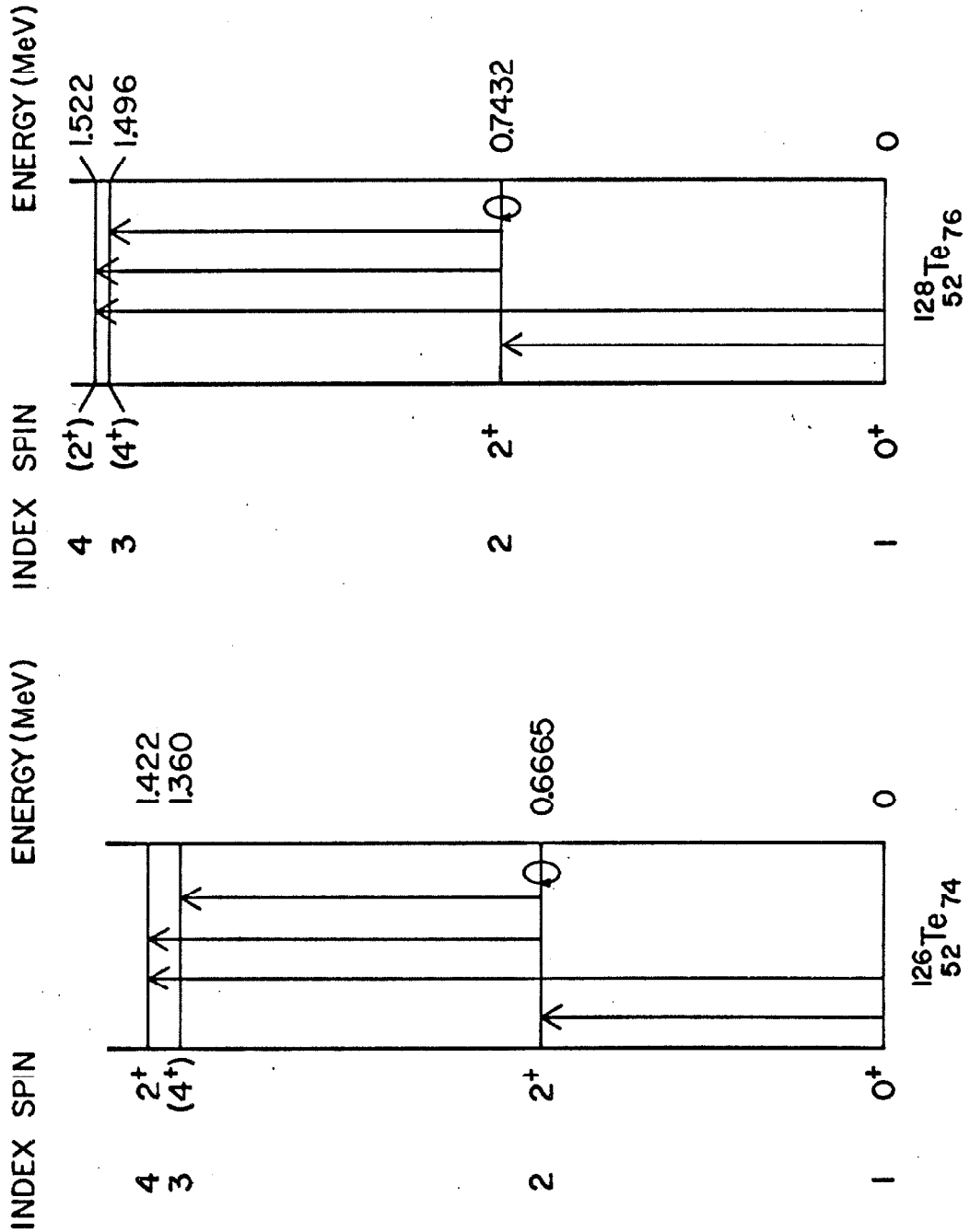
ENERGY (MeV)
1.522
1.496
0.7432
0
INDEX
SPIN
4
3
2
1
(2+)
(4+)
2+
0+
128 52Te76
ENERGY (MeV)
1.422
1.360
0.6665
0
INDEX
SPIN
4
3
2
1
2+
(4+)
2+
0+
126 52Te74

FIGURE 12

FIGURE 13

Spectra of ^{4}He ions scattered from ^{114}Cd in the angular range $155^{o} < \theta < 175^{o}$. The position of the window used to gate the time-to-pulse-height spectrum is indicated. The three large peaks in the singles spectrum are due to scattering from cadmium, oxygen, and carbon, respectively. The smaller peaks are due to ^{4}He ions which have lost some of their energy in passing through the dead layers on the surface edges of the sensitive area of the counter. The coincidence spectrum shows a displacement relative to the singles spectrum due to the lower energy of the inelastically scattered projectiles. A small peak in the coincidence spectrum due to random coincidences appears at the energy of the elastic peak. The peak-to-tail ratios for the singles and coincidence spectra are seen to be the same, indicating that all the counts above the window are due to scattering from cadmium.

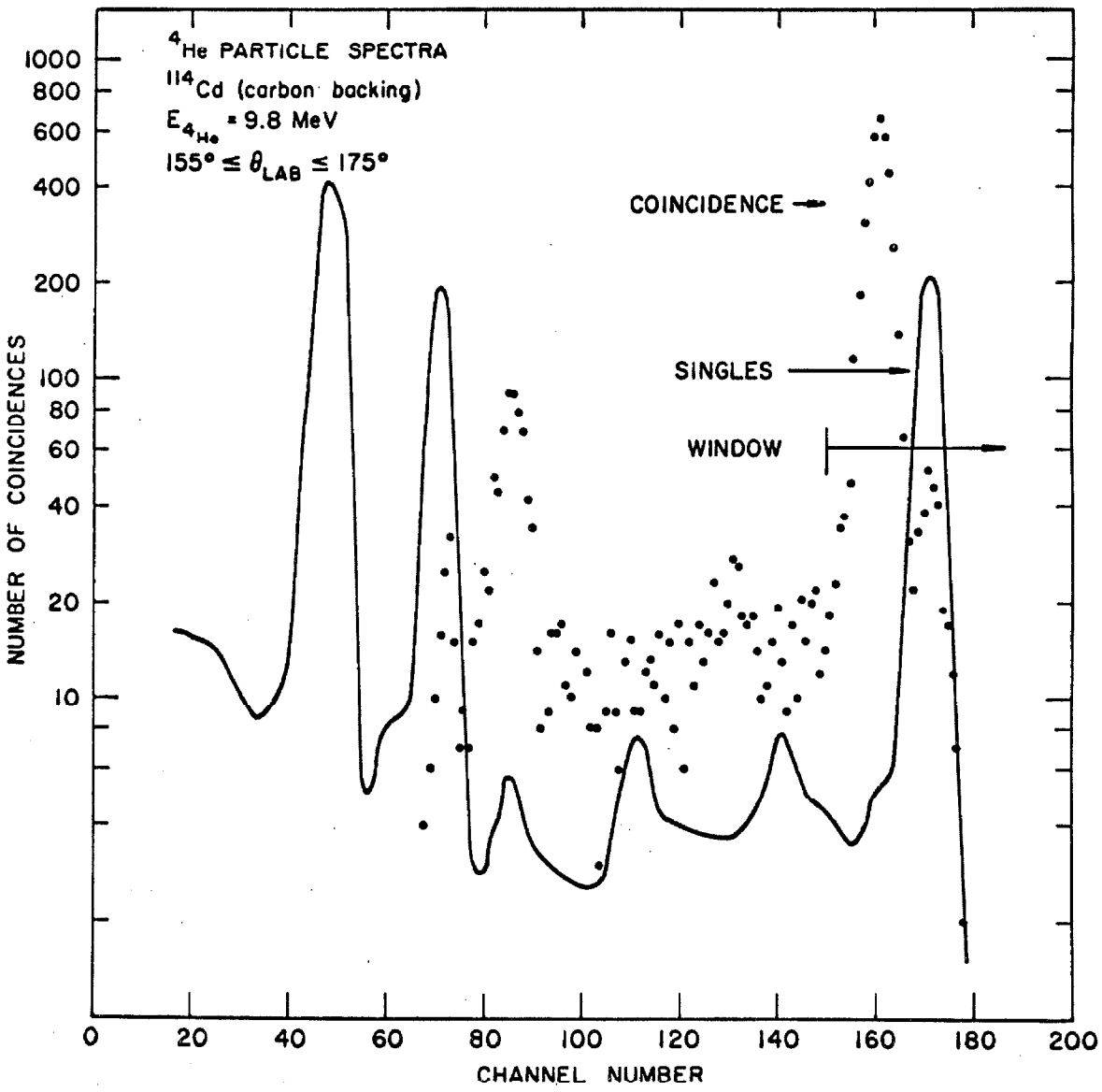
^{4}He PARTICLE SPECTRA
^{114}Cd (carbon backing)
$E_{^4He}$ = 9.8 MeV
155° ≤ θ_{LAB} ≤ 175°
COINCIDENCE
SINGLES
WINDOW
NUMBER OF COINCIDENCES
1000
800
600
400
200
100
80
60
40
20
10
0
20
40
60
80
100
120
140
160
180
200
CHANNEL NUMBER

FIGURE 13

FIGURE 14

Comparison of the experimental quantities $P = d\sigma_2/\Sigma_i d\sigma_i$ for ^4He, ^{12}C, and ^{16}O bombardment of ^{114}Cd with those calculated in first order perturbation theory. The deviations from unity are attributed mainly to the quadrupole moment of the first 2^+ state. The three solid lines represent the results of a computer calculation in which the two parameters M_{12} and M_{22} were varied to obtain the best fit to the experimental data. $P_{\text{first order}}$ was calculated using the fitted value of M_{12}. The dotted points were not included in the analysis. The experimental errors and those quoted for M_{12} and M_{22} are random only. (Pages 29, 35)

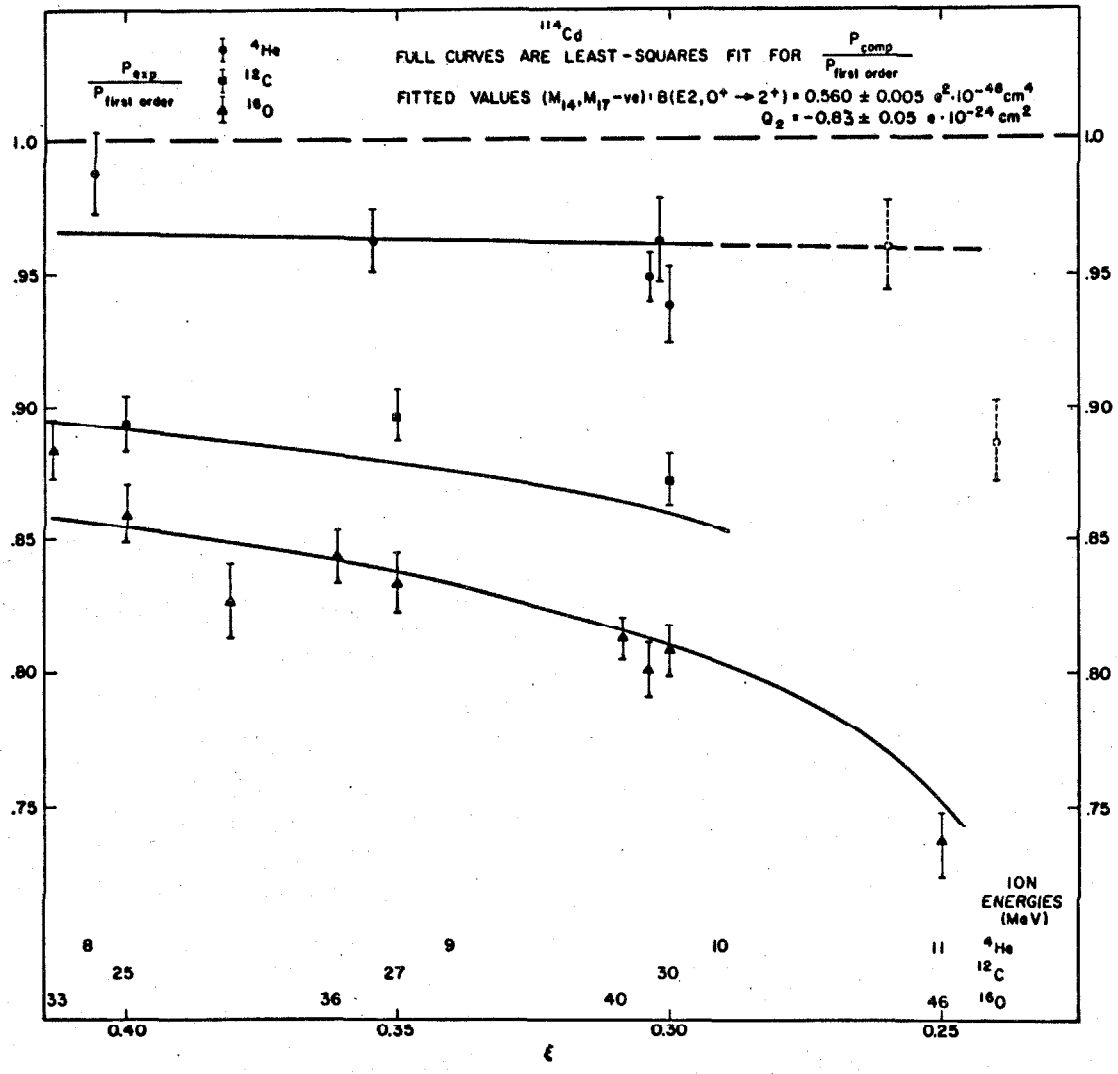
^{114}Cd
FULL CURVES ARE LEAST-SQUARES FIT FOR $\frac{P_{comp}}{P_{first\ order}}$
FITTED VALUES $(M_{14}, M_{17}-ve)\cdot B(E2, 0^+ \rightarrow 2^+) = 0.560 \pm 0.005\ e^2 \cdot 10^{-48} cm^4$
$Q_2 = -0.83 \pm 0.05\ e \cdot 10^{-24} cm^2$
$\frac{P_{exp}}{P_{first\ order}}$
^{4}He
^{12}C
^{16}O
1.0
.95
.90
.85
.80
.75
ION ENERGIES (MeV)
8
9
10
11
^{4}He
25
27
30
^{12}C
33
36
40
46
^{16}O
0.40
0.35
0.30
0.25
ε

FIGURE 14

FIGURE 15

Analogue of Figure 14 for ^{116}Cd. (Pages 29, 35)

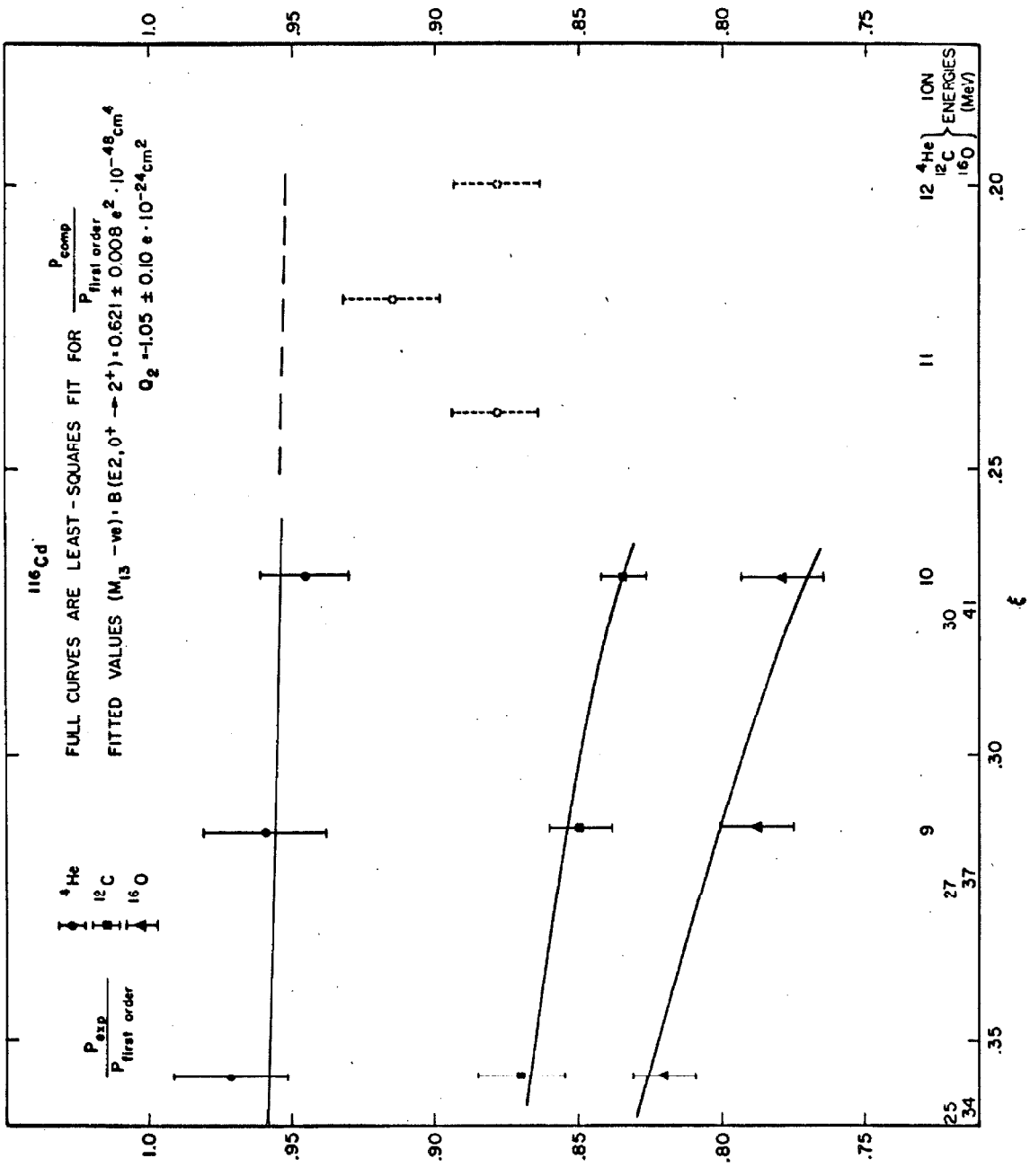
116Cd
FULL CURVES ARE LEAST-SQUARES FIT FOR P_comp / P_first order
FITTED VALUES (M13 -ve) · B(E2, 0+ → 2+) = 0.621 ± 0.008 e² · 10⁻⁴⁸ cm⁴
Q2 = -1.05 ± 0.10 e · 10⁻²⁴ cm²
P_exp / P_first order
4He
12C
16O
ION ENERGIES (MeV)
12 4He
12C
16O
ξ
1.0
.95
.90
.85
.80
.75
.20
.25
.30
.35
11
10
9
30
41
27
37
25
34

FIGURE 15

FIGURE 16

Comparison of the experimental quantities P_{exp} for ^{4}He and ^{16}O bombardment of ^{126}Te with those calculated from first order perturbation theory. The deviations from unity are attributed mainly to the quadrupole moment of the first 2^{+} state. The solid lines represent the results of a computer calculation in which the two parameters M_{12} and M_{22} were varied to fit the experimental data. $P_{first\ order}$ was calculated using the fitted value of M_{12}. The dotted ^{4}He points were not included in the analysis. The experimental errors and those quoted for M_{12} and M_{22} are random only. (Pages 29, 35)

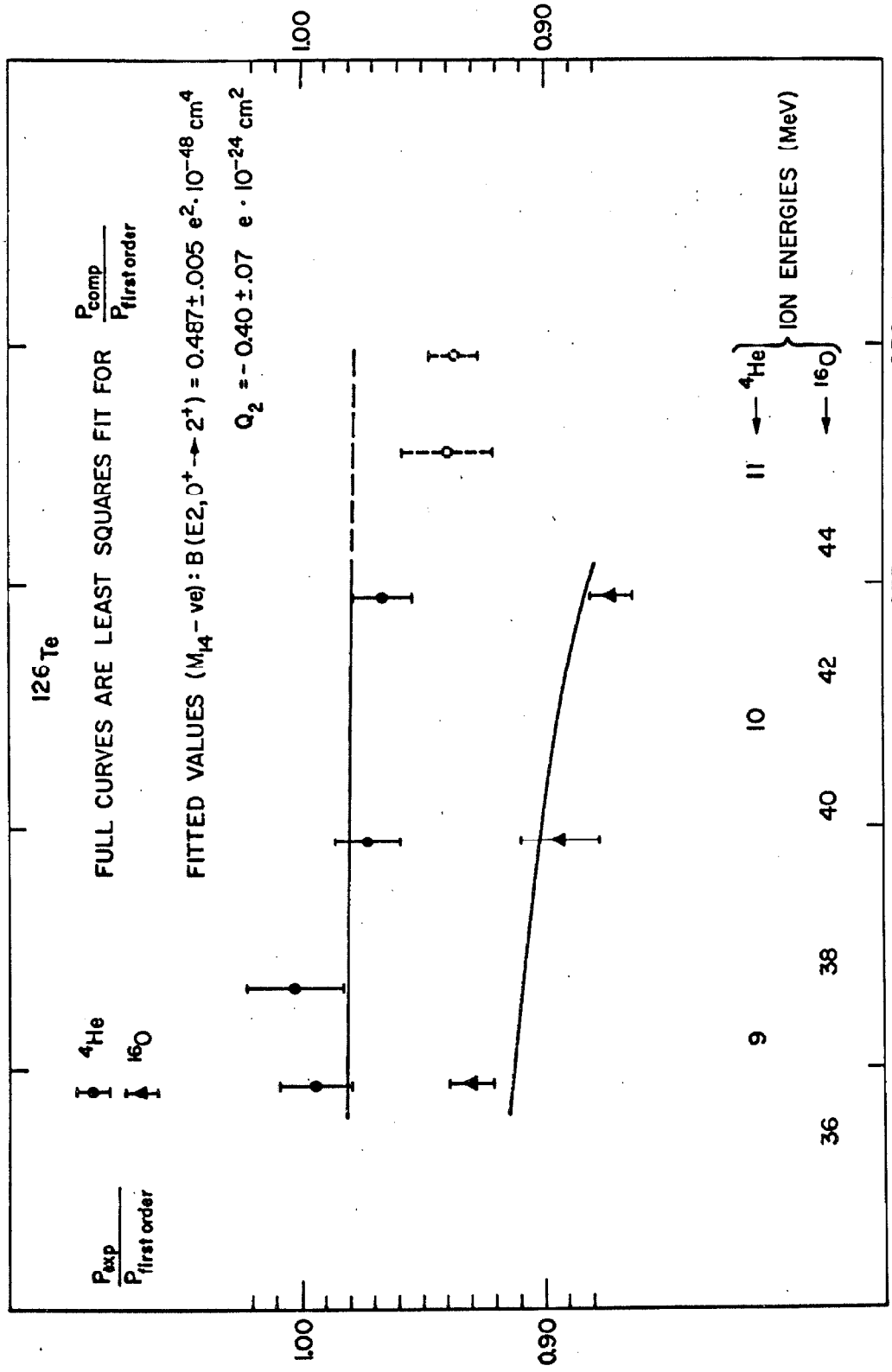
^{126}Te
FULL CURVES ARE LEAST SQUARES FIT FOR $\frac{P_{comp}}{P_{first\ order}}$
FITTED VALUES (M_{14} - ve): B(E2, $0^+ \rightarrow 2^+$) = 0.487±.005 $e^2 \cdot 10^{-48}$ cm^4
Q_2 = - 0.40 ± .07 e · 10^{-24} cm^2
^{4}He
^{16}O
$\frac{P_{exp}}{P_{first\ order}}$
1.00
0.90
ION ENERGIES (MeV)
^{4}He
^{16}O
9
10
11
36
38
40
42
44
0.30
0.35
0.40
0.45
ξ

FIGURE 16.

FIGURE 17

Analogue of Figure 16 for ^{128}Te. (Pages 29, 35)

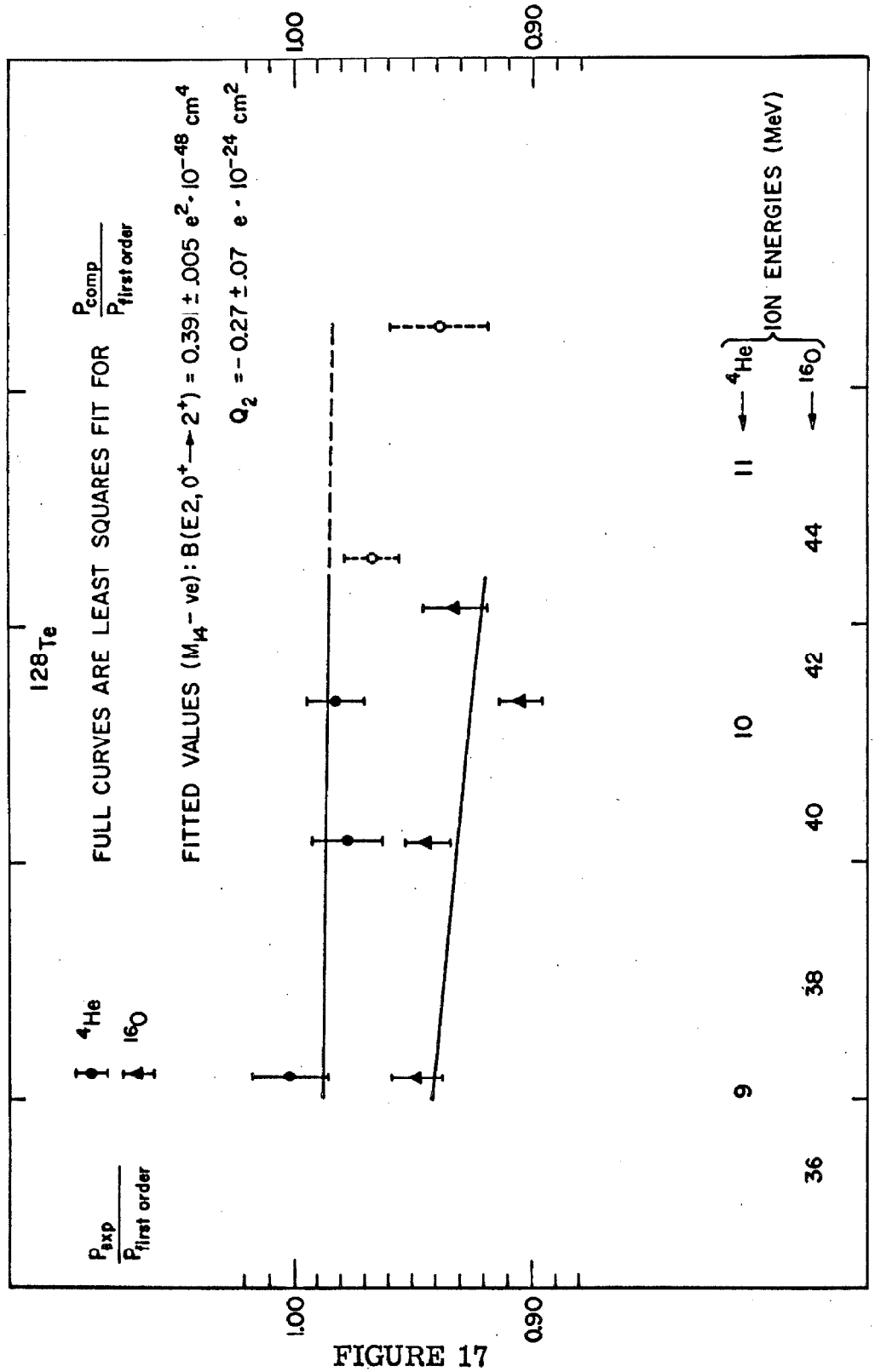
128Te
FULL CURVES ARE LEAST SQUARES FIT FOR $\frac{P_{comp}}{P_{first\ order}}$
FITTED VALUES (M_{14} - ve): B(E2, $0^+ \rightarrow 2^+$) = 0.39 ± .005 $e^2 \cdot 10^{-48}$ cm^4
Q_2 = - 0.27 ± .07 e · 10^{-24} cm^2
$\frac{P_{exp}}{P_{first\ order}}$
4He
16O
1.00
0.90
9
10
11
36
38
40
42
44
ION ENERGIES (MeV)
4He
16O
0.50
0.45
0.40
0.35
ξ

FIGURE 17

FIGURE 18

The data and least-squares fit of Figure 14 replotted but now normalized to P_{comp} ($Q_2 = 0$), the latter being the value of P computed with $M_{22} = Q_2 = 0$ and with all other matrix elements the same as before. Here the dispersion between curves corresponding to the different bombarding ions is due entirely to a non-zero quadrupole moment of the first 2^+ state. (Page 37)

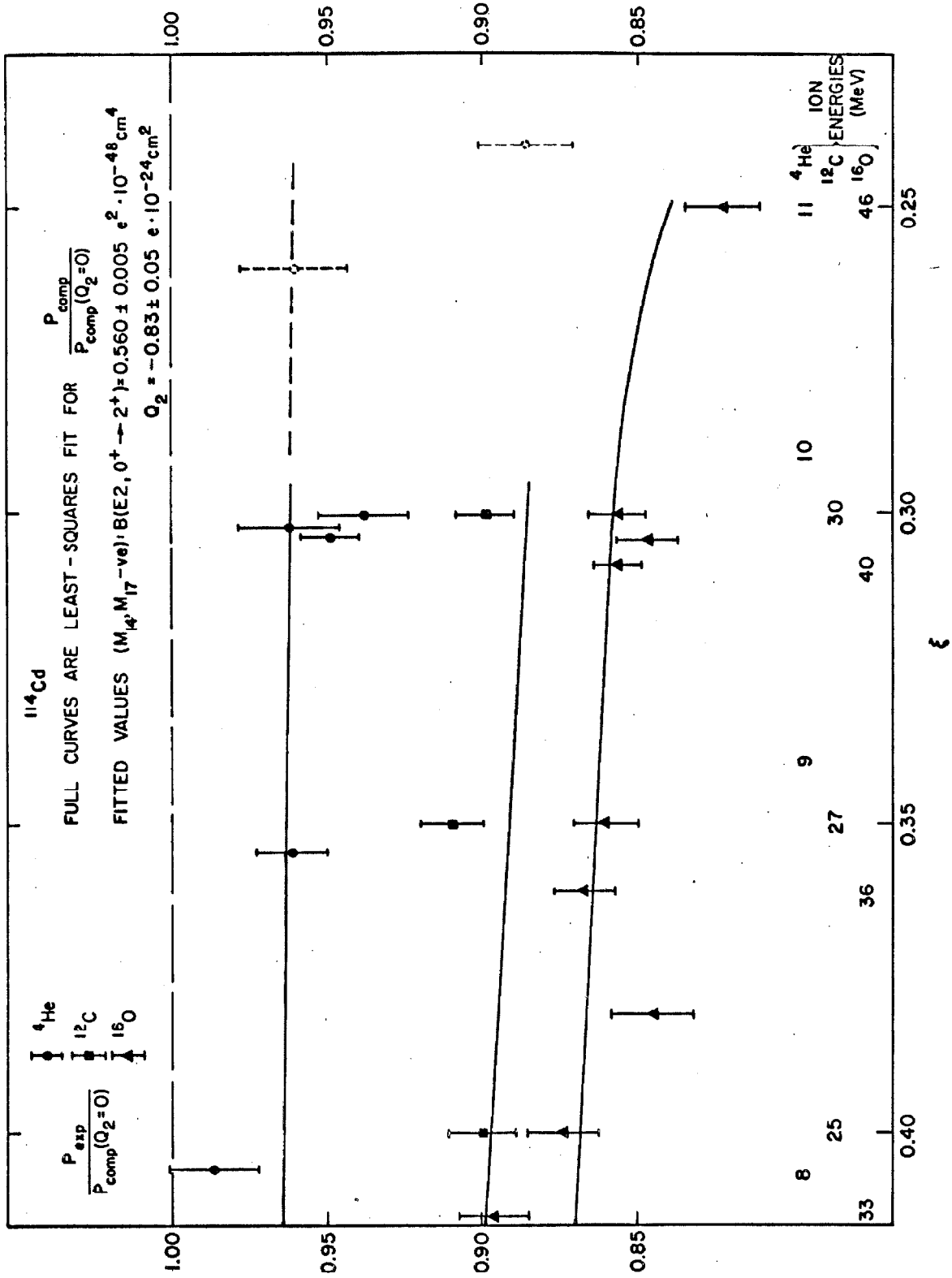
114Cd
FULL CURVES ARE LEAST-SQUARES FIT FOR $\frac{P_{comp}}{P_{comp}(Q_2=0)}$
FITTED VALUES $(M_{14}, M_{17}\text{-ve})$: B(E2, $0^+ \rightarrow 2^+$) = 0.560 ± 0.005 $e^2 \cdot 10^{-48}$ cm^4
Q_2 = −0.83 ± 0.05 $e \cdot 10^{-24}$ cm^2
$\frac{P_{exp}}{P_{comp}(Q_2=0)}$
4He
12C
16O
1.00
0.95
0.90
0.85
ION ENERGIES (MeV)
4He
12C
16O
11
10
9
8
46
30
27
25
40
36
33
0.25
0.30
0.35
0.40
ξ

FIGURE 18

FIGURE 19

Analogue of Figure 18 for ^{116}Cd. (Page 37)

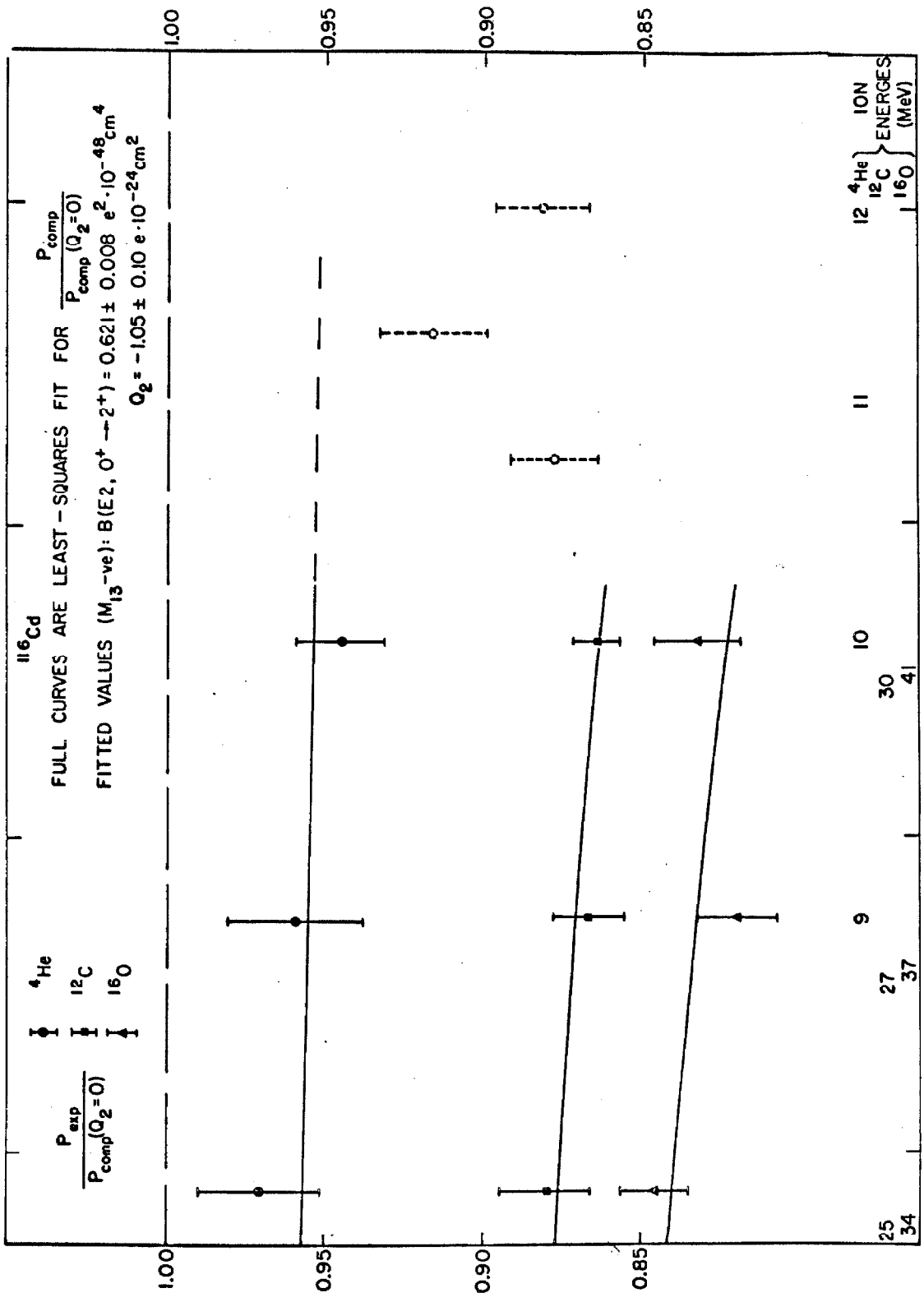
^{116}Cd
FULL CURVES ARE LEAST-SQUARES FIT FOR $\frac{P_{comp}}{P_{comp}(Q_2=0)}$
FITTED VALUES (M_{13}-ve): B(E2, $0^+ \rightarrow 2^+$) = 0.621 ± 0.008 $e^2 \cdot 10^{-48} cm^4$
Q_2 = -1.05 ± 0.10 $e \cdot 10^{-24} cm^2$
$\frac{P_{exp}}{P_{comp}(Q_2=0)}$
^4He
^{12}C
^{16}O
1.00
0.95
0.90
0.85
ION ENERGIES (MeV)
^4He 12
^{12}C 11
^{16}O 10
9
0.20
0.25
0.30
0.35
ξ
41
30
37
27
34
25

FIGURE 19

FIGURE 20

The data and least-squares fit of Figure 16 but now normalized to $P_{comp}(Q_2 = 0)$, the latter being the value of P computed with $M_{22} = Q_2 = 0$ and with all other matrix elements the same as before. Here the dispersion between curves corresponding to different bombarding ions is due entirely to a non-zero quadrupole moment of the first 2^+ state. (Page 37)

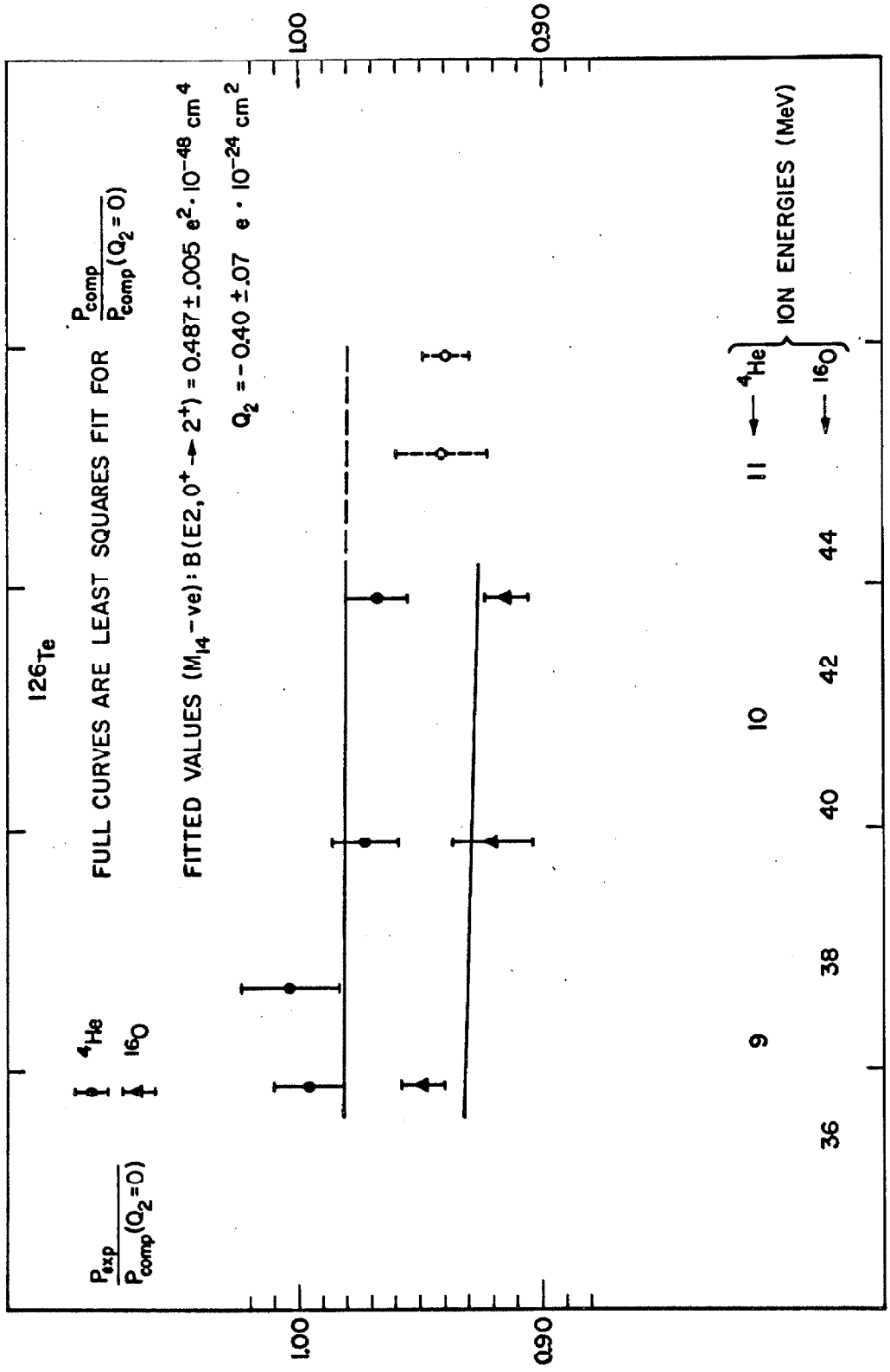
126Te
FULL CURVES ARE LEAST SQUARES FIT FOR $\frac{P_{comp}}{P_{comp}(Q_2=0)}$
FITTED VALUES (M_{14} -ve): B(E2, $0^+ \rightarrow 2^+$) = 0.487 ± .005 $e^2 \cdot 10^{-48}$ cm^4
Q_2 = - 0.40 ± .07 $e \cdot 10^{-24}$ cm^2
$\frac{P_{exp}}{P_{comp}(Q_2=0)}$
4He
16O
1.00
0.90
9
10
11
4He
16O
ION ENERGIES (MeV)
36
38
40
42
44
0.45
0.40
0.35
0.30
ξ

FIGURE 20

FIGURE 21

Analogue of Figure 20 for ^{128}Te. (Page 37)

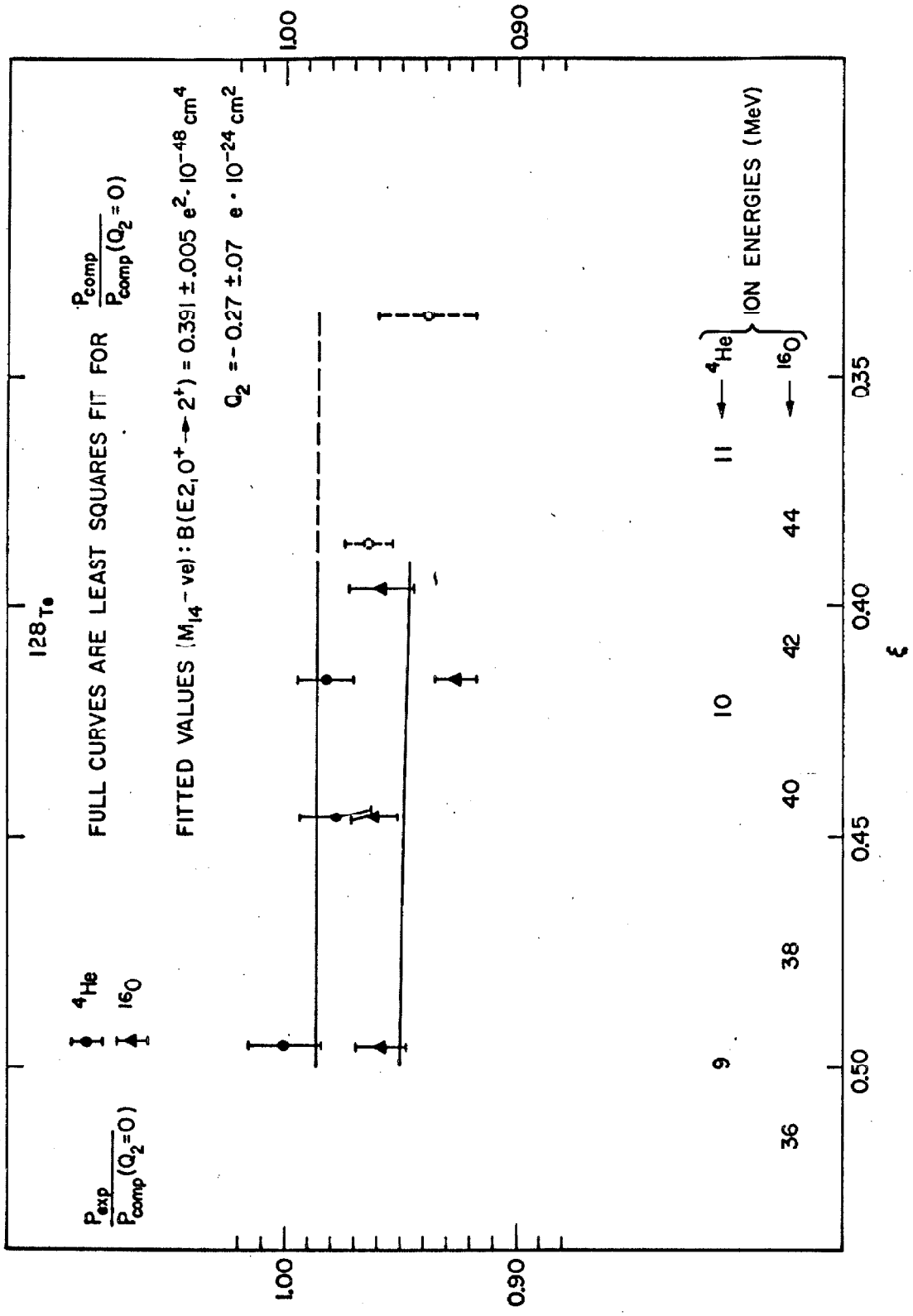
128Te
FULL CURVES ARE LEAST SQUARES FIT FOR $\frac{P_{comp}}{P_{comp}(Q_2=0)}$
FITTED VALUES (M_{14} - vel): B(E2, $0^+ \rightarrow 2^+$) = 0.391 ± .005 $e^2 \cdot 10^{-48}$ cm^4
Q_2 = - 0.27 ± .07 $e \cdot 10^{-24}$ cm^2
$\frac{P_{exp}}{P_{comp}(Q_2=0)}$
^4He
^{16}O
1.00
0.90
ION ENERGIES (MeV)
^4He
^{16}O
9
10
11
36
38
40
42
44
0.50
0.45
0.40
0.35
ξ

FIGURE 21

FIGURE 22

Systematic variation of some properties of the cadmium and tellurium isotopes. In each case the maximum and minimum values of $M_{22}/|M_{22}|$ are plotted (corresponding to both signs of the interference term $P^{(12)}_{0^+\to 2'^+\to 2^+}$). The energy and transition moment ratios have been obtained from Cookson and Darcey (1965) and McGowan, et al., (1965). The errors for the cadmium B(E2)-ratios are typically 20% while those for the corresponding values in tellurium are probably 30% to 40%. (Page 51)

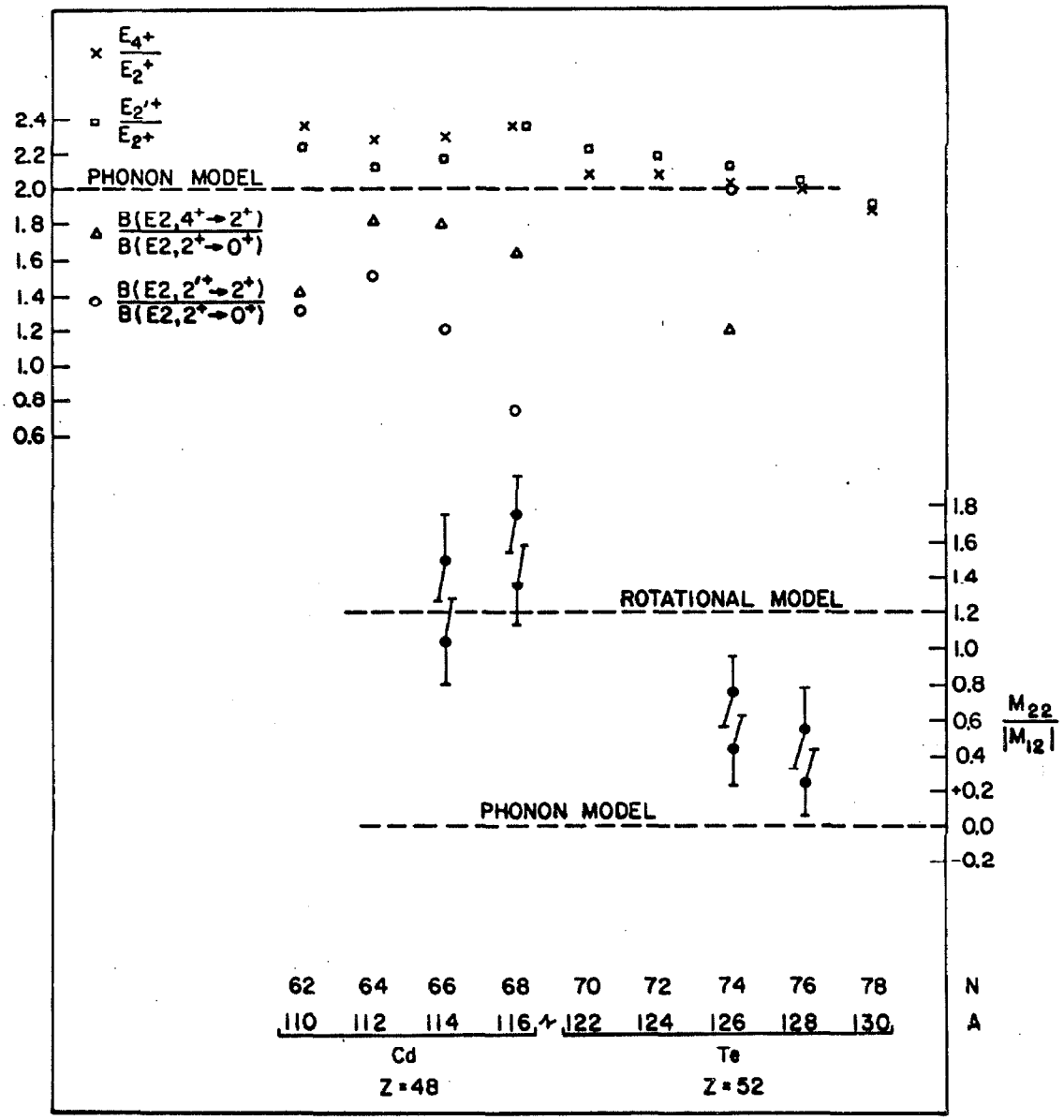
$\frac{E_{4^+}}{E_{2^+}}$
$\frac{E_{2'^+}}{E_{2^+}}$
PHONON MODEL
$\frac{B(E2,4^+\to 2^+)}{B(E2,2^+\to 0^+)}$
$\frac{B(E2,2'^+\to 2^+)}{B(E2,2^+\to 0^+)}$
2.4
2.2
2.0
1.8
1.6
1.4
1.2
1.0
0.8
0.6
ROTATIONAL MODEL
PHONON MODEL
1.8
1.6
1.4
1.2
1.0
0.8
0.6
0.4
+0.2
0.0
-0.2
$\frac{M_{22}}{|M_{12}|}$
62 64 66 68 70 72 74 76 78 N
110 112 114 116 122 124 126 128 130 A
Cd
Z=48
Te
Z=52

FIGURE 22

FIGURE 23

Momentum spectrum of elastically and inelastically scattered ions at a laboratory angle of 150^{o} following bombardment of a thin ^{114}Cd target by 9.76 MeV ^{4}He ions. This spectrum was recorded in four overlapping measurements with an array of 16 counters in the focal plane of the spectrometer. (Page 60)

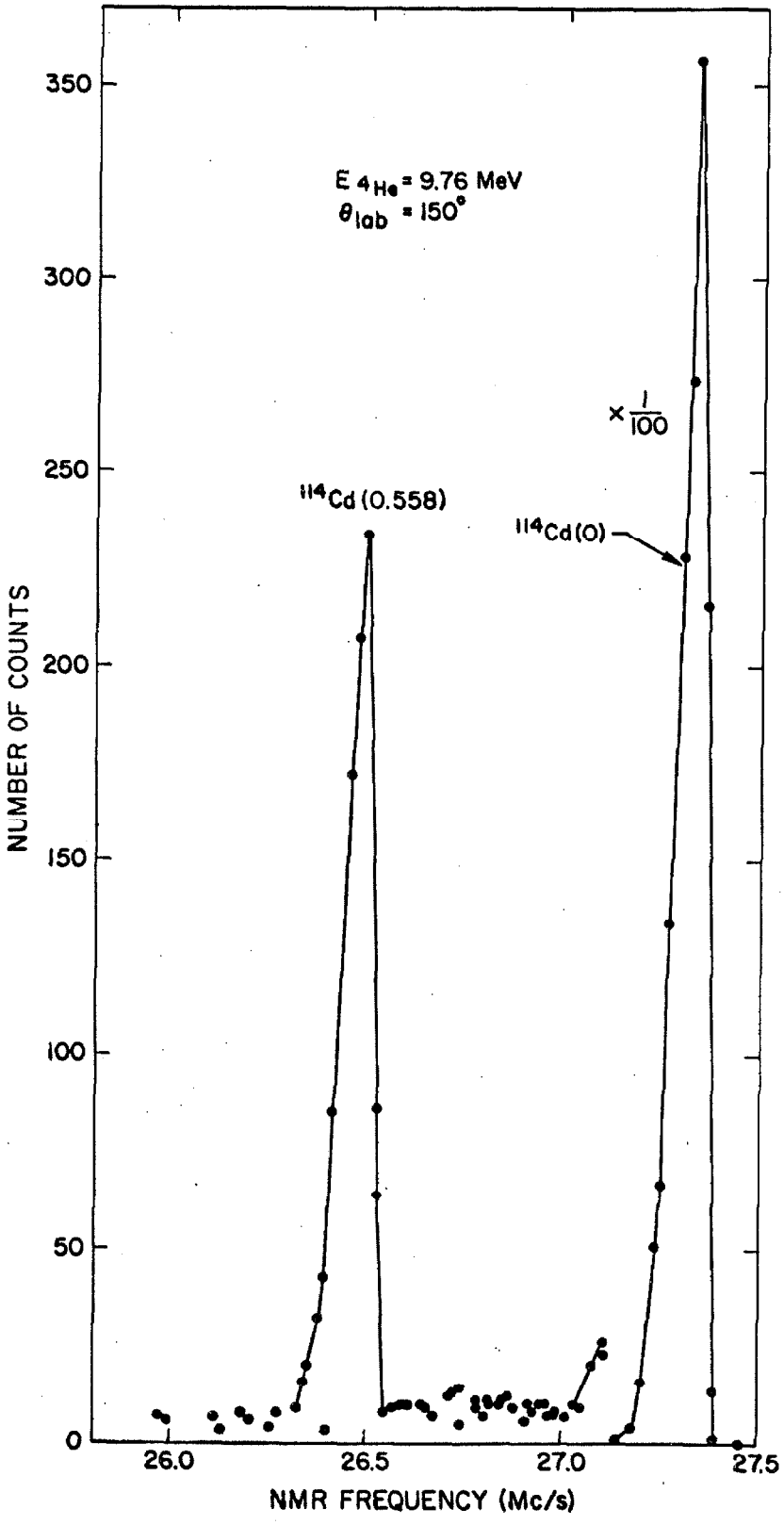
E 4He = 9.76 MeV
θlab = 150°
× 1/100
114Cd (0.558)
114Cd (0)
NUMBER OF COUNTS
NMR FREQUENCY (Mc/s)
0
50
100
150
200
250
300
350
26.0
26.5
27.0
27.5

FIGURE 23

FIGURE 24

Momentum spectrum of elastically and inelastically scattered ions at a laboratory angle of 150^{o} following bombardment of a thin ^{114}Cd target by 40.7 MeV ^{16}O ions. This spectrum was recorded in two overlapping measurements by an array of 16 counters in the focal plane of the spectrometer. (Page 60)

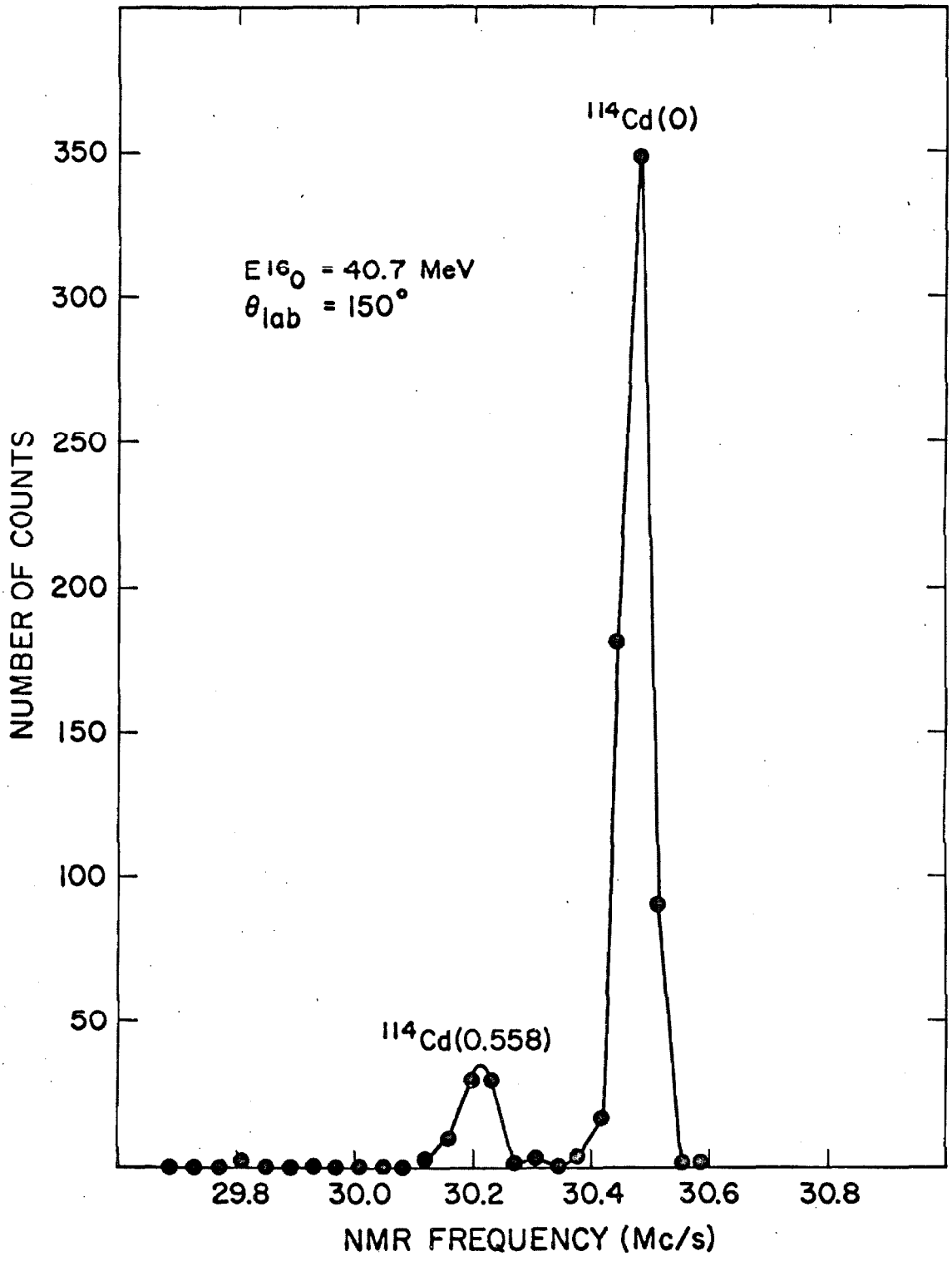
^{114}Cd(0)
E^{16}_{O} = 40.7 MeV
θ_{lab} = 150°
^{114}Cd(0.558)
NUMBER OF COUNTS
350
300
250
200
150
100
50
29.8
30.0
30.2
30.4
30.6
30.8
NMR FREQUENCY (Mc/s)

FIGURE 24

FIGURE 25

Gamma-ray spectra from the bombardment of ^{126}Te by 42 MeV ^{16}O ions. The spectra were taken with a 20 cc lithium-drifted germanium detector. The coincidence spectrum was gated by a window placed on the 667 keV $2^+ \rightarrow 0^+$ transition photopeak recorded by a 10.2-cm-long x 12.7-cm-diameter NaI detector. The background consists almost entirely of real coincidences whose source was most likely the $^{12}C(^{16}O, p\,\alpha)^{23}Na$ reaction due to carbon accumulation on the target. The arrow indicates a coincidence peak from the $2^+ \rightarrow 0^+$ transition and the horizontal bar indicates the expected position of the $4^+ \rightarrow 2^+$ gamma ray. (Page 62)

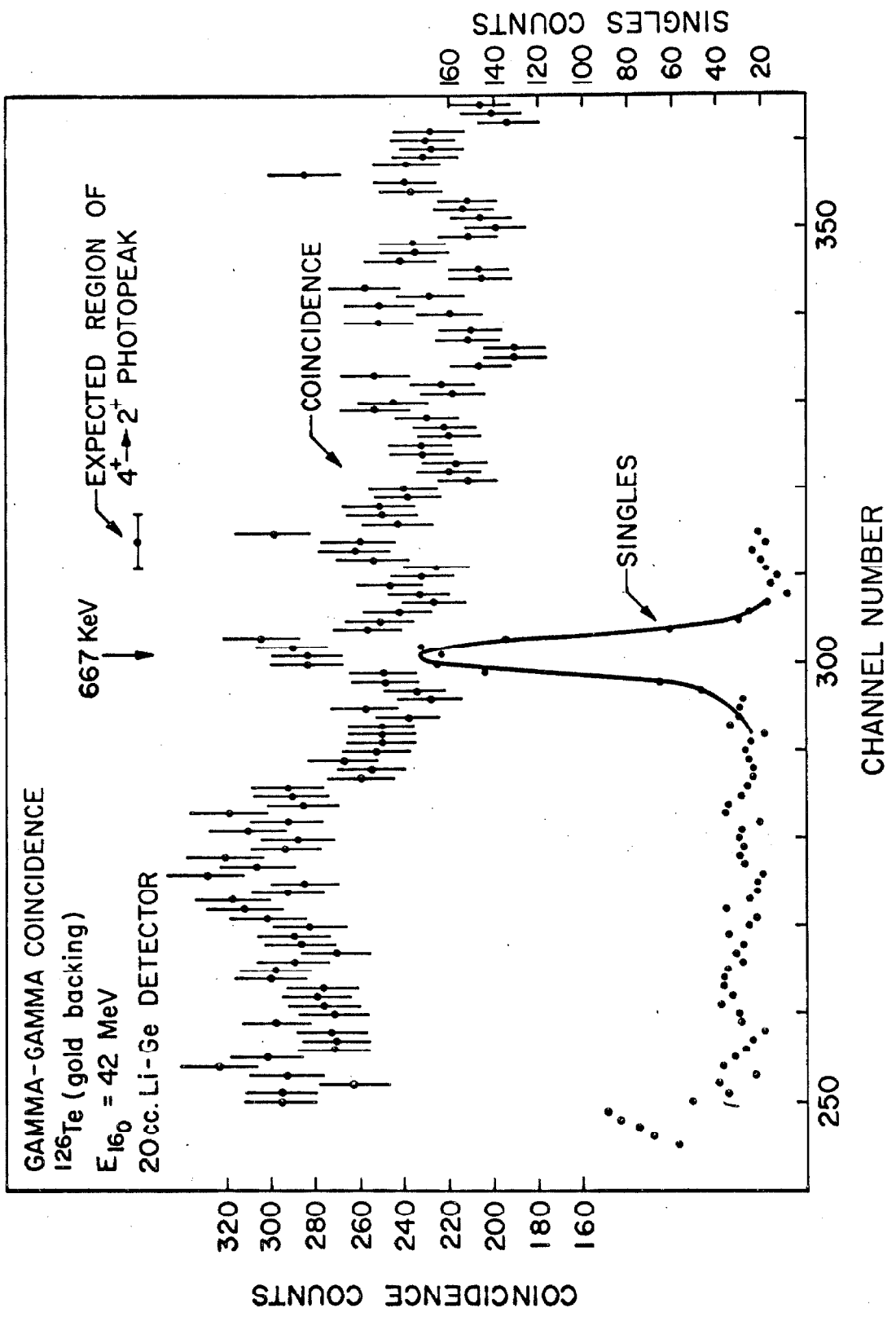
GAMMA-GAMMA COINCIDENCE
126Te (gold backing)
E16O = 42 MeV
20cc. Li-Ge DETECTOR
667 KeV
EXPECTED REGION OF
4+→2+ PHOTOPEAK
COINCIDENCE
SINGLES
COINCIDENCE COUNTS
SINGLES COUNTS
CHANNEL NUMBER

FIGURE 25